Fiber-Reinforced Concrete for Bridge Decks

Final Report
December 2021

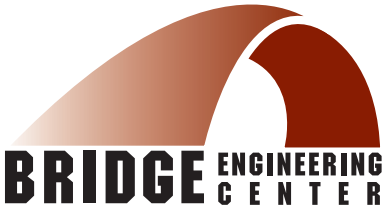

IOWA STATE UNIVERSITY
Institute for Transportation

Sponsored by
Iowa Highway Research Board
(IHRB Project TR-767)
Iowa Department of Transportation
(InTrans Project 19-679)

About the Bridge Engineering Center

The mission of the Bridge Engineering Center (BEC) is to conduct research on bridge technologies to help bridge designers/owners design, build, and maintain long-lasting bridges.

About the Institute for Transportation

The mission of the Institute for Transportation (InTrans) at Iowa State University is to save lives and improve economic vitality through discovery, research innovation, outreach, and the implementation of bold ideas.

Iowa State University Nondiscrimination Statement

Iowa State University does not discriminate on the basis of race, color, age, ethnicity, religion, national origin, pregnancy, sexual orientation, gender identity, genetic information, sex, marital status, disability, or status as a US veteran. Inquiries regarding nondiscrimination policies may be directed to the Office of Equal Opportunity, 3410 Beardshear Hall, 515 Morrill Road, Ames, Iowa 50011, telephone: 515-294-7612, hotline: 515-294-1222, email: eooffice@iastate.edu.

Disclaimer Notice

The contents of this report reflect the views of the authors, who are responsible for the facts and the accuracy of the information presented herein. The opinions, findings and conclusions expressed in this publication are those of the authors and not necessarily those of the sponsors.

The sponsors assume no liability for the contents or use of the information contained in this document. This report does not constitute a standard, specification, or regulation.

The sponsors do not endorse products or manufacturers. Trademarks or manufacturers' names appear in this report only because they are considered essential to the objective of the document.

Iowa DOT Statements

Federal and state laws prohibit employment and/or public accommodation discrimination on the basis of age, color, creed, disability, gender identity, national origin, pregnancy, race, religion, sex, sexual orientation or veteran's status. If you believe you have been discriminated against, please contact the Iowa Civil Rights Commission at 800-457-4416 or Iowa Department of Transportation's affirmative action officer. If you need accommodations because of a disability to access the Iowa Department of Transportation's services, contact the agency's affirmative action officer at 800-262-0003.

The preparation of this report was financed in part through funds provided by the Iowa Department of Transportation through its "Second Revised Agreement for the Management of Research Conducted by Iowa State University for the Iowa Department of Transportation" and its amendments.

The opinions, findings, and conclusions expressed in this publication are those of the authors and not necessarily those of the Iowa Department of Transportation.

Technical Report Documentation Page

1. Report No.	2. Government Accession No.	3. Recipient's Catalog No.
IHRB Project TR-767		

4. Title and Subtitle	5. Report Date
Fiber-Reinforced Concrete for Bridge Decks	December 2021
	6. Performing Organization Code

7. Author(s)	8. Performing Organization Report No.
Behrouz Shafei (orcid.org/0000-0001-5677-6324), Peter Taylor (orcid.org/0000-0002-4030-1727), Brent Phares (orcid.org/0000-0001-5894-4774), and Maziar Kazemian (orcid.org/0000-0002-3067-4597)	InTrans Project 19-679

9. Performing Organization Name and Address	10. Work Unit No. (TRAIS)
Bridge Engineering Center Iowa State University 2711 South Loop Drive, Suite 4700 Ames, IA 50010-8664	11. Contract or Grant No.

12. Sponsoring Organization Name and Address	13. Type of Report and Period Covered
Iowa Highway Research Board Iowa Department of Transportation 800 Lincoln Way Ames, IA 50010	Final Report
	14. Sponsoring Agency Code IHRB Project TR-767

15. Supplementary Notes

Visit https://bec.iastate.edu/ for color pdfs of this and other research reports.

16. Abstract

Concrete is made of multiple ingredients that begin in a plastic phase and become solid over time. Additionally, it is well established that concrete is exposed to various stressors from the initial hours of pouring, making it prone to cracking. The multiphase nature of concrete along with these stressors require the consideration of several factors, especially for the design of concrete bridge decks that are exposed to aggressive environmental and mechanical stressors simultaneously. Due to the low early-age strength of concrete, even small-scale tensions can result in cracking and consequently decrease the longevity of the concrete structure.

In order to address these issues, a three-stage framework was designed for this project. In Stage 1, multiple binder compositions were investigated for their performance in terms of early-age plastic shrinkage by recording capillary pressure development, monitoring crack width, and determining strain development by means of digital image correlation. After binder modification, in Stage 2 different dosages of microfibers were added to concrete mixtures to compensate for the concrete's low tensile strength and control cracking during the life of the concrete. To measure the efficiency of the microfibers, drying shrinkage, compressive and splitting tensile strength, and rapid chloride migration tests were carried out to determine the cracking potential and mechanical and durability properties of fiber-reinforced concrete (FRC). In Stage 3, three types of macrofibers (i.e., polypropylene [PP], alkali-resistant [AR] glass, and polyvinyl alcohol [PVA]) were incorporated at multiple dosages into FRC that already contained microfibers to enhance the post-peak strength of the concrete. The compressive, splitting tensile, and flexural strengths of the concretes were recorded as the pre-peak mechanical properties, and the toughness and residual flexural strength were recorded as the post-peak mechanical properties.

The results show that Class F fly ash, as opposed to silica fume and Type K (expansive) cement, contributes most to the early-age cracking resistance of concrete. Furthermore, increasing PP microfiber content significantly reduced the cracking potential and enhanced the mechanical properties and chloride resistance of concrete. In the case of hybrid FRC (FRC containing both microfibers and macrofibers), AR glass macrofibers introduced superior performance compared to PP and PVA macrofibers, in terms of pre- and post-peak mechanical properties.

17. Key Words	18. Distribution Statement
bridge deck concrete—concrete toughness—concrete shrinkage—fiber-reinforced concrete—hybrid fibers—mechanical properties	No restrictions.

19. Security Classification (of this report)	20. Security Classification (of this page)	21. No. of Pages	22. Price
Unclassified.	Unclassified.	147	NA

Form DOT F 1700.7 (8-72) **Reproduction of completed page authorized**

FIBER-REINFORCED CONCRETE FOR BRIDGE DECKS

Final Report
December 2021

Principal Investigator
Behrouz Shafei, Associate Professor
Bridge Engineering Center, Iowa State University

Co-Principal Investigators
Brent Phares, Research Structural Engineer
Bridge Engineering Center, Iowa State University

Peter Taylor, Director
National Concrete Pavement Technology Center, Iowa State University

Research Assistant
Maziar Kazemian

Authors
Behrouz Shafei, Peter Taylor, Brent Phares, and Maziar Kazemian

Sponsored by
Iowa Highway Research Board and
Iowa Department of Transportation
(IHRB Project TR-767)

Preparation of this report was financed in part
through funds provided by the Iowa Department of Transportation
through its Research Management Agreement with the
Institute for Transportation
(InTrans Project 19-679)

A report from
Bridge Engineering Center
Institute for Transportation
Iowa State University
2711 South Loop Drive, Suite 4700
Ames, IA 50010-8664
Phone: 515-294-8103 / Fax: 515-294-0467
https://bec.iastate.edu/

TABLE OF CONTENTS

ACKNOWLEDGMENTS ix

EXECUTIVE SUMMARY xi

CHAPTER 1. INTRODUCTION 1

- Research Significance 1
- Objectives 1
- Report Organization 1

CHAPTER 2. LITERATURE REVIEW 2

- Early-Age Cracking in Concrete 2
- Methods of Mitigating Shrinkage Cracking in Concrete 3
- Types of Shrinkage in Concrete 5
- Factors Affecting Plastic Shrinkage 6
- Methods to Mitigate Plastic Shrinkage Cracking 8

CHAPTER 3. SUPPLEMENTARY AND ALTERNATIVE CEMENTITIOUS MATERIALS 12

- Pozzolanic SCMs 12
- Alternative Cementitious Materials 21

CHAPTER 4. FIBER REINFORCEMENT IN CONCRETE 26

- Mechanism of Crack Mitigation 27
- Fiber Types 28
- Comparison Among Synthetic and Glass Fibers 55

CHAPTER 5. EXPERIMENTAL PROGRAM 59

- Material Properties 59
- Mixing Procedure 60
- Stage 1. Binder Investigation 61
- Stage 2. Microfiber Investigation 69
- Stage 3. Hybrid Fiber Investigation 81

CHAPTER 6. RESULTS AND DISCUSSION 86

- Stage 1. Binder Investigation 86
- Stage 2. Microfiber Investigation 99
- Stage 3. Hybrid Fiber Investigation 107

CHAPTER 7. CONCLUSIONS AND RECOMMENDATIONS 115

- Key Findings 115
- Conclusions and Recommendations 117

REFERENCES 118

LIST OF FIGURES

Figure 1. Spalling of concrete due to steel rebar corrosion 3
Figure 2. Fibers used in the study: (a) from top to bottom, PVA, PP, and AR glass macrofibers and (b) PP microfibers 60
Figure 3. Restrained slab instrumented with CPSS sensors 64
Figure 4. Concrete ring undergoing restrained shrinkage....71
Figure 5. Concrete cylinder and bearing device loaded into the testing machine 75
Figure 6. RMT setup: (1) cathode in NaCl solution, (2) anode in NaOH solution, (3) specimen in rubber sleeve, (4) power supply....80
Figure 7. Three-point bending test setup 84
Figure 8. Capillary pressure development rates for Specimens 0-0 (Control), 7.5K-0, and 15K-0 86
Figure 9. Capillary pressure development rates for Specimens 0-15FA, 7.5K-15FA, and 15K-15FA 87
Figure 10. Capillary pressure development rates for Specimens 0-7.5SF, 7.5K-7.5SF, and 15K-7.5SF 87
Figure 11. Onset and rate of plastic shrinkage cracking for Specimens 0-0, 7.5K-0, and 15K-0 89
Figure 12. Onset and rate of plastic shrinkage cracking for Specimens 0-15FA, 7.5K-15FA, and 15K-15FA 89
Figure 13. Onset and rate of plastic shrinkage cracking for Specimens 0-7.5SF, 7.5K-7.5SF, and 15K-7.5SF....90
Figure 14. Final tensile strain chart for Specimen 0K 94
Figure 15. Final tensile strain map for Specimen 0K 94
Figure 16. Final tensile strain chart for Specimen 7.5K 95
Figure 17. Final tensile strain map for Specimen 7.5K 95
Figure 18. Final tensile strain chart for Specimen 15K 96
Figure 19. Final tensile strain map for Specimen 15K 96
Figure 20. Final tensile strain chart for Specimen 22.5K 97
Figure 21. Final tensile strain map for Specimen 22.5K 97
Figure 22. Compressive strain development for Mix 1 (0.0% fiber)....99
Figure 23. Compressive strain development for Mix 2 (0.25% fiber)....100
Figure 24. Compressive strain development for Mix 3 (0.50% fiber)....100
Figure 25. Compressive strain development for Mix 4 (1.0% fiber)....101
Figure 26. Mean compressive strain development for all FRC mixes....101
Figure 27. Tensile strength of FRC mixes at 7, 14, and 28 days....103
Figure 28. Cracking potential over time for all FRC mixes 104
Figure 29. 28-day compressive strength of FRC mixes....106
Figure 30. Rapid chloride migration test results for (a) mean chloride penetration depth and (b) migration coefficient 107
Figure 31. Water reducer demand of hybrid FRC mixes....108
Figure 32. Compressive strength of hybrid FRC with PP macrofibers 109
Figure 33. Compressive strength of hybrid FRC with AR glass macrofibers 109
Figure 34. Compressive strength of hybrid FRC with PVA macrofibers....110

Figure 35. Splitting tensile strengths of hybrid FRC with PP, AR glass, and PVA macrofibers.....111
Figure 36. Flexural strengths of hybrid FRC with PP, AR glass, and PVA macrofibers.....113

LIST OF TABLES

Table 1. Base mixture proportions (lb/yd^3).....59
Table 2. Chemical composition of the binders used in the study (% weight) 59
Table 3. Physical and mechanical properties of the fibers used in the study.....60
Table 4. Test matrix for plastic shrinkage cracking in restrained concrete slabs 61
Table 5. Test matrix for strain measurement by digital image correlation.....66
Table 6. Test matrix for cracking age of concrete under restrained shrinkage.....69
Table 7. Test matrix for splitting tensile strength.....73
Table 8. Test matrix for compressive strength of concrete.....76
Table 9. Test matrix for chloride penetration by rapid migration.....78
Table 10. Test matrix for flexural strength 82
Table 11. Plastic shrinkage cracking images for Type K concrete slabs.....91
Table 12. Plastic shrinkage cracking images for fly ash concrete slabs 91
Table 13. Plastic shrinkage cracking images for silica fume concrete slabs and control sample 92
Table 14. Toughness of FRC specimens.....114

ACKNOWLEDGMENTS

This work was sponsored by the Iowa Highway Research Board and the Iowa Department of Transportation. The authors would like to thank the technical advisory committee on this project: Michael Nop, Curtis Carter, Todd Hanson, Jesse Peterson, Steve Seivert, and Joseph Stanisz. The research team would also like to acknowledge the staff of the Portland Cement Concrete Pavement Materials and Research Laboratory and Structural Engineering Research Laboratory at Iowa State University for their support in performing the experimental work.

EXECUTIVE SUMMARY

Bridge deck concretes are exposed to multiple stressors that endanger the performance and life cycle of the bridge. If special attention is not dedicated to the material design and construction of the reinforced concrete structures, cracks would be generated and would propagate into the concrete, providing channels for corrosive agents (such as chloride ions and carbon dioxide) to penetrate into the concrete at a pace much faster than that of uncracked concrete. The penetration of these destructive agents results in corrosion of the rebars and a decrease in the structural performance of the reinforced concrete. At this point, the structure needs to be either repaired, which hinders the operation of the structure, or demolished and built again. Either of these options imposes significant economic and operational expenses on the structure. Therefore, a comprehensive study should be carried out to investigate the multiple factors threatening the longevity of concrete structures.

Due to its large surface area, bridge deck concrete is significantly prone to shrinkage-induced cracking caused by water evaporation, either through plastic shrinkage when the concrete is in a semiplastic phase or through drying shrinkage over longer periods. The low tensile strength of ordinary portland cement concrete is responsible for shrinkage-induced cracking, which can be reduced by modifying the binder composition or by adding fibers to the concrete to provide additional tensile strength capacity.

Since ancient times, people have been putting fibers, such as straw and hair, into mortars and bricks to improve their tensile properties. These ancient and simple methods of concrete reinforcement have now been transformed into advanced methods that involve using discontinuous fibers distributed randomly throughout the concrete matrix. Moreover, conventional concrete is a brittle material by nature. To compensate for this characteristic and avoid the sudden brittle failure of concrete structures, reinforcement materials are embedded into the concrete.

To address the concerns noted above, this project aimed to investigate multiple crack mitigation scenarios under shrinkage-induced cracking conditions, which are the most important crack-inducing parameters in bridge deck concrete. Furthermore, the post-peak performance of concrete was emphasized, with the workability of the concrete being considered as a restrictive factor.

To pursue the aforementioned objectives, a comprehensive study was conducted that consisted of three stages:

- Stage 1. Binder Investigation. This stage was designed to investigate the performance of multiple binder compositions in terms of mitigating early-age cracking. To do so, 7.5% and 15% of portland cement was substituted with expansive (Type K) cement, Class F fly ash, and silica fume. Plastic shrinkage tests were conducted on slab specimens, and the capillary pressure development and crack widths of the slabs were recorded for six hours. Additionally, the digital image correlation (DIC) technique was employed on the mixtures made with Type K cement to record the strain development. The results of this stage led to

the determination of the binder composition of the concrete on which tests were performed in the subsequent stages of this research.

- Stage 2. Microfiber Investigation. In this stage, microfibers were added to the concrete to further enhance the performance of the concrete against tensile stresses. In particular, polypropylene (PP) microfibers at dosages of 0.25%, 0.50%, and 1.0% of the concrete volume were investigated during this stage. Drying shrinkage tests and splitting tensile strength tests were conducted to measure the cracking potential of the fiber-reinforced concrete (FRC). Furthermore, compressive strength tests and rapid chloride migration tests were carried out to determine the mechanical and durability properties of the FRC.

- Stage 3. Hybrid Fiber Investigation. This stage was dedicated to identifying the pre-peak and post-peak properties of hybrid FRC (FRC containing both microfibers and macrofibers). It is well known that microfibers are most effective in controlling the low tensile stresses (such as shrinkage tension) and macrofibers contribute to the post-peak strength of the concrete when macrocracks are generated. In this stage, three macrofiber types, i.e., PP, alkali-resistant (AR) glass, and polyvinyl alcohol (PVA), at various dosages were added to concrete containing two amounts of PP microfibers. The compressive, splitting tensile, and flexural strengths of the mixtures were recorded and reported as the pre-peak mechanical properties of the hybrid FRC. Additionally, the toughness and residual flexural strength of the mixtures were measured and recorded as the post-peak behavior of the hybrid FRC.

The results of this three-stage study can be used to determine a suitable mix design for the application of fiber-reinforced concrete for bridge decks.

Key Findings of the Research

Stage 1:

- In general, increasing the proportion of Type K expansive cement resulted in an increase in the rate of capillary pressure development for all types and percentages of supplementary cementitious materials (SCMs) investigated in this project. Silica fume was found to have a negative effect on the rate of capillary pressure development, while Class F fly ash decreased the rate of capillary pressure. Therefore, Class F fly ash was incorporated into the mix design of the FRC in subsequent stages of this research.

- For each type of concrete investigated, an increase in Type K expansive cement led to a reduction in plastic shrinkage crack widths at six hours after casting. For concrete containing Class F fly ash or silica fume, increasing the dosage of Type K cement resulted in a reduction in the rate of plastic shrinkage crack propagation, provided that adequate workability was achieved through the use of superplasticizer.

- The DIC results suggest that after the six-hour testing period, the specimens experienced reduced plastic shrinkage-induced tensile strain at the location of cracking with increasing

proportions of Type K expansive cement up to 22.5%. Doses of Type K cement up to 22.5% showed a substantial relative reduction in plastic shrinkage-induced tensile strain.

Stage 2:

- For PP microfiber percentages from 0.25% up to 1.0% by volume, an increase in fiber proportion did not significantly affect the rate of drying-induced strain development or the final magnitude of strain in a concrete ring.

- Tensile strength increased with both age and PP microfiber percentage among all ages and mixes of FRC for fiber doses up to 1.0% by volume. The largest relative increase in tensile strength occurred at lower PP microfiber doses in the range of 0.25%. The ability of PP microfibers to improve the tensile strength of concrete decreased in efficiency at fiber volumes of 1.0% or higher.

- Cracking potential, defined as the ratio of the maximum shrinkage-induced stress experienced by an FRC mix to the tensile strength of the same FRC mix, decreased with an increase in PP microfiber percentage for fiber doses up to 1.0%. At volumes of 1.0% and higher, the relative reduction in cracking potential significantly decreased compared to the relative reduction in cracking potential at lower doses.

- In general, the data show that the 28-day compressive strength of FRC increases with PP microfiber proportion for fiber doses up to 1.0% by volume. At PP microfiber volumes of 1.0% and higher, the relative increase in compressive strength provided by the fibers significantly decreased compared to the relative increase in compressive strength at lower doses.

- An increase in PP microfiber proportion up to 1.0% by volume corresponded to a decrease in the rate and magnitude of chloride ion penetration into FRC after 24 hours. Increasing the fiber dosage to 1.0% appeared to result in less efficient mitigation of chloride penetration compared to the mitigation provided at lower fiber proportions.

Stage 3:

- PVA macrofibers reduced the workability of FRC more significantly than AR glass and PP macrofibers due to the water absorption of the PVA fibers.

- PP and PVA macrofibers reduced the compressive strength of concrete, while AR glass macrofibers provided a compressive strength similar to that of the control sample. In the case of hybrid FRC, the addition of AR glass macrofibers resulted in superior compressive strength, which was augmented by increasing the macrofiber dosage.

- FRC with PP macrofibers showed weaker performance under tensile loads compared to FRC with AR glass or PVA macrofibers.

- The mechanical test results suggest that AR glass macrofibers show a promising synergy with PP microfibers, which makes AR glass macrofibers an appropriate choice for hybrid FRC.

- Regardless of the fiber combination and dosage, the FRC samples studied in Stage 3 exhibited a flexural strength similar to or higher than that of the control sample. FRC with PP macrofibers showed superior performance in terms of flexural strength when no microfibers were added to the mixture. However, when microfibers were introduced into the mixture, FRC with PP macrofibers lost its superiority. Furthermore, in hybrid FRC with low macrofiber dosages (i.e., 0.125% and 0.1875%), AR glass FRC had the highest flexural strength. However, at a macrofiber dosage of 0.25%, PVA FRC outperformed the FRCs with other macrofibers.

- The addition of AR glass macrofibers to concrete, even at a dosage of 0.125%, provided FRC with some level of post-peak residual strength and toughness. However, PP and PVA macrofibers provided FRC with post-peak flexural strength and toughness at dosages of 0.25% and 0.1875%, respectively. Moreover, at a macrofiber dosage of 0.5%, AR glass FRC, in contrast to PP or PVA FRC, showed a well-formed residual flexural strength stretching beyond 1/150 of the span length.

Summary of the Findings and Recommendations

Based on the research conducted and the literature reviewed for this study, it can be concluded that replacing a portion of portland cement with Class F fly ash has a positive effect on the resistance of concrete to plastic shrinkage as well as on the workability and long-term durability of concrete. Although the addition of Type K cement showed promise in restricting crack width, it increased the rate of capillary pressure development in concrete, which has a destructive effect on the resistance of concrete to plastic shrinkage. Therefore, it is not recommended that Type K cement be included in final mix designs, while it is recommended that Class C fly ash replace 20% of the portland cement to address dimensional stability, workability, and durability concerns.

The addition of PP microfibers, even in doses as low as 0.25% by volume, proved to significantly reduce the cracking potential of concrete due to drying shrinkage. Furthermore, PP microfibers were found to be helpful in enhancing the mechanical and chloride resistance of FRC, but increasing the volume of PP microfibers beyond a certain percentage decreased the fibers' efficiency. On the other hand, PP microfibers, similar to other microfibers, increase the water demand of concrete, which is a restrictive operational parameter. Therefore, practical considerations limit the dosage of PP microfibers; the maximum practical dosage is recommended to be 0.125%, which corresponds to 2 lb/yd^3.

Another drawback of microfibers is their inability to provide post-peak strength, which can be addressed with the addition of macrofibers. Based on the pre- and post-peak mechanical strength results, AR glass monofilaments are recommended to be used as macrofibers. These fibers showed superior performance over PP and PVA macrofibers. The recommended fiber combination is 0.125% PP microfiber along with 0.25% AR glass macrofiber, which can satisfy practical restrictions as well as provide suitable pre- and post-peak mechanical properties.

CHAPTER 1. INTRODUCTION

Research Significance

Properly designed structural concrete exhibits favorable strength, durability, and economic properties, which makes it an attractive choice for transportation infrastructure applications. Despite its many advantages, concrete is susceptible to damage resulting from prolonged or harsh environmental exposure. The inherent relative weakness of concrete under tensile loading makes concrete highly vulnerable to cracking when applied tensile stresses exceed the low tensile strength of concrete. The vulnerability of concrete elements to cracking is even greater at an early age, when the concrete is just beginning to set and has not developed its full tensile strength. Cracks that develop in a concrete element serve as locations at which water and corrosive agents may infiltrate the concrete. In the presence of steel reinforcing, the penetration of water and corrosive agents into a concrete element leads to corrosion of the steel and subsequent spalling and deterioration of the concrete.

To extend the service life of reinforced concrete, as well as ensure the safety of concrete structures during service, it is imperative to mitigate cracking, particularly while the concrete is beginning to set. While crack reduction efforts are a common topic of research, many improvements can be made regarding the understanding, application, and practicality of the crack mitigation techniques that can be employed to enhance the longevity and consequently reduce the maintenance cost of structures.

Objectives

This project was conducted in three stages to find a solution for the aforementioned concerns. In this first stage, a binder composition suitable for mitigating the early-age cracking potential of the concrete matrix was selected. In the second task, different dosages of microfibers were added to concrete mixtures as reinforcement against early-age cracking, and the fibers' influence on the cracking potential and the mechanical and durability properties of the concrete were investigated. In the third stage, three different macrofibers were investigated for their contribution to pre-peak and post-peak mechanical strength in hybrid fiber-reinforced concrete (FRC) mixtures (FRC containing both microfibers and macrofibers).

Report Organization

The report is organized into the following chapters:

- Chapter 2. Literature Review
- Chapter 3. Supplementary and Alternative Cementitious Materials
- Chapter 4. Fiber Reinforcement in Concrete
- Chapter 5. Experimental Program
- Chapter 6. Results and Discussion
- Chapter 7. Conclusions and Recommendations

CHAPTER 2. LITERATURE REVIEW

Early-Age Cracking in Concrete

The initial hours immediately after casting concrete are vital for the performance and service life of the concrete element. During approximately the first 12 hours after casting a concrete specimen, the concrete changes from a plastic, functionally liquid state (immediately after pouring), to a semiplastic state (as the concrete initially sets), to a rigid state (after the concrete fully sets) (Esping and Löfgren 2005, Schmidt and Slowik 2009, Sayahi 2019).

The change in a concrete specimen from a liquid state to a rigid state is accompanied by a reduction in free water. The primary mechanisms contributing to the reduction in free water as concrete hydrates are (1) evaporation and (2) chemical hydration reactions. Evaporation occurs in a concrete specimen as free water evaporates from the exposed surface. During the dormant period, gravity draws aggregates toward the bottom of the element, which in turn pushes water toward the top surface in a process known as bleeding (Cohen et al. 1990, Schmidt and Slowik 2009, Allahham et al. 2016, Sayahi 2019). It is important to note that initially bleeding may occur at a higher rate than evaporation. In this case, bleed water simply accumulates at the top of the concrete specimen, creating a film of water on the concrete surface (Schmidt and Slowik 2009, Sayahi 2019).

However, at some point when the settlement of aggregates is finished and bleeding slows, the evaporation rate exceeds the bleeding rate. When this occurs, the concrete no longer has a protective film of water on top, and therefore it dries out and the risk of shrinking-related cracking increases (Cohen et al. 1990, Sayahi 2019). During this phase, instead of water evaporating from the top surface of the concrete, capillary water begins to evaporate from between aggregates. The evaporation of water from between aggregates causes a negative capillary pressure and subsequent contraction of the concrete specimen (Shaeles and Hover 1988, Schmidt and Slowik 2009, Allahham et al. 2016, Sayahi 2019, Vosoughi 2019).

In addition, water is consumed during hydration reactions as concrete hydrates. Water is essential in hydrating the cementitious materials in concrete, which allows for the formation of the cement matrix that binds the aggregates together and gives concrete its strength as well as other mechanical properties. Various products of the hydration reactions may occupy less space than was previously occupied by water. As a result, the concrete specimen contracts, similar to the effect of evaporation (Bentz and Jensen 2004, Sayahi 2019).

Experiments have shown that free, unrestrained shrinkage of concrete simply causes the concrete specimen to contract and does not cause noteworthy crack development (Cohen et al. 1990, Schmidt and Slowik 2009). However, nearly all structural applications of concrete are restrained in some way, whether in the form of internal reinforcement, construction joints, or formwork. In a restrained concrete specimen, the negative pressure and contraction caused by evaporation and hydration reactions result in tensile stresses because the restraining mechanisms do not allow the concrete to contract freely.

Concrete develops its compressive and tensile strength over a long period of time after setting has occurred. As a result, in its early age concrete has very little tensile strength compared with the already low tensile strength of a fully matured specimen. If the tensile stresses induced by negative pressures and restraining forces should exceed the low tensile strength of a young concrete element, cracking may occur. The surface tension generated as water is extracted from capillaries serves as the driving mechanism of shrinkage in concrete. As such, cracking originates from the empty capillaries from which the water has evaporated (Cohen et al. 1990, Slowik et al. 2008, Schmidt and Slowik 2009, Allahham et al. 2016, Sayahi 2019).

Early-age shrinkage cracking is typically very shallow because the pores that lose the most water are near the surface of the concrete (Schmidt and Slowik 2009). However, these cracks are critical in terms of the ingress of water and other chemicals into a concrete element. Early-age shrinkage cracks allow for water to enter a concrete specimen. For water alone, the alkaline environment created by the concrete surrounding the steel reinforcement protects the steel from oxidization and corrosion. However, if chlorides (such as deicing salts) are present in the water, this protective alkaline environment is destroyed, and the steel reinforcement will begin to rust (PCA 2002, Qi 2003) (see Figure 1).

Figure 1. Spalling of concrete due to steel rebar corrosion

As such, it is especially important to mitigate early-age shrinkage cracking in concrete elements located in freeze-thaw climates or marine environments.

Methods of Mitigating Shrinkage Cracking in Concrete

Several methods of mitigating shrinkage cracking in concrete have been researched and are utilized in practice. These methods are tailored to address the different mechanisms that result in different types of shrinkage. (The various types of shrinkage experienced in a concrete element are explained in greater detail in the following section.)

To address plastic shrinkage cracking, mitigation techniques typically aim to keep the concrete surface wet and avoid excessive evaporation. Because plastic shrinkage cracking results from

excessive moisture loss, plastic shrinkage cracking may be controlled through various wet curing methods. Wet curing methods may include covering the concrete element with a waterproof barrier or misting the concrete element with water (referred to as fogging) (Shaeles and Hover 1988, Schmidt and Slowik 2009, Sayahi 2019).

However, compared to no special curing measures, wet curing is often labor intensive and impractical for large elements. A potentially easier, but perhaps unreliable, method of controlling evaporation and subsequent plastic shrinkage cracking is to avoid casting concrete on a day with unfavorable conditions, such as high heat or strong winds.

Autogenous shrinkage cracking, which results from the chemical hydration reactions between cementitious materials and water, are not affected by wet curing methods, which only provide additional water to the surface of a concrete element. Instead, to mitigate excessive moisture loss due to hydration reactions, extra water may be provided evenly throughout the concrete bulk. The even distribution of water throughout an entire concrete element may be accomplished through internal curing (Vosoughi 2019). For internal curing, the mechanism of delivering water evenly throughout the concrete is to include a percentage of porous aggregate that will act as a water carrier and evenly distribute internal curing water throughout the inside of a concrete element, replenishing the water lost to autogenous shrinkage.

Shrinkage cracking may also be addressed through chemical means with the use of shrinkage-reducing admixtures (SRAs). SRAs reduce the amount of cracking by reducing the surface tension at the capillaries, which leads to lower shrinkage forces in concrete (Mora-Ruacho et al. 2009). It is crucial to note that while SRAs are useful in mitigating shrinkage cracking (particularly autogenous), they are a chemical admixture that may affect the strength and modulus of elasticity of a concrete specimen (Mora-Ruacho et al. 2009, Niu et al. 2019, Sayahi 2019).

Finally, additional reinforcement in the form of fibers may be included in the concrete mix to mitigate shrinkage cracking. Unlike the above methods of crack mitigation, which aim to address the root cause of shrinkage cracking directly (i.e., water loss through evaporation and through consumption by cement hydration reactions), fiber reinforcement helps to mitigate shrinkage cracking by increasing the tensile strength of the concrete element (Banthia and Gupta 2006, Bertelsen et al. 2019, Hemalatha and Ramesh 2019). In addition, the even distribution of fibers throughout the entire concrete element tends to improve crack distribution.

As such, the concrete surface may experience many microcracks that do not propagate to form larger, more severe cracks (Bertelsen et al. 2019). Finally, a matrix of fibers dispersed throughout the concrete is thought to help prevent aggregate from settling due to gravity, thereby reducing the amount of water lost in the bleeding process (Banthia and Gupta 2006, Bertelsen et al. 2019).

Types of Shrinkage in Concrete

In general, three categories of shrinkage in concrete have been identified. Plastic shrinkage refers to shrinkage that occurs before setting. Autogenous shrinkage also starts at an early age, but its effects last longer than those of plastic shrinkage as the concrete continues to hydrate. Finally, drying shrinkage may be thought of as long-term shrinkage starting after setting and taking place over the course of years as a concrete element dries. The following sections discuss the mechanisms behind plastic, autogenous, and drying shrinkage.

Plastic Shrinkage

Plastic shrinkage is shrinkage that takes place between the casting of concrete and the time of final set, or when the concrete changes from a plastic phase into a rigid phase. Several factors influence the plastic shrinkage of a concrete specimen, such as temperature, relative humidity, and wind speed near the concrete surface (Cohen et al. 1990, Battaglia 2012, Schmidt and Slowik 2009, Allahham et al. 2016, Sayahi 2019). When, as in most cases, a concrete element is restrained due to internal reinforcement, construction joints, formwork, etc., plastic shrinkage is not allowed to occur freely, which results in tensile forces in the concrete. This makes early-age concrete particularly vulnerable to cracking, as the tensile strength of the concrete is still in its developing stages (Shaeles and Hover 1988, Schmidt and Slowik 2009).

The mechanism of plastic shrinkage is “rapid and excessive moisture loss” (Sayahi 2019). As moisture leaves a concrete specimen through bleeding and evaporation, and when the evaporation rate exceeds the bleeding rate, negative pressure develops in the capillaries between aggregates (Shaeles and Hover 1988, Cohen 1990, Schmidt and Slowik 2009, Sayahi 2019). This negative pressure arises due to the surface tension of the capillary water between aggregates. As water escapes the concrete due to evaporation, the menisci of the water in the pores between particles become more pronounced, the surface tension of which causes negative pressure on the two adjacent particles (Shaeles and Hover 1988, Schmidt and Slowik 2009).

This capillary pressure increases as evaporation continues until, at a certain point, the surface tension of the capillary water breaks, allowing air to enter the pore system. This event in which air enters the system of pores, bringing the capillary pressure down to atmospheric pressure, is referred to as air-entry time (Scarpas et al. 2012, Sayahi 2019). An important consideration regarding capillary pressure within a concrete specimen is the fact that the breaking of the surface tension within a pore is a local event as opposed to a global one. That is, the maximum capillary pressure that causes air entry at one location may not be equal to the pressure that causes air entry at another location, and neither value represents the behavior of the concrete element as a whole (Shaeles and Hover 1988, Cohen 1990, Schmidt and Slowik 2009).

Autogenous Shrinkage

Autogenous shrinkage may occur simultaneously with plastic shrinkage, as well as for several hours after plastic shrinkage stops. While autogenous shrinkage can similarly be attributed to

moisture loss in a concrete specimen, the driving mechanism of moisture loss is not evaporation, as with plastic shrinkage. Rather, moisture is lost through consumption in the hydration reactions of the cement particles (Bentz and Jensen 2004, Sayahi 2019).

While the method of moisture loss differs between plastic and autogenous shrinkage, both result in the tendency for the concrete element to shrink as a result of the buildup of negative pressure in the concrete bulk. Instead of negative pressure arising from the surface tension in the pores between particles, as is the case with plastic shrinkage, for autogenous shrinkage the negative pressure stems from the hydration reaction products occupying less space than the water consumed during the reaction (Bentz and Jensen 2004, Schmidt and Slowik 2009). Certain products of the hydration reaction between water and the cementitious materials in concrete occupy less space than the water consumed to carry out the reaction, leading to empty space inside the concrete bulk. If air is not able to reach this portion of the concrete element, then the empty space resulting from the hydration reaction will apply a negative pressure to the restrained concrete. Similar to plastic shrinkage cracking, if the tensile stresses caused by the negative pressure due to autogenous shrinkage exceed the tensile strength of the concrete specimen, then autogenous shrinkage cracks form (Bentz and Jensen 2004, Schmidt and Slowik 2009, Sayahi 2019, Vosoughi 2019). While autogenous shrinkage cracking does not fall within the scope of research for this project, it may occur simultaneously with plastic shrinkage cracking, and therefore it is important to be aware of the mechanisms and factors leading to autogenous shrinkage cracking.

Drying Shrinkage

Long-term drying shrinkage occurs much more slowly and at a much later time than both plastic and autogenous shrinkage. The mechanism of long-term drying shrinkage is somewhat similar to that of plastic shrinkage, although on a much slower timeline. Over the course of months and years, water slowly evaporates from a fully hardened concrete element, resulting in negative pressure inside the concrete. While the tensile strength in a concrete element experiencing long-term drying shrinkage is surely fully developed, the tensile stresses induced by negative pressure may exceed the relatively low tensile strength of concrete, leading to cracking. Several factors may influence the formation of long-term drying shrinkage cracks, including aggregate size, water content, temperature, and relative humidity (Shaeles and Hover 1988, Cohen et al. 1990, Schmidt and Slowik 2009, Allahham et al. 2016, Sayahi 2019, Vosoughi 2019). Long-term drying shrinkage cracking is not within the scope of research for this project, and because it occurs so much later than plastic shrinkage cracking, there should not be any potential for confusion between the two types of cracking.

Factors Affecting Plastic Shrinkage

As discussed earlier, the rate and magnitude of plastic shrinkage in concrete is dependent on several factors. The following sections provide an overview of common factors that play key roles in the progression of plastic shrinkage as it occurs in concrete.

Evaporation

As previously mentioned, evaporation of water is a key factor in the formation of plastic shrinkage cracks. Evaporation provides an indication of the probability that plastic shrinkage cracking will occur in a recently cast concrete element (Sayahi 2019). The rate of evaporation is so critical to plastic shrinkage cracking that the American Concrete Institute (ACI) specifies that preventative measures must be taken if the evaporation rate exceeds a given limit (Cordon and Thorpe 1965). Primary factors that affect the rate of water evaporation from a concrete specimen are air temperature, concrete temperature, wind speed near the concrete surface, and relative humidity (Cohen et al. 1990, Schmidt and Slowik 2009, Leemann et al. 2014, Sayahi 2019). If conditions can be kept such that evaporation is limited, the likelihood of plastic shrinkage cracking decreases. However, these environmental factors are, at best, difficult to plan for and, at worst, impossible to avoid. Certain concrete elements are more vulnerable than others to severe evaporation. For example, a concrete footing placed below grade likely has very little exposed surface area subject to evaporation. As a result, minimal water is lost, and plastic shrinkage cracking is likely only a minor consideration. Compare this scenario to that of a concrete bridge deck, for example. Comparatively, the surface area-to-volume ratio of a concrete bridge deck is much higher than that of a concrete footing. The difference only increases when comparing the exposed surface area-to-volume ratio of the two elements. As a result, a bridge deck is far more susceptible to moisture loss through evaporation and the subsequent plastic shrinkage cracking that may result (Scarpas et al. 2012, Combrinck et al. 2018).

Bleeding

Bleeding is the process in which water present in freshly poured concrete rises to the top of the specimen, collecting in a thin layer on the concrete surface (Cohen et al. 1990, Henkensiefken et al. 2010, Schmidt and Slowik 2009, Allahham et al. 2016).

Bleed water is forced upward because gravity causes the solid aggregate in a concrete element to settle toward the bottom. The bleeding rate depends on several factors, including water-to-cementitious materials (w/c) ratio, particle gradation, concrete viscosity, and the rate at which water is consumed by the hydration of cement particles (Banthia and Gupta 2006, Cohen et al. 1990, Schmidt and Slowik 2009, Sayahi 2019). Concrete geometry also affects the bleeding rate. For example, a thin, flat element such as a bridge deck has less distance for bleed water to travel to the top surface of the concrete and will experience a greater rate of bleeding than, for example, a concrete footing. Due to an increasing desire to lower the w/c ratio in concrete mix designs, less mix water is typically available in a freshly poured specimen, leading to a lower bleeding rate in more recent concrete mix designs compared to older mixes (Slowik et al. 2008, Sayahi 2019).

While a thin layer of bleed water helps delay the evaporation of capillary water and subsequent plastic shrinkage cracking, excessive bleeding comes with its own disadvantages. For example, excessive bleeding may be the result of a large amount of particle settlement (e.g., through over-vibration), which in turn promotes plastic settlement cracking (Schmidt and Slowik 2009, Combrinck et al. 2018).

Capillary Pressure

As the evaporation rate exceeds the bleeding rate in a concrete element, capillary water begins to evaporate. As pore water evaporates from between solid particles, the menisci of the veins of capillary water move lower into the pores. The surface tension of the menisci creates attractive forces on the adjacent particles, which in turn creates an overall negative pressure inside the pore system of a concrete element. As evaporation continues and the menisci of the pore water between particles continue to move lower, the radii of the menisci decrease. Eventually, the radii become too small and the menisci of the pore water between the solid particles break, allowing air to enter the pores (Shaeles and Hover 1988, Slowik et al. 2008, Allahham et al. 2016, Sayahi 2019). These locations at which air enters the pore system create weak points in the concrete surface. Such weak points may serve as starting locations for cracking, particularly plastic shrinkage cracking (Slowik et al. 2008, Battaglia 2012, Schmidt and Slowik 2009, Sayahi 2019).

The time and capillary pressure magnitude at which air enters the concrete pore system are very localized occurrences (Shaeles and Hover 1988, Sayahi 2019, Vosoughi 2019). Particularly for a concrete element with a large surface area (e.g., a bridge deck), several interconnected factors may lead to different capillary pressure behaviors at many locations. As such, capillary pressure magnitude is not to be thought of as intrinsic to the concrete mix, or even representative of the mix as a whole.

Tensile Strain

The development of capillary pressure alone does not lead to plastic shrinkage cracking. If a concrete element is restrained in some way, as is often the case, then the negative pressure created within the concrete bulk as a result of plastic shrinkage will lead to the development of tensile strain as the concrete attempts to contract while restrained (Cohen et al. 1990, Battaglia 2012, Sayahi 2019). Experimental results regarding tensile strength development in concrete have shown that the strain capacity of concrete is lowest around the time of initial setting, or approximately around six hours after casting (Slowik et al. 2008, Scarpas et al. 2012). Plastic shrinkage cracks in concrete may be visible even earlier, after approximately one to two hours. As discussed previously, if the tensile stress or strain exceeds the tensile capacity of the concrete, plastic shrinkage cracks begin to develop.

Methods to Mitigate Plastic Shrinkage Cracking

Several methods exist to address the issue of plastic shrinkage cracking in concrete. An overview of some strategies to reduce plastic shrinkage cracking is presented below. Two methods, the use of supplementary cementitious materials (SCMs) and the use of fiber reinforcement, are the focus of this research and are discussed in further detail in Chapters 3 and 4, respectively.

Traditional Curing Methods

The issues related to excessive moisture loss through evaporation and subsequent plastic shrinkage cracking are well documented, and, as such, a number of traditional wet curing methods exist for mitigating plastic shrinkage cracking. The common mechanism of mitigating plastic shrinkage cracking through traditional curing methods is the regulation of evaporation. A relatively straightforward example of a traditional wet curing method is the use of a waterproof barrier (e.g., plastic film) to cover the concrete and prevent excess moisture loss through evaporation. Another method of keeping the concrete surface wet is fogging, or applying a mist of water near the concrete surface, increasing the relative humidity of the concrete's environment (Shaeles and Hover 1988, Sayahi 2019, Vosoughi 2019). Other more sophisticated methods of rewetting concrete have been researched, such as pressure-regulated automated concrete wetting (Schmidt and Slowik 2009). A primary disadvantage of many traditional wet curing methods is the labor required to set up and maintain the curing apparatus. For example, it is often impractical, if not impossible, to completely wrap a concrete beam in plastic. The large surface area of bride decks also presents difficulties for traditional wet curing methods.

Internal Curing

Another potential disadvantage of traditional curing methods is that while such methods all focus on limiting evaporation and providing extra water at the concrete surface, water is being consumed throughout the concrete bulk. As a result, to completely avoid cracking, extra curing water is often needed not only at the concrete surface but also evenly dispersed throughout the concrete itself (Vosoughi 2019). In order to distribute water evenly throughout a concrete mixture, a broad spectrum of materials, such as superabsorbent polymers (SAPs), porous lightweight aggregates (LWAs), and natural pozzolans, can be utilized. SAPs have been observed to act as internal water reservoirs in the concrete matrix (Kang et al. 2018, Tan et al. 2020). Additionally, a certain percentage of fine aggregates can be substituted with porous aggregates, which hold extra curing water in their pores (PCA 2002, Vosoughi 2019). Similarly, a portion of cement can be replaced with porous natural pozzolans such as rice husk ash (RHA) and natural zeolite, which are capable of water desorption in hardened concrete (Van Tuan et al. 2011, Pezeshkian et al. 2020).

As water evaporates from the capillaries, creating negative pressure, a concrete element is able to supplement the pore water lost to evaporation with extra internal curing water stored in the internal curing agents. Replenishing the evaporated water in such a way stops the process of excessive negative pressure buildup as well as the infiltration of air into the pore system, the combination of which contributes to plastic shrinkage cracking (Sayahi 2019, Vosoughi 2019). In addition, when the internal curing agent is LWA, while the internal curing water is being sucked out of the porous aggregate by negative capillary pressure, the fully rigid behavior of the aggregate allows for the displacement of water without deformation. In contrast, early-age concrete cracks from excessive moisture loss because the concrete is a weak solid initially after setting (Shaeles and Hover 1988, Sayahi 2019, Vosoughi 2019).

Supplementary Cementitious Materials

As opposed to traditional wet curing methods and internal curing, SCMs may be used as a chemical method to limit shrinkage and the associated cracking. While wet curing and internal curing utilize a more mechanical approach to provide extra water to the surface and bulk of a concrete element, respectively, the addition of SCMs affects the water consumption of a concrete mix at a chemical level. Adding SCMs into a concrete mix alters the hydration reaction between water and cementitious materials, which in turn changes the growth rate of the cement matrix (Leemann et al. 2014, Kwan and Chu 2018). In addition, SCMs alter the curing process of concrete in such a way as to reduce the overall rate of evaporation from the concrete element (Mora-Ruacho 2009, Leemann et al. 2014, Sayahi 2019).

Because they address concrete hydration at the chemical level, SCMs are often employed as a method to mitigate autogenous shrinkage cracking in concrete. However, while SCMs may be useful in inhibiting shrinkage crack development, it is important to consider their effects on the mechanical properties of concrete, particularly strength and modulus of elasticity. In particular, the rate of strength gain may be slowed, which would leave a concrete element more vulnerable to early-age cracking (Mora-Ruacho 2009, Leemann et al. 2014, Sayahi 2019).

Fiber Reinforcement

Plastic shrinkage cracks develop when the induced tensile stresses (as a result of moisture loss and negative internal pressure) exceed the relatively low tensile strength of early-age concrete (Cohen et al. 1990, Battaglia 2012, Allahham et al. 2016, Vosoughi 2019). The methods of plastic shrinkage cracking mitigation discussed above are all similar in the sense that they achieve crack control through some form, whether mechanical or chemical, of reducing excessive moisture loss in a concrete specimen. The addition of fiber reinforcement throughout a concrete mixture is a method of plastic shrinkage cracking mitigation that addresses cracks after they have formed. While fiber reinforcement does not prevent cracking from occurring, the fibers are able to bridge newly formed cracks and prevent them from propagating excessively.

Fibers offer their own tensile strength, much higher than that of early-age concrete, for immediate help in reducing plastic shrinkage cracking (Banthia and Gupta 2006, Bertelsen et al. 2019, Hemalatha and Ramesh 2019). While the tensile strength of typical fiber reinforcement is likely well above the tensile stresses induced by plastic shrinkage, the mechanical strength of the fiber reinforcement alone is not enough to eliminate plastic shrinkage cracking. Due to the semiplastic nature of concrete during the early stages of hydration, the concrete is not fully bonded to the fiber reinforcement during the time when plastic shrinkage cracking may occur (Hemalatha and Ramesh 2019, Sayahi 2019).

However, in addition to crack-bridging behavior, evenly distributed fiber reinforcement helps to achieve a more uniform cracking pattern. As a result, the addition of fiber reinforcement yields a concrete element with small, evenly distributed microcracks rather than a few large, concentrated cracks (see Figure 3). Smaller cracks bridged by fiber reinforcement are much less likely to

propagate and form relatively large cracks that allow for the ingress of water and harmful chemicals (Bertelsen et al. 2019).

Lastly, fiber reinforcement provides a matrix of fibers distributed throughout a concrete element that helps to prevent settling of aggregates. The even distribution of fibers throughout a concrete specimen helps to better distribute the weight of each aggregate within the surrounding cement matrix as it hydrates and develops strength. By limiting the settlement of aggregates, the amount of bleed water forced to the concrete surface is minimized (Banthia and Gupta 2006, Bertelsen et al. 2019). As a result, more of the mix water is held in the concrete bulk where it may be utilized, similarly to internal curing water, to replenish water that is lost to either evaporation or the hydration of cementitious materials.

CHAPTER 3. SUPPLEMENTARY AND ALTERNATIVE CEMENTITIOUS MATERIALS

In an effort to improve both the strength and durability of concrete mixtures, SCMs, as well as alternative cementitious materials to portland cement, are often employed for the range of benefits they offer. SCMs may be considered in terms of two general categories depending on the types of behavior the SCMs exhibit in concrete: pozzolanic and cementitious. Within the scope of this project, the only type of SCM investigated was pozzolanic. Alternative cementitious materials to portland cement are not considered SCMs, but rather materials that are independently cementitious.

Pozzolanic SCMs

Pozzolanic SCMs, or pozzolans, are defined as follows by the Portland Cement Association (PCA):

> A pozzolan is defined as a siliceous or siliceous and aluminous material that in itself possesses little or no cementitious value, but that will, in finely divided form and in the presence of moisture, chemically react with calcium hydroxide at ordinary temperatures to form compounds having cementitious properties. (Thomas 2007)

Calcium hydroxide ($Ca(OH)_2$), a product of the reaction that occurs during the hydration of portland cement, is utilized as a reactant in the pozzolanic reaction. The general portland cement reaction and general pozzolanic reaction are shown below.

Portland cement reaction:

PORTLAND CEMENT + WATER → C-S-H + CH + HEAT

Pozzolanic reaction:

POZZOLAN + CH + WATER → C-S-H + HEAT

where:

C-S-H = calcium silicate hydrate

CH = calcium hydroxide, $Ca(OH)_2$

Calcium silicate hydrate (C-S-H) is the primary product resulting from the hydration of portland cement. In addition, it is the compound that provides most of concrete's strength. It should be noted that the ratio of calcium to silicate present in the C-S-H product is not rigidly defined. The

lack of a well-defined ratio of calcium to silicate makes the notation C-S-H preferable when discussing the calcium silicate hydrate product of a portland cement hydration reaction.

Another product of the portland cement hydration reaction is calcium hydroxide (CH), commonly known as slacked lime. In contrast to C-S-H, CH does not contribute to the strength of the concrete and, in fact, acts as something of a weak point in the final hardened cement matrix (Thomas 2007, Leemann et al. 2014). As shown in the portland cement and pozzolanic reactions above, CH is a product of the portland cement reaction. This is to say that in a typical plain concrete, the hydration of portland cement produces a byproduct, CH, that is in fact detrimental to the overall strength of the hardened cement matrix. However, as seen from the pozzolanic reaction, CH is a reactant consumed by the added pozzolan. This indicates that the addition of a pozzolanic SCM reduces the quantity of CH in the final hardened cement matrix, which, as a result, improves the strength of the concrete compared to plain portland cement concrete (Takemoto and Uchikawa 1980). In addition, the product of the pozzolanic reaction is C-S-H, which increases the strength of the cement matrix. In essence, a pozzolanic SCM will consume CH and produce C-S-H, which serves to increase the ultimate strength of the final concrete element.

While a pozzolanic SCM may increase the ultimate strength of the cement matrix and the overall concrete element, its addition comes with other effects that must be considered and may even cause adverse consequences. For example, depending on the pozzolanic SCM used, the workability of the concrete may increase or decrease (Henkensiefken et al. 2010, Khan et al. 2020). Should workability decrease, the concrete mix may require the addition of high-range water-reducing admixtures (HRWRAs) in order to achieve workability without altering the water-to-binder (w/b) ratio. Additionally, while the ultimate strength of concrete may be increased through the use of a pozzolanic SCM, the rate of strength development may be reduced (Bentz and Jensen 2004, Ghourchian et al. 2018a). Depending on the application of the concrete element, a trade-off of delayed strength development for higher ultimate strength may not be desirable. Another consequence of pozzolanic SCMs is their effect on the bleeding rate of freshly poured concrete. The addition of fine particles, as well as the consumption of water in the pozzolanic reaction, may reduce the amount of bleed water for a freshly poured concrete element (Thomas 2007, Ghourchian et al. 2018b). The reduced bleeding rate of concrete mixes with pozzolanic SCMs can lead to accelerated development of negative capillary pressure and subsequent plastic shrinkage cracking (Ghourcian 2018c, Khan et al. 2020). Pozzolanic SCMs offer the significant advantage of increased ultimate strength, but care must be taken to achieve the proper mix with consideration of all other properties.

Fly Ash

Fly ash has been in use as a pozzolanic SCM since the mid-1900s (Sutter et al. 2013). It is a byproduct from the burning of coal for electricity generation. Pulverized coal is blown into the burning section of a boiler, where the coal is burned to produce heat. In this burning zone, the noncombustible inorganic materials (e.g., quartz, calcite, gypsum, pyrite, feldspar) melt and fuse together in liquid form. After the droplets are blown away from the combustion chamber by

exhaust gases, they cool and form glassy, spherical particles referred to as fly ash. The fly ash is collected by precipitators for use as an SCM (Thomas 2007, Sutter et al. 2013).

Because fly ash is a byproduct of the combustion of coal, the chemical composition and resulting performance of the fly ash is dependent on the composition of the coal used in the power plant. A wide range of both domestic and imported coals (e.g., anthracite, bituminous, lignite) are burned in the US, and therefore the properties of fly ash are dependent on the location, the source of the coal, and the burning method used for each power plant (Thomas 2007).

In general, fly ash is categorized into two classes. The criterion for determining the class of a fly ash is percentage by mass of calcium oxide (CaO), also known as quicklime or burnt lime and referred to in practice as calcium content. Calcium content in fly ash is an indicator of the behavior of the fly ash both individually and mixed with concrete as an SCM. Calcium content provides insight into the reactivity and potential pozzolanic behavior of a fly ash (Khan et al. 2020). In addition, calcium content is a helpful indicator of the ability of a fly ash to accomplish the following: reduce the heat of hydration in concrete, mitigate expansion resulting from the alkali-silica reaction, and defend against sulfate attack in concrete (Thomas 2007). The effects of fly ash on concrete are explored in more detail in the following sections.

The following two sections discuss the effect of calcium content on the behavior and classification of fly ash. Based on calcium content, fly ash is divided into the following two categories: Class F fly ash and Class C fly ash.

Class F Fly Ash

Class F fly ash refers to fly ash that meets the requirements of a Class F designation as outlined in ASTM C618, Standard Specification for Coal Fly Ash and Raw or Calcined Natural Pozzolan for Use in Concrete. Both chemical and physical requirements are in place for the designation of Class F fly ash. The chemical requirements for a fly ash to be considered Class F are as follows:

$SiO_2 + Al_2O_3 + Fe_2O_3 \geq 50\%$ and $CaO \leq 18\%$

with: $SO_3 \leq 5.0\%$

moisture content $\leq 3.0\%$

loss on ignition $\leq 6.0\%$

A Class F fly ash is sourced from the combustion of anthracite or bituminous coal that meets the chemical requirements specified for a Class F fly ash. The primary compounds from which fly ash is composed are silicon dioxide (SiO_2), aluminum oxide (Al_2O_3), iron (III) oxide (Fe_2O_3), and calcium oxide (CaO). Other compounds may be present in relatively small quantities, such as magnesium oxide (MgO) and sulfur trioxide (SO_3). The ASTM C618 specification for Class F

fly ash may, in essence, be thought of as saying that a fly ash with a calcium content of at most 18% is classified as a Class F fly ash. Because Class F fly ash, by definition, has an upper limit on calcium oxide that restrains the maximum calcium content percentage, a Class F fly ash may be referred to in practice as a low-calcium fly ash (Thomas 2007, Sutter 2016).

Predictably, because calcium content is the basis of classification for fly ash, calcium content is the primary indicator of the behavior of a fly ash in a concrete element. The predominant components of low-calcium (i.e., Class F) fly ash are alumino-silicate glasses composed of silicon dioxide and, in smaller quantities, crystalline quartz, mullite, hematite, and magnetite to varying degrees. The crystalline structure of the minerals composing Class F fly ash are essentially inert in the presence of water alone, requiring calcium hydroxide to react and form compounds with cementitious value (Nochaiya et al. 2010). This behavior, by definition, classifies Class F fly ash as a pozzolanic material.

Class C Fly Ash

Class C fly ash is, unsurprisingly, classified in a very similar manner to Class F fly ash. Class C fly ash refers to fly ash that meets the requirements of a Class C designation as outlined in ASTM C618. Both chemical and physical requirements are in place for the designation of Class C fly ash. The chemical requirements for a fly ash to be considered Class C are as follows:

$SiO_2 + Al_2O_3 + Fe_2O_3 \geq 50\%$ AND $CaO > 18\%$

with: $SO_3 \leq 5.0\%$

moisture content $\leq 3.0\%$

loss on ignition $\leq 6.0\%$

A Class C fly ash is produced from the combustion of lignite or sub-bituminous coal that meets the chemical requirements for a Class C fly ash. As noted above, the primary components of Class C fly ash are the same as those of Class F fly ash, only in different proportions. Namely, Class C fly ash is also composed primarily of silicon dioxide, aluminum oxide, iron (III) oxide, and calcium oxide, with essentially negligible amounts of magnesium oxide and sulfur trioxide. Considering fly ash once again in terms of calcium content, the ASTM C618 specification for Class C fly ash may be interpreted as saying that a fly ash with a calcium content greater than 18% is classified as a Class C fly ash. In contrast to Class F fly ash, Class C fly ash has, by definition, a lower bound on the allowable calcium content and may be referred to in practice as a high-calcium fly ash (Thomas 2007, Sutter 2016).

High-calcium (i.e., Class C) fly ash varies in both composition and behavior from its lower calcium Class F counterpart. Class C fly ash is primarily composed of calcium-alumino-silicate glasses, which include the same minerals as Class F fly ash (i.e., quartz, mullite, hematite, and magnetite), as well as other crystalline phases not present in Class F fly ash. Some of the

crystalline minerals found in Class C fly ash react with water alone, as opposed to those present in Class F fly ash. The fact that some minerals in Class C fly ash react with water, in addition to the presence of the generally more reactive calcium-alumino-silicate glass, cause high-calcium Class C fly ash to react more quickly and exhibit both pozzolanic and cementitious properties, in contrast to the slower reacting and strictly pozzolanic Class F fly ash (Ramachandran et al. 1964, Thomas 2007).

As outlined above, calcium content provides the primary indication of fly ash behavior in concrete, as well as the sole basis of classification of fly ash as Class C or Class F (provided that the source coal meets the prescribed chemical requirements of ASTM C618). With a calcium content of 18% or lower, fly ash is classified as Class F and exhibits strictly pozzolanic behavior in concrete. As calcium content increases above 18%, fly ash changes classification to Class C and begins to independently exhibit cementitious behavior as well as pozzolanic behavior. Note that, while uncommon, a fly ash containing a high enough calcium content will exhibit enough cementitious behavior that it may be used as the sole cementing agent to produce a concrete element of moderate strength (Nochaiya et al. 2010).

Effects of Fly Ash on Concrete Properties

The effects of fly ash on concrete are numerous. Both the fresh and hardened properties of concrete are affected by the addition of fly ash, as described in the following sections.

Workability

Adding fly ash with an appropriately high fineness and low carbon content reduces the water demand of concrete, improving workability and allowing for a reduction in water content for a concrete element. The potential decrease in w/c ratio resulting from the addition of fly ash provides an additional potential source of strength in hardened concrete. An approximate estimation for the degree of water reduction possible due to fly ash is roughly 3% water reduction for every 10% fly ash substitution for portland cement (Mora-Ruacho et al. 2009, Leemann et al. 2014).

The increase in workability, and the subsequent potential for water reduction, due to fly ash is in part a result of the spherical shape of fly ash particles. The spherical shape of the particles allows them to act as bearings, causing fresh concrete to flow and consolidate more easily than a plain portland cement concrete with the same slump (Thomas 2007).

In order to take advantage of the workability benefits of fly ash, a concrete mix should be well proportioned. A fly ash with lower fineness and a relatively high carbon content allows for lower amounts of water reduction. In fact, at a certain coarseness, substituting fly ash for portland cement actually increases water demand.

Bleeding

Considering a well-proportioned concrete and a fine, low-carbon fly ash, the addition of fly ash reduces bleeding due to the decrease in w/c ratio. Depending on the proportioning and water content, bleeding may be eliminated in a concrete element. The elimination of bleed water leaves a concrete element vulnerable to plastic shrinkage cracking, and appropriate drying conditions must be established to prevent such cracking (Ghourcian et al. 2018).

In the event that fly ash is used as an SCM but no reduction in water content is made, bleeding may increase relative to a typical portland cement concrete due to the decrease in water demand. While bleed water offers some protection against plastic shrinkage cracking, care must be taken to avoid the detrimental effects of excessive bleeding, such as significant aggregate segregation (Eisenbeisz 2001). Proper gradation of aggregates should be sufficient to control excess bleed water.

Air Entrainment

Fly ash contains unburned carbon from the coal firing process, which results in the need for a higher proportion of air-entraining agents to ensure adequate air voids in the concrete. In addition, because fly ash composition is dependent on the coal used at the power plant, as the carbon content of Class F fly ash increases, so too does the demand for air-entraining admixtures. Loss on ignition is an indirect method of measuring carbon content in fly ash. Typically, high-calcium Class C fly ash requires less air-entraining admixture compared to low-calcium Class F fly ash (Nochaiya et al. 2010).

Setting Time

In general, both Class F and Class C fly ash tend to extend concrete setting time. Class F fly ash in particular is fairly predictable in its tendency to delay both initial and final setting. The delay in setting caused by Class F fly ash is often a welcome benefit during hot weather casting. During cold weather, however, the setting time of concrete may be significantly delayed, causing issues with pouring and finishing concrete without freezing as the concrete sets. To counteract the issue of delayed cold weather setting, accelerating admixtures may be used in conjunction with Class F fly ash (Ghourchian et al. 2018a, Ghourchian et al. 2018b).

Heat of Hydration

The reduction in the heat of hydration is often an attractive benefit of fly ash substitutions for large concrete structures. For very large concrete structures where the heat of hydration can become very high, such as dams, high proportions of fly ash have been used successfully to reduce the rate at which heat develops and the maximum temperature reached within the concrete. Class F fly ash has historically been popular for mitigating issues related to heat of hydration in concrete. In fact, past research has indicated that the rate of heat development due to hydration increases with the calcium content of fly ash, discouraging the use of Class C fly ash

for heat reduction. However, such findings have been contradicted by more recent research and experimental results in which Class C fly ash has been used successfully to limit heat development (Sutter 2016).

Compressive Strength Development

Both Class F and Class C fly ash exhibit pozzolanic behavior and therefore tend to increase the ultimate strength of concrete. While the ultimate strength of concrete increases in the long term due to fly ash substitution, the rate of strength development tends to decrease with increasing proportions of fly ash. Depending on the application of the concrete element, the trade-off of reduced early-age strength in exchange for higher ultimate strength may not be desirable.

The rate of strength development, and consequently the early-age strength of the concrete, is dependent on temperature. The effect of temperature on strength development becomes more severe when fly ash is substituted for portland cement because the pozzolanic reaction is more heavily influenced by temperature than the cementitious reaction. At higher temperatures, concrete containing fly ash tends to develop strength very quickly from approximately zero to three days, and afterwards strength increases relatively slowly until the ultimate strength is reached. Under more typical ambient conditions, fly ash concrete develops early-age strength relatively slowly, but the ultimate strength increases beyond that of portland cement concrete as well as hot-cured fly ash concrete (Thomas 2007).

Silica Fume

Similar to fly ash, silica fume first saw use in the US in the mid-1900s. Silica fume is produced as a byproduct of manufacturing silicon or ferro-silicon alloys. Electric arc furnaces emit flue gasses that contain an extremely fine powder primarily composed of silicon and oxygen, which is percolated and collected in a baghouse filtration system (King 2012).

The combustion of quartzite, coal, and woodchips produces gasses containing silica fume powder. The primary compound making up silica fume is noncrystalline silicon dioxide (SiO_2). The chemical behavior of silicon dioxide paired with the high surface area-to-volume ratio of the extremely fine particles makes silica fume very reactive. Particles of silica fume are on the order of 100 times smaller than a typical particle of portland cement. Because silica fume particles are so fine, special safety measures must be taken when handling unprocessed silica fume. As such, silica fume for commercial use comes in the form of a densified powder or a slurry (Eisenbeisz 2001, King 2012).

As mentioned, silica fume is very reactive. Specifically, silica fume behaves as a pozzolan, readily reacting with water and CH produced by the hydration of portland cement to produce C-S-H. While silica fume is pozzolanic and does not exhibit independent cementitious behavior, the high degree of pozzolanic reactivity makes silica fume useful as an SCM (Takemoto and Uchikawa 1980, Toutanji et al. 1998, Khan 2020).

Silica fume for use as a cementitious material in concrete should meet the requirements outlined in ASTM C1240, Standard Specification for Silica Fume Used in Cementitious Mixtures. Both chemical and physical requirements are in place for the designation of cementitious silica fume. The chemical requirements for silica fume used as a cementitious material are as follows:

$SiO_2 \geq 85\%$

with: moisture content $\leq 3.0\%$

loss on ignition $\leq 5.0\%$

Silica fume, in contrast to fly ash, is sourced from materials with less uncertainty regarding their composition. The production of silicon requires the smelting of very pure (i.e., >99%) quartzite, also referred to as orthoquartzite at such a purity. Because orthoquartzite contains more than 99% silicon dioxide, there is added certainty as to the chemical composition of a given silica fume, which by ASTM standards must be at least 85% silicon dioxide. However, because other, less pure combustibles are used in the production of silicon (e.g., coal), the chemical composition of a given silica fume is not guaranteed and must be checked against the ASTM standard to ensure quality before use as a cementitious material. The need for quality control of silica fume is amplified when considering the common application of silica fume as an SCM in high-strength concrete. Due to the highly pozzolanic nature of silica fume, concrete containing silica fume benefits greatly from the added strength due to the rapid pozzolanic reaction consuming CH and producing C-S-H. As such, silica fume finds common use in high-strength concrete (Cohen et al. 1990, King 2012, Nochaiya et al. 2010).

Effects of Silica Fume on Concrete Properties

Similar to fly ash, the use of silica fume has a number of effects on both the fresh and hardened properties of concrete. The effects of silica fume on concrete are outlined in the following sections.

Workability

Due to the extreme fineness of silica fume particles, the water demand of silica fume concrete is higher than that of concrete with only portland cement. Very fine silica fume particles increase the overall surface area of the cementitious materials significantly, which requires increased water content to achieve adequate workability. In order to design an appropriately workable concrete mix containing silica fume, superplasticizers (also called HRWRAs), are incorporated into the mix. Such admixtures allow for the desired slump to be achieved without increasing the w/b ratio and subsequently reducing the ultimate strength of the concrete (Combrinck et al. 2018).

Bleeding

In conjunction with workability, silica fume has a marked effect on the bleeding rate of freshly poured concrete. Again, the very fine particle size of silica fume greatly increases the surface area of the cementitious materials, increasing water demand and the amount of water required to achieve wetting. As such, less water is available as bleed water in silica fume concrete compared to typical portland cement concrete. A significant reduction in bleed water makes a concrete element more vulnerable to plastic shrinkage cracking, as evaporation is not sufficiently counteracted by the presence of bleed water (Jaber 2007, King 2012).

Heat of Hydration

As a highly reactive pozzolanic material, silica fume serves to increase the rate of hydration of portland cement. Silica fume particles provide nucleation sites at which hydration products, namely C-S-H and CH, may be formed. The nucleation sites provided by silica fume accelerate hydration of the cementitious materials. As a result, silica fume tends to increase the heat of hydration in concrete. The increase in heat development is particularly notable while the concrete is at an early age. The increased heat of hydration resulting from silica fume requires careful consideration, particularly in large concrete structures. If the proportion of silica fume is high and a concrete element is sufficiently large, heat development may occur much faster than heat dissipation. In such cases, the excess heat retained in the concrete element can cause added stresses that may adversely affect the structure. In colder climates, an increase in the heat of hydration may be a welcome benefit during winter, as added heat can help promote a more moderate drying environment (Jaber 2007, King 2012).

Compressive Strength Development

Because silica fume is a highly reactive pozzolanic material, it readily consumes CH from cement hydration and produces C-S-H. As such, the addition of silica fume as an SCM tends to significantly increase the ultimate strength of concrete. In addition, unlike in fly ash concrete, the strength development in concrete containing silica fume occurs at a greater rate than that of plain portland cement concrete. The similarity in strength development for concrete containing only portland cement and concrete with silica fume eliminates the trade-off observed with fly ash between low early-age strength and increased ultimate strength. In contrast, silica fume concrete develops significantly increased ultimate strength at a similar rate to typical concrete with only portland cement. In fact, for the same w/b ratio, concrete containing silica fume exhibits increased compressive strength at any given time over portland cement concrete. This significant increase in the ultimate strength of concrete provided by silica fume is the cause for silica fume's popularity as an SCM in high-strength concrete.

While silica fume is able to provide a higher concrete compressive strength compared to fly ash, it is important to note that, in contrast to fly ash, silica fume is more expensive by mass than portland cement. Although silica fume is attractive for its ability to increase the ultimate strength of concrete, if such a strength increase is not explicitly necessary, the economic impacts of silica

fume substitution can make its use as an SCM undesirable or impractical (Eisenbeisz 2001, King 2012).

Note that with an increasing level of substitution of silica fume for portland cement above the typical range of 5% to 10%, the trend of increased compressive strength does not continue. Substitutions of silica fume above the range of 5% to 10% begin to show decreased compressive strength compared to concrete with only portland cement (Silica Fume Association 2014).

Alternative Cementitious Materials

Alternative cementitious materials refer to those materials other than conventional portland cement that possess independent cementitious behavior. Alternative cementitious materials are similar in several ways to pozzolanic SCMs, and the two share a number of the characteristics discussed in the previous section. However, while a pozzolanic SCM does not, by definition, possess cementitious value—i.e., it does not undergo a cementitious hydration reaction with the addition of water alone—and only forms products with cementitious properties in the presence of CH, an alternative cementitious material is capable of independently undergoing a hydration reaction that results in products containing cementitious properties. As a result, the hydration reaction for an alternative cementitious material is very similar to the hydration reaction for portland cement (Mora-Ruacho et al. 2009). Specifically, the primary product resulting from the hydration reaction of alternative cementitious materials is C-S-H, which provides most of the strength to a concrete element. In general, the reaction occurs as follows:

Alternative cementitious material reaction:

ALTERNATIVE CEMENTITIOUS MATERIAL + WATER → C-S-H + CH + HEAT

It is important to note that, unlike pozzolanic SCMs, alternative cementitious materials do not consume CH as a part of their hydration reaction. Because alternative cementitious materials are capable of producing compounds with cementitious properties in the absence of CH as a reactant, alternative cementitious materials do not consume CH, which could potentially result in less compressive strength gain compared to pozzolanic SCMs (Leemann et al. 2014).

Type K Shrinkage-Compensating Cement

Along with fly ash and silica fume, Type K shrinkage-compensating cement (SCC) first saw use in the US in the mid-1900s, although its use remained relatively sparse until the later part of the century. Type K SCC is named for the innovative use of a chemical compound commonly referred to as Klein's Compound after Alexander Klein of the University of California–Berkeley. The compound is a naturally occurring form of calcium sulfoaluminate named Ye'elimite after Har Ye'elim, a hill near the Dead Sea in the southern district of Israel where the compound was first discovered in nature (Hargis et al. 2014).

In the 1960s, Alexander Klein utilized calcium sulfoaluminate in cement, giving rise to the name Klein's Compound and eventually to the designation Type K SCC. Type K cement combines calcium sulfaluminate with anhydrite and lime. The hydration of the anhydrite and lime forms gypsum and calcium hydroxide. Calcium sulfoaluminate, or Ye'elimite, forms monosulfoaluminate and aluminum hydroxide upon hydration. With the addition of gypsum, the Ye'elimite reacts with water to form ettringite and aluminum hydroxide (Cordon and Thorpe 1965, Hargis et al. 2014). The formation of ettringite upon hydration of Type K SCC is the key component to the expansive nature, and resulting shrinkage-compensating characteristics, of Type K cement (Rice 2012).

Ettringite formation results in expansion of the cement paste, which serves to counteract shrinkage in restrained concrete and subsequent plastic shrinkage cracking. Two primary theories attempt to explain the mechanism of expansion due to ettringite formation in a cement paste (Ramsayer 2017, Rice 2012). These theories, the crystal growth theory and the swelling theory, and their effects on cement paste expansion due to ettringite formation are discussed in greater detail in the following sections.

Three classifications of SCC are covered by ASTM specifications: Types K, M, and S. For an SCC to be classified as Type K, it must meet the requirements outlined in ASTM C845, Standard Specification for Expansive Hydraulic Cement. Both chemical and physical requirements are in place for the classification of expansive hydraulic cement. The chemical requirements for Type K expansive cement are that the cement contains the following:

anhydrous calcium aluminosulfate: $(CaO)_4Al_2O_3 3SO_3$

calcium sulfate: $CaSO_4$

uncombined calcium oxide: CaO

with: $MgO \leq 6.0\%$

insoluble residue $\leq 1.0\%$

loss on ignition $\leq 4.0\%$

Note that the chemical requirements regarding the presence of calcium sulfate and the maximum proportions of magnesium oxide, insoluble residue, and carbon content (measured indirectly through loss on ignition) apply to Types K, M, and S expansive cement. Only the inclusion of anhydrous calcium aluminosulfate and uncombined calcium oxide are unique to an expansive cement of Type K (Battaglia 2012).

Expansion Mechanism in Type K SCC

Two theories have attempted to explain the mechanism driving the expansion of cement paste in Type K SCC due to ettringite formation. Both theories are discussed in the following sections. Currently, it is generally accepted that neither theory fully encompasses the mechanism of expansion. However, it is thought that each theory can explain the expansion due to ettringite formation during different stages of cement hydration.

Crystal Growth Theory

The crystal growth theory states that the mechanism of expansion in a Type K expansive cement is the formation and growth of ettringite crystals. The crystals are thought to form on the surfaces of the anhydrous calcium aluminosulfate, or Ye'elimite, particles, which are the particles responsible for the expansive nature of Type K SCC. Subsequent growth of the ettringite crystals causes outward crystallization pressure, which results in expansive force within the cement paste (Cohen 1983).

The crystal growth theory applied to Type K expansive cement makes a series of assumptions regarding ettringite crystal formation. First, it is assumed that the Ye'elimite particles are spherical and uniformly distributed in a solution of water, calcium hydroxide, and dissolved sulfates. Immediately upon hydration of the Type K SCC, the surfaces of the Ye'elimite are assumed to be coated in a dense layer of ettringite. Topochemical hydration then occurs, which causes an increase in the thickness of the ettringite layer surrounding the Ye'elimite particles. As this process continues, the layer of ettringite crystals continues to grow outward, eventually exceeding the thickness of the surrounding solution. At this point, the growing ettringite layers coating adjacent Ye'elimite particles meet, pushing the adjacent particles apart and causing expansion of the Type K cement paste. The theory of ettringite crystal growth pushing adjacent Ye'elimite particles apart and resulting in cement expansion is the crystal growth theory (Battaglia 2012, Han et al. 2016).

Swelling Theory

The swelling theory of expansion due to ettringite formation hypothesizes that expansion results from the adsorption of water molecules to the surface of ettringite crystals rather than from the formation of the crystals themselves. In the swelling theory, it is believed that the pressure created by water adsorption to the surface of ettringite crystals is responsible for the expansive behavior of Type K SCC (Cohen 1983).

The explanation of the swelling theory for the expansive behavior in Type K SCC is built upon two primary assumptions regarding the hydration of the cement and the behavior of ettringite crystals. The first assumption is that ettringite is formed following a through-solution mechanism as opposed to a topochemical mechanism. Through-solution formation of ettringite refers, in general, to the formation of ettringite crystals by precipitation in a supersaturated solution. Specifically, a supersaturated solution of calcium oxide, aluminum oxide, and sulfur oxide

allows for the crystallization of ettringite as a precipitate throughout the solution. This formation mechanism differs from topochemical formation, where ettringite crystals are formed on the surface of existing solid calcium aluminate in the presence of dissolved sulfate ions (Battaglia 2012, Han et al. 2016).

The second assumption of swelling theory is that the hydration rate of Ye'elimite decreases significantly in the presence of saturated calcium hydroxide, which results in gel-like, colloid-sized ettringite crystals. The relatively high surface area-to-volume ratio of the colloidal particles provides many potential points for water to adsorb to the ettringite. A large number of colloidal ettringite particles with water molecules adsorbed to their surface results in swelling pressure as adsorptive forces cause adjacent particles to push against each other. The swelling pressure generated due to water adsorption by ettringite results in the expansive behavior of Type K SCC (Rouquerol et al. 1994, Han et al. 2016).

Effects of Type K SCC on Concrete Properties

In addition to promoting expansive behavior, the substitution of expansive Type K SCC influences several properties of both fresh and hardened concrete (Shi et al. 2019, 2020a, 202b, 202c). The effects of Type K SCC are outlined in the following sections.

Workability

In general, the addition of Type K SCC tends to reduce the workability of fresh concrete compared to typical portland cement concrete. The reduction in workability resulting from substitution of Type K SCC is caused by the increased fineness of the expansive cement versus portland cement, as well as the consumption of water in the formation of ettringite. Increasing the overall fineness of the cementitious materials increases the cement surface area, resulting in the need for increased water consumption to fully hydrate the cement. In addition, water is consumed in the formation of the ettringite crystals that give Type K SCC its expansive properties. In order to achieve the desired workability in concrete containing expansive cement, HRWRAs may be added to increase slump without altering the w/c ratio (Hoff and Mather 1978, Bentz and Jensen 2004, Ghourchian et al. 2018a).

Bleeding

Similar to the effect of Type K SCC on workability, the addition of expansive cement tends to reduce the rate and magnitude of bleeding in fresh concrete. The reduction in bleeding, much like the reduction in workability, results from the increased water demand exhibited by Type K SCC. As additional water is required to fully hydrate the expansive cement, less free water is available for bleeding. In addition, the consumption of water in the formation of ettringite causes a reduction in the bleed water available in fresh concrete. As an acceptable level of workability is achieved through the use of HRWRAs to avoid increasing the w/c ratio, concrete with Type K SCC will also see a reduction in bleed water. While a reduced amount of bleed water, in general, makes concrete more vulnerable to plastic shrinkage cracking, the expansive nature of Type K

SCC serves to counteract plastic shrinkage cracking, mitigating the risk of plastic shrinkage cracking even in the presence of reduced bleed water (Shizong et al. 1995, Ghourchian et al. 2018b).

Heat of Hydration

In general, the heat of hydration in concrete containing Type K SCC is similar to that exhibited by typical portland cement concrete. Therefore, in regard to heat of hydration, Type K SCC may be used in relatively large proportions for large-scale concrete structures without risking increased thermal stresses compared to portland cement. However, when substituting Type K SCC in a large concrete structure, care must be taken regarding the expansive nature of the cement because a proportionate level of expansion will yield a relatively large magnitude of overall volume change (Nagataki and Gomi 1998).

Compressive Strength Development

The addition of Type K SCC tends to result in increased compressive strength compared to concrete containing only portland cement. The increase in strength is attributed to several effects of substituting Type K SCC. The increased fineness of Type K SCC provides an increased cement surface area for hydration to occur, promoting an increase in the cement hydration products. In addition, the increased water demand resulting from the use of expansive cement reduces the free water present in the concrete. The increase in ettringite formation from Type K SCC also causes the density of the cement paste to increase, which in turn results in higher compressive strength (Nagataki and Gomi 1998).

Effects of Type K SCC on Other Concrete Properties

The expansive nature of Type K SCC has important effects on the permeability, and consequently the durability, of a concrete element. In practice, a concrete element is restrained by the presence of reinforcement and formwork. As such, concrete containing expansive cement is not allowed to expand freely. Instead, the concrete element attempts to expand within its restraints, which generates a net compressive stress within the concrete and, in turn, reduces the permeability. A reduction in permeability mitigates the risk of water and corrosive agents penetrating the concrete and causing corrosion of the steel reinforcement. As a result, the expansive nature of Type K SCC may positively impact the durability of a given concrete element (Hargis et al. 2014, Leemann et al. 2014, Ghourchian et al. 2018c).

CHAPTER 4. FIBER REINFORCEMENT IN CONCRETE

Conventional concrete is a brittle material by nature with relatively weak performance in tension. To compensate for this characteristic and avoid the sudden brittle failure of concrete structures, reinforcement materials are embedded into the concrete.

Since ancient times, people have been putting fibers, such as straw and hair, into mortars and bricks to improve their tensile properties. These ancient and simple methods of concrete reinforcement have now been transformed into advanced methods that involve using discontinuous fibers distributed randomly throughout the concrete matrix. The resulting composite material is called fiber-reinforced cementitious composite, even though there are other names for concretes, mortars, or pastes that include fibers within their matrices. The performance of any FRC, and similar cementitious composites, is known to be greatly influenced by the physical, chemical, and mechanical properties of the fibers used in the cementitious matrix.

The specifications that fibers within FRC should be randomly distributed and discontinuous are important for differentiating the mechanism of tensile reinforcement in FRC from that in conventional concrete containing steel or fiber reinforcing bars. In conventionally reinforced concrete, the rebar is designed and placed to maximize the efficiency of the bars, while FRC relies on a randomly distributed matrix of fibers so that the entire concrete element contains fibers that provide tensile reinforcement evenly throughout the concrete. Additionally, the fibers in FRC are discontinuous or discrete, while in conventionally reinforced concrete the rebar (flexural rebar, in particular) is effectively continuous along the entire length of the concrete element. While longitudinal rebar, for example, does not literally extend to the face of a concrete beam, the bars are continuous throughout regions in which flexural stresses are significant and require the tensile strength of rebar. This condition differs from that of FRC, in which the fibers are relatively short and, as a result, discontinuous. Discontinuity allows for a network of fibers to achieve random distribution throughout a concrete element, eliminating the need to carefully design the placement of reinforcement.

As a case in point, consider a continuous concrete slab reinforced with conventional rebar. At inflection points in the deflected shape, where the moment in the slab changes sign, the location of the rebar must change in order to ensure that the reinforcement lies along the tension face of the slab to avoid excessive cracking or failure. If the same slab were reinforced with a network of discrete fibers randomly distributed throughout the concrete, the fibers near the tension face of the slab are simply able to engage and provide tensile reinforcement regardless of which face is experiencing tension.

The main fiber properties that govern their performance in both fresh and hardened concrete include the dimensions of the fibers, elastic modulus, tensile strength, ultimate strain, and bonding and chemical compatibility with the cement matrix. The different fiber materials used in current practice can be grouped into four main categories: metallic, glass, synthetic, and natural. Metallic fibers, as the name suggests, refer to fibers that are made from metals. The most common type of metallic fiber used is steel fibers, but stainless steel fibers have recently gained attention because of their high corrosion resistance. Glass fibers are broadly defined as fibers that

are derived from naturally occurring minerals or rocks. The two general types of glass materials used as fiber reinforcement in cementitious matrices are silica and basalt glass. Synthetic fibers are considered manmade fibers that are neither metallic nor glass fibers. A wide variety of synthetic fibers are deemed suitable for application in FRC, including but not limited to PP, nylon, polyvinyl alcohol (PVA), polyolefin (PO), carbon, polyethylene (PE), polyester, acrylic, and aramid. Natural fibers are fibers that occur in nature within the organic tissue of plants.

Mechanism of Crack Mitigation

As mentioned above, the typical motivation for adding fibers to concrete is the crack-bridging behavior exhibited by the fibers and, consequently, the reduction in crack width and propagation. The crack reduction benefit of fiber reinforcement extends beyond the mitigation of tensile cracking in a concrete element under tensile stress. The tensile strength and crack-bridging ability of fiber reinforcement helps to prevent or practically eliminate plastic shrinkage cracking in an FRC element. The degree of crack mitigation provided by fiber reinforcement depends on the type of fiber, the proportion of the fiber in concrete, and the shape of the fibers themselves.

To understand the mechanism of crack mitigation for fiber reinforcement, it is necessary to discuss the propagation of a crack in concrete from the micro to the macro level. A crack in concrete originates at the interfacial transition zone (ITZ), or the interface between aggregates and hydrated cement. Tensile stresses applied within the ITZ result in the formation of microcracks, invisible to the naked eye. Multiple ITZ locations experience microcracking under tensile stresses. As these microcracks propagate throughout the cement paste, they eventually meet other microcracks and combine to eventually form a larger macrocrack. At this stage, although a macrocrack has developed, the concrete has not necessarily lost all tensile capacity. Aggregate interlock may still be sufficient to bridge the macrocracks at this point, allowing the concrete to retain a small amount of tensile strength. However, once the macrocracking progresses and exceeds the aggregate interlock, the concrete has lost all tensile capacity at the crack location and, if unreinforced, the concrete would fail in tension at this point (Dopko 2018, Hemalatha and Ramesh 2019).

Considering the different scales and stages of cracking in concrete, fibers of various sizes are beneficial in addressing all stages of crack development. To this end, both microfibers and macrofibers are used in FRC for their unique benefits.

In general, fiber reinforcement mitigates cracking most effectively if the stiffness, or elastic modulus, of the fibers is similar to or higher than that of the concrete. Fibers with higher stiffness than the surrounding concrete are able to successfully bridge and prevent cracking without simply deforming along with the crack, as would be the case for fibers of low stiffness. Depending on the application, different fiber materials may be used to achieve the desired concrete strength improvement behavior. At early ages, for example, when concrete strength is relatively low, microfiber materials with lower elastic moduli may successfully bridge microcracks, improve early-age strength, and reduce plastic shrinkage cracking. For a significant increase in ultimate strength, fiber materials with a higher elastic modulus are better suited as reinforcement (Dopko 2018, Niu et al. 2019, Diab et al. 2020).

Microfibers refer to fibers of relatively small diameter and high length-to-dimeter ratio, or aspect ratio, with lengths typically less than 18 mm. Microfibers are primarily used to mitigate the propagation of microcracks throughout the ITZ and cement matrix. These fibers bridge the microcracks by remaining anchored in the cement paste on either side and provide tensile strength across the cracks. The microcrack controlling behavior of microfibers makes them most effective at increasing early-age strength in FRC at stages prior to the formation of large macrocracks.

Macrofibers are characterized by their increased lengths (and reduced aspect ratios) compared to microfibers. There is no set standard that defines the size boundaries between microfibers and macrofibers, which creates some overlap in the definitions. However, macrofibers are rarely shorter than 18 mm and generally have diameters that are larger than 0.1 mm.

Macrofibers are effective at bridging the cracks in concrete that have grown past the micro stage. This is because macrofibers are large enough to provide stress transfer across crack openings when a single crack has formed from the growth of multiple microcracks. If the fiber-matrix bond condition is held constant, the higher the elastic modulus of the macrofiber, the smaller the crack width under the same applied load. This feature relies on the existence of a sufficient bond between the fibers and the matrix to develop the strength of the individual fibers and utilize their high tensile stiffness. Besides reported exceptions for fibers with a high modulus of elasticity (Huang and Zhao 1995, Yao et al. 2003, Sorelli et al. 2005, Dopko et al. 2018), macrofibers do not significantly influence the strength parameters of concrete prior to crack formation. The effectiveness of macrofibers at bridging cracks depends on the maximum aggregate size as well. In general, for larger maximum size aggregates, longer fibers are more effective at improving post-crack performance, while for smaller maximum size aggregates, shorter fibers can be equally (if not more) effective (Huang and Zhao 1995).

Because microfibers are most effective at improving performance parameters at an early age (by reducing plastic shrinkage cracks) and macrofibers are most effective for post-crack ductility and macrocrack control in FRC, the proper choice of fiber geometry is of utmost importance for achieving the expected performance for the target application.

It is worthwhile to note that microfibers and macrofibers affect concrete differently outside of their crack mitigation and strength increasing behaviors. In particular, microfibers more severely impact the workability of fresh concrete than macrofibers. Because microfibers exhibit a relatively high surface area-to-volume ratio compared to macrofibers, microfibers tend to decrease the workability of concrete because the cement paste must coat the large surface area of the fiber network. In order to combat the reduced workability of concrete with microfiber reinforcement, HRWRAs are often used as a supplement. Macrofibers similarly decrease the workability of fresh concrete, but to a lesser extent than microfibers (Yin et al. 2015).

Fiber Types

As touched on in the previous section, the behavior desired from fiber reinforcement depends on the specific needs of the designer. A method of drastically altering the behavior of fiber

reinforcement is to change the material type of the fiber. Four of the five properties that govern the performance of fiber reinforcement—tensile strength, elastic modulus, ultimate strain, and bonding and chemical compatibility with the cement matrix—are material properties and vary with the material chosen for fiber reinforcement. Only fiber shape is not affected by material choice, although one could argue that the ability to alter the shape of a single fiber beyond the typical cylindrical shape is dependent on the malleability of the fiber material.

Steel Fibers

As proven by conventional steel reinforcement, steel exhibits a sufficiently high tensile strength, stiffness, and ultimate strain for use as reinforcement in concrete. As such, the dimensions of steel fiber reinforcement heavily impact the successful use of steel fibers in FRC. Because it is known that steel shows favorable chemical behavior as reinforcement in concrete (assuming no infiltration of water) and is capable of adequate bond strength with concrete, the fiber dimensions are the primary consideration for successful steel fiber reinforcement. Bond strength may be thought of as a result of fiber dimensions; adequate development length paired with deformations in reinforcement are well known to provide adequate steel-to-concrete bond strength (Eren and Marar 2010).

Steel possesses a fairly unique level of malleability, which allows fibers made of steel be bent into various shapes that the fibers will maintain upon addition into a concrete mix. Typically, the failure mechanism of steel reinforcing fibers varies with time as concrete strength develops. At early ages, when the cement matrix in which the fibers are embedded has relatively low strength, steel fibers generally fail by pull-out because the cement paste does not have adequate strength to anchor the steel fiber and develop its full tensile strength. At later ages, as concrete strength reaches its ultimate value, steel fibers tend to fail by fracture. As a result, the bond strength of steel fibers is often increased by deforming or shaping the fibers to increase the performance of steel fibers in early-age, low strength concrete (Eren and Marar 2010, Kwan and Chu 2018).

Several types of deformations exist for steel fiber reinforcement. The goal of deforming steel fiber reinforcement is to increase the bond strength between the steel and cement matrix either through increased fiber surface area or added anchorage at the fiber ends. Such mechanisms of increasing bond strength are also found in full-sized steel reinforcement. In particular, the development length of typical steel rebar may be reduced by the use of deformed (i.e., nonsmooth) rebar or the addition of hooked or L-shaped bars. Similarly, the development length of steel fiber reinforcement is reduced through deforming the surface or anchoring the fiber ends.

A specific deformation type may be desirable based on the specific application of the fiber reinforcement. For example, for a given aspect ratio, fibers with hooked-end anchorage tend to be more effective than crimped fibers at increasing the flexural strength of concrete. However, for higher strength concrete mixes, fibers twisted about their longitudinal axis tend to show improved composite behavior compared to hooked-end fibers. For a given concrete mix and application, care must be taken to select the most effective type of steel fiber deformation (Dopko 2018, Kwan and Chu 2018).

In addition to bridging cracks and improving the strength of concrete, steel fiber reinforcement may significantly affect the slump of fresh concrete. The stiffness of steel fibers may tend to impede flow and reduce the workability of concrete. In order to maximize the workability of steel FRC, fiber volume should be kept to a manageable level, fibers should be added slowly, and the concrete should not be over-mixed. Over-mixing of steel FRC may reduce workability because slump tends to decrease more severely as the magnitude of fiber deformation increases. Over-mixing of steel FRC allows for the potential for increased fiber deformation and a subsequent unintended reduction in workability (Qi 2003).

Glass Fibers

In regard to fiber reinforcement, glass fibers refer to those derived from melted constituent material that is then extruded into very thin strips, which upon cooling form long, thin, filament-sized strands. As the melted constituent material is extruded into filament form, the strands are coated with a material called sizing. Glass fiber sizing, in its most general form, consists of a film former and a coupling agent. The film former is a chemical compound that forms a film around glass strands, which serves several purposes. The film formed on glass strands protects, lubricates, and consolidates the fibers. Once resin is introduced to the glass strands, the film former encourages the separation of the strands to promote even resin distribution. The coupling agent in glass fiber sizing acts as a bonding agent between the individual glass strands and the applied resin coating, allowing for hydrophilic glass to bond with hydrophobic resin. A typical glass fiber used as concrete reinforcement is composed of roughly 200 individual strands, with each strand coated in sizing and cut to the desired length.

Note that, if desired, the conglomeration of individual strands into a single fiber may be undone upon wetting. Dispersion of individual strands in such a way provides concrete with microfiber reinforcement for the mitigation of microcracks. In contrast, fibers may be designed to remain intact upon hydration. Allowing fibers to remain in their consolidated form greatly decreases their overall aspect ratio, causing the fibers to behave as macrofibers. Such behavior is useful for the mitigation of macrocracks (Dopko 2018).

Two primary types of glass fibers are typically used as concrete reinforcement: silica glass and basalt glass. Silica, also known as silicon dioxide (SiO_2) or quartz, occurs naturally in quartzite at concentrations typically around 90% to 95%. Basalt, a naturally occurring extrusive igneous rock, typically contains silica contents of around 40% to 50%. Due to the relatively large percentages of silicon dioxide present in both quartzite and basalt, the resulting silica and basalt glass fibers exhibit many chemical similarities. The chemical difference between silica and basalt glass fibers lies in the proportions of other chemicals besides silicon dioxide. In particular, silica glass fibers contain a relatively high proportion of boron oxides, while basalt glass fibers contain relatively high levels of sodium oxides, iron, potassium, and magnesium (Hemalatha and Ramesh 2019).

While glass fibers tend to show desirable mechanical performance when used as reinforcement in cement matrices, chemical incompatibility may hinder their behavior. Specifically, the alkaline environment created by cement shows a tendency to degrade glass fibers not resistant to

alkalinity. Both basalt and silica glass fibers exhibit complete deterioration and strength loss after being subjected to alkaline or acidic environments. After exposure to an alkaline environment, both basalt and silica glass fibers show pitting corrosion on their surfaces. As a result of pitting, the fibers are left with a reduced cross-sectional area and consequently a lower tensile strength. It should be noted that the similarity in chemical deterioration for both types of glass fiber results from the similarity in the fibers' chemical makeup (Wu et al. 2015, Kwan and Chu 2018).

Typical basalt and silica glass fibers may be chemically modified to produce alkali-resistant (AR) glass fibers and prevent issues of alkali-induced deterioration. Such fibers are produced by the addition of zirconium oxides. Compatibility with an alkaline environment is achieved chemically by the substitution of some zirconium dioxide for the silicon dioxide present in the basalt and silica. The addition of alkali-resistant zirconium dioxide results in a protective layer of zirconium dioxide surrounding each fiber and, consequently, chemical compatibility with the surrounding cement matrix. The combination of zirconium dioxide coating to ensure chemical stability and fiber sizing to prevent clumping and promote fiber bonding allows glass fibers to be utilized as effective concrete reinforcement (Wu et al. 2015, Dopko 2018).

Although their production methods are similar overall, the production of silica glass fibers often involves the use of additives to improve the physical properties of this type of fiber. Basalt glass fiber production, however, does not require additives, resulting in less consistent fiber properties in the finished product. Furthermore, basalt fiber production is usually a simpler process, making basalt glass fibers less expensive than silica glass fibers (Fiore et al. 2015). Generally, basalt glass fibers have a higher strength and elastic modulus than silica glass fibers, although these features remain highly dependent on the parent material and manufacturing process.

Silica Glass

Glass fibers are manufactured by extruding melted parent material into a filament form. During the extrusion process, the filaments are coated with a material called sizing, which equips the fibers with the desired surface texture and interfacial properties for the matrix within which they will be used. For glass fibers used in concrete, individual sizing-coated glass filaments are typically gathered into strands of around 200 filaments and cut to desired lengths. Depending on the production process and intended use, glass strands can be made to disperse back into their filament (microfiber) form when they come in contact with water (water dispersible) or they can be manufactured to remain as integral strands (macrofibers). A relatively new type of glass macrofiber has recently been developed by impregnating glass strands with an alkali-resistant polymer resin. This type of resin-impregnated fiber follows the same concept as glass fiber-reinforced polymer (GFRP) rebar, only on a smaller scale.

The two main types of glass fibers that have been used frequently in practice as reinforcement in cementitious composites include silica glass and basalt glass. Due to the chemical similarity of their parent materials, the final fiber products are also chemically similar. Basalt and silica glass fibers contain high amounts of silicon dioxide (typically 40% to 70%), depending on the composition of the parent material. The main difference between basalt and silica glass fibers is that basalt glass fibers tend to have significant levels of iron, potassium, magnesium, and sodium

oxides, while silica glass fibers typically have low levels of these oxides but can contain significant levels of boron oxides (Deák and Czigány 2009).

It is generally accepted that AR silica glass fibers mixed in cementitious matrices lose some of their reinforcing effectiveness over time because of their chemical sensitivity to the alkaline environment, as explained in the previous section (Gao et al. 2003, Scheffler et al. 2009). In order to help improve the long-term performance of AR glass FRC, Song et al. (2015) investigated modifying the binder using a partial replacement of ordinary portland cement with calcium sulfoaluminate cement. The study found that the proposed method greatly improved the long-term performance of the composites. After 10 years of aging, the modified composites retained substantial ductility compared to the control specimens, which showed no post-crack residual strength after 10 years of exposure. The cited study clearly reflects that if proper mixture design considerations are employed, glass fiber degradation can be substantially decreased (Song et al. 2015).

In addition to the methods of adding zirconium to the chemical structure of glass, applying alkali-resistant sizing to the filament surface during production, or changing the chemistry of the concrete matrix, glass fiber strands can be impregnated with alkali-resistant and surface-bonding resins, such as epoxy and vinyl ester, to improve their long-term durability. These types of polymer-impregnated glass fibers are made into concrete macrofibers that are relatively new to the concrete industry and are essentially miniature versions of GFRP rebars. The alkali degradation of GFRP macrofibers is not fully described in the literature. However, due to the similarities that these fibers share with GFRP rebars, research describing the durability of GFRP rebar can cautiously be extrapolated to describe the long-term durability of GFRP macrofibers.

Investigations that have utilized accelerated aging techniques have all reported concerns about the durability of glass-based fibers in concrete. Significant amounts of degradation and strength loss have been found, especially under high temperature exposure and aggressive chemical environments (Benmokrane et al. 2002, Micelli and Nanni 2004, Sayyar et al. 2013. These studies have sparked major concerns in the concrete industry about the level of safety provided by the structures that use GFRP as primary reinforcement. These concerns motivated several case studies and critical reviews to characterize the level of GFRP strength degradation for in-service structures (Nkurunziza et al. 2005, Mufti et al. 2007, Karim and Shafei 2021a). These efforts found that the degradation reported from accelerated aging tests on GFRP products largely overestimated the actual level of degradation in the field. Several case studies reported little to no GFRP degradation for in-service structures, owing to the effective protection provided by the polymer resin. The studies also concluded that accelerated aging tests do not necessarily represent the conditions of in situ concrete because of the use of elevated temperatures and the unlimited supply of hydroxyl ions (Mufti et al. 2007).

Although several studies have focused on the bond properties of silica GFRP bars in concrete, few studies are available concerning the bond properties of silica glass fibers in concrete, which can be highly different from the bond properties of silica GFRP bars due to differences in size and shape between the materials. In a study conducted by Scheffler et al. (2017), the pull-out properties of AR glass fibers with two types of sizing were investigated under quasi-static and

high-rate (i.e., high-impact) loading protocols. Upon measuring the local interfacial shear strength and critical energy release rate, it was found that regardless of the sizing type, the interfacial friction stress decreases when a high-rate load is applied, mainly because of smoothing of the surface asperities of the AR glass fibers. The study concluded that it is possible to control the pull-out behavior of AR glass fibers through adopting an appropriate sizing, which can significantly help to adjust the FRC's post-peak mechanical properties (Scheffler et al. 2017).

AR glass fibers can be used in FRC made with conventional mixing procedures. However, it has been reported that high fiber volumes are difficult to achieve when using glass fiber filaments in concrete made with conventional mixing procedures because the fibers tend to disperse into the matrix unevenly. Therefore, an increase in w/c ratio or additional mixing is required (Bentur and Mindess 2006), though additional mixing can potentially damage the fibers and compromise their long-term performance (Johnston 2014). It should be noted that the effect of AR glass fibers on the workability of conventionally mixed concrete is highly dependent on the aspect ratio and surface area of the fibers, which can be drastically increased for filament strands compared to integral strands. A study by Ghugal and Deshmukh (2006) reported that AR glass microfibers (up to 4.5% cement weight) were mixed into FRC containing coarse aggregates with no mixing difficulties. The study employed a high w/c ratio of 0.51 to increase workability, but there was no indication of using water-reducing admixtures (Ghugal and Deshmukh 2006).

Several studies have reported that the addition of glass fibers does not have a significant effect on the compressive strength of FRC, and in some cases they only marginally increase the compressive strength (Ghugal and Deshmukh 2006, Barluenga and Hernández-Olivares 2007, Söylev and Özturan 2014, Arslan 2016, Ibrahim 2016). However, Khan and Ali (2016) reported contradictory results, which can be attributed to the relatively long glass fibers used in that study, although the silica glass fibers performed better than nylon fibers. Söylev and Özturan (2014) compared the effect of steel, glass, and PP fibers on the compressive strength of specimens with two w/c ratios, 0.45 and 0.60. The study used air curing and moist curing methods and found that glass and PP fibers had rather similar performance, while steel fibers increased the compressive strength of the specimens (Söylev and Özturan 2014).

Arslan (2016) observed that basalt glass macrofibers have a more pronounced contribution to compressive strength than silica glass fibers. Kizilkanat et al. (2015) reported a similar observation for microfibers. Furthermore, Barluenga and Hernández-Olivares (2007) indicated that low-dosage additions of glass fibers (e.g., 600 to 900 g/m^3) do not change the flexural strength of FRC. However, including more silica glass fibers improves the splitting tensile and flexural strengths of FRC (Mirza and Soroushian 2002, Söylev and Özturan 2014, Kizilkanat et al. 2015, Arslan 2016, Khan and Ali 2016). Silica glass fibers have shown a higher contribution to splitting tensile and flexural strengths compared to nylon and PP fibers while delivering marginally lower strengths compared to steel and basalt glass fibers (Söylev and Özturan 2014, Khan and Ali 2016). Arslan (2016) also indicated that, regardless of volume fraction, the FRC's modulus of elasticity remains unchanged overall with the addition of silica glass fibers. Owing to developments in the recycling industry, silica glass fibers can be extracted from GFRP, but they are in the form of fiber clusters that contain some remaining polymer and filler materials (Arslan 2016). Dehghan et al. (2017) utilized this technology and examined the mechanical properties of

recycled glass FRC and reported an increase in the FRC's tensile strength, despite a decrease in its compressive strength.

Regardless of fiber length and volume fraction, silica glass fibers have been found to increase the ductility and toughness of concrete (Mirza and Soroushian 2002, Söylev and Özturan 2014, Kizilkanat et al. 2015). Furthermore, the splitting tensile and flexural energy absorption of concrete has been reported to increase despite a decrease in compression energy absorption (Arslan 2016, Khan and Ali 2016). Silica glass fibers have delivered superior performance in increasing the toughness of concrete compared to nylon fibers, while their performance has been similar to that of PP fibers. On the other hand, steel fibers have significantly outperformed glass fibers (Söylev and Özturan 2014, Khan and Ali 2016). Arslan (2016) used a range of 0.5 to 3.0 kg/m^3 of silica glass fibers to measure the fracture energy of a set of beam samples. It was reported that adding 1.0 kg/m^3 silica glass fibers yielded the maximum efficiency and increased the fracture energy up to 35% higher than that of plain concrete. It was also noted that the specimens with silica glass fibers achieved a higher ductility and energy dissipation capacity compared to basalt FRC specimens (Arslan 2016).

Small additions of glass fibers have been found to be effective in controlling shrinkage-induced cracking. Barluenga and Hernández-Olivares (2007) studied drying shrinkage under both free and restrained conditions and found that even the addition of very small amounts of glass microfibers (600 g/m^3) contributes significantly to reducing the cracked area and the length of cracks in both standard concrete and SCC. It was also concluded that, although increasing the fiber content increases the concrete's ability to withstand drying shrinkage, the efficiency of the fibers begins to diminish beyond a certain dosage (Barluenga and Hernández-Olivares 2007). Furthermore, Soranakom et al. (2008) indicated that the addition of silica glass fibers enhances the resistance of concrete to drying shrinkage cracking by delaying the time of cracking and lowering the crack width. In the case of restrained plastic shrinkage, Malathy et al. (2007) tested different volume fractions of silica glass microfibers and found that the fibers are very effective in controlling plastic shrinkage, even in concretes containing silica fume.

Basalt Glass

With regard to chemical durability, basalt glass fibers show an alkali degradation similar to that of E-glass fibers (Wei et al. 2010, Wu et al. 2015). To overcome this drawback, a range of methods has been examined in the literature that further the development of AR basalt glass fibers. Rybin et al. (2013) studied the alkali resistance and mechanical properties of basalt glass fibers coated with zirconyl chloride octahydrate. The study found that the surface-coated fibers undergo delayed strength degradation under alkali exposure (Rybin et al. 2013). This was also attributed to the surface coating thickness and density. Lipatov et al. (2015) investigated the addition of zirconium oxides to basalt fibers during their manufacturing process. The study found that the solubility limit of zirconium in basalt glass was 7.1%, which was much less than that of silica glass. Despite the inability to reach a high zirconium content during manufacturing, AR basalt glass fibers with a zirconium content of 5.7% showed an alkali degradation (in terms of weight loss) similar to that of AR silica glass fibers with a zirconium content of 18.8%. The strength degradation of the AR basalt glass fibers was substantially higher than that of the AR

silica glass fibers. However, the compressive, tensile, and flexural strengths of the hardened mortars prepared with the basalt glass fibers that had an optimal zirconium content remained similar to those of the mortars prepared with AR silica glass fibers (Lipatov et al. 2015).

Mingchao et al. (2008) tested the chemical resistance of AR basalt glass fibers by boiling them in distilled water, salt solution, and acid solution. It was reported that the AR basalt glass fibers underwent stiffness and strength degradation in acid solution. In alkali solution, however, their stiffness was mostly maintained, but their strength underwent a gradual decline. Similar to AR silica glass fibers, filaments of basalt glass fibers have been impregnated with alkali-resistant polymer resins in recent years to create basalt fiber-reinforced polymer (BFRP) macrofibers (Mingchao et al. 2008). The same long-term durability characteristics discussed in the section on silica glass fibers above are valid for basalt glass fibers as well. Considering the lack of studies focusing on basalt glass fibers, this extrapolation can be justified, especially because the same alkali-resistant polymer resins are used to impregnate both GFRP and BFRP.

According to Jiang et al. (2014), scanning electron microscope (SEM) images of concrete mixtures reinforced with both basalt glass microfibers and macrofibers revealed that chopped basalt glass fibers are densely covered with hydration products after seven days of curing, which creates a satisfactory bond with the concrete matrix. However, after 28 days of curing, the SEM images showed a gap between the individual fibers and the concrete matrix, suggesting the possibility of debonding at later ages (Jiang et al. 2014). Arslan (2016) reported the presence of a partial bond between basalt glass macrofibers and the concrete matrix, contributing to an increase in the mechanical strength of FRC. Furthermore, the study reported that all the fibers failed by pull-out and no fiber rupture was observed. This can be attributed to the high tensile strength of the basalt glass fibers outperforming the strength of the fiber-matrix bond (Arslan 2016).

Ayub et al. (2014) studied how the addition of high volumes (up to 3.0%) of basalt microfibers affects the workability of pozzolanic concrete (with high-range water-reducing admixtures) and reported no mixing problems. Though the authors noted that the microfiber contents used were high, the achievement of a satisfactory slump demonstrated that with a proper mixture design, the use of admixtures, and the use of a high-energy mixer, high volumes of glass microfibers can be incorporated into FRC that contains coarse aggregates (Ayub et al. 2014). In the case of basalt macrofibers, Arslan (2016) reported no workability issues when using up to 3.0% of this type of fiber in concrete. This was further supported by a review of SEM images, which showed that the basalt macrofibers were well dispersed within the concrete mixture. In contrast, silica glass fibers were observed to flocculate (Arslan 2016).

Since basalt glass fibers have a density that is similar to that of the concrete matrix, BFRP macrofibers at volumes of up to 4.0% have been reported to mix well in concrete using conventional mixing procedures, compared to most other fibers (Patnaik et al. 2013). In a study by Branston et al. (2016), BFRP fibers were found to clump at a volume of 2.0%; however, no superplasticizer had been used. For SCC with a maximum aggregate size of 16 mm, it has been reported that BFRP macrofibers with an aspect ratio of 65 are detrimental to flowability at

volumes over 1.15%, likely due to the stiffness and size of the fibers (Branston et al. 2016, Mohammadi Mohaghegh 2016).

Different results have been reported for the mechanical properties of basalt FRC. Yang and Lian (2011) found that for chopped water-dispersible basalt microfibers, a dosage of 0.3% to 0.5% is optimal for increasing the compressive strength of FRC, while other studies reported that the addition of high volumes of basalt microfibers and macrofibers does not have a significant effect on the mechanical properties of FRC (Yang and Lian 2011, Jiang et al. 2014, Ayub et al. 2014). On the other hand, Kabay (2014) found that basalt microfibers with lengths of 12 and 24 mm that were dispersed at low volumes (2.0 and 4.0 kg/m^3) decreased the compressive strength of the FRC as the fiber volume increased for both normal and high-strength concrete. These contradictory results originate from different fiber characteristics and different concrete mixtures. While lower fiber contents can improve the packing of concrete, higher fiber contents, along with lower water-to-cement ratios, can cause the addition of fiber to have negative effects on the compressive strength of FRC.

Studies have shown that basalt glass fibers enhance the splitting tensile and flexural strengths of FRC, regardless of the fiber content and fiber length (Yang and Lian 2011, Ayub et al. 2014, Kabay 2014). Furthermore, Jiang et al. (2014) found that longer fibers outperform shorter ones in improving splitting tensile and flexural strengths. Saradar et al. (2018) investigated the flexural strengths of 12 mm long basalt, steel, glass, PP, and PO fibers at 0.1% of volume fraction. The study found that all the fibers increased the flexural strength of concrete; however, the basalt and steel fibers made the highest contribution, followed by the PO, glass, and PP fibers (Saradar et al. 2018). Similarly, other studies have confirmed the superior splitting tensile and flexural strength performance of basalt glass fibers in comparison to silica glass fibers (Kizilkanat et al. 2015, Arslan 2016). Branston et al. (2016) investigated the effectiveness of chopped basalt filament microfiber bundles compared to BFRP macrofibers and concluded that the filament basalt fibers can increase pre-crack flexural and compressive strengths in concrete while the BFRP fibers decreased compressive strength and increased flexural strength at higher volumes. Patnaik et al. (2013) reported that BFRP macrofibers increased the flexural strength of concrete with increasing fiber content.

Basalt glass fibers are known to be effective in enhancing the post-peak mechanical properties of concrete (Patnaik et al. 2013). Jalasutram et al. (2017) reported that the addition of basalt glass fibers to concrete can increase the deformability and flexural toughness of basalt FRC. Furthermore, the addition of basalt fibers has been determined to be more effective than the addition of silica glass fibers in increasing the ductility and crack resistance of FRC (Jalasutram et al. 2017). This trend is reversed for fracture energy, where silica glass fibers outperform basalt glass fibers (Kizilkanat et al. 2015, Arslan 2016). Branston et al. (2016) compared the effectiveness of chopped basalt filament microfiber bundles to that of BFRP macrofibers (minibars) and concluded that the BFRP macrofibers had a much better post-peak performance. When a 2.0% volume of 43 mm long BFRP macrofibers was tested under flexure, an outstanding post-crack performance characterized by high ultimate strength, high residual strength, and initial post-crack strain hardening, followed by gradual strain softening at high deflections, was recorded (Branston et al. 2016).

In a study by Adhikari (2013) on BFRP macrofibers, it was found that the ratio of the average post-crack residual strength to the first crack strength can reach 0.75 with a fiber volume of 2.0% and as high as 1.00 with a fiber volume of 4.0%. This clearly indicated that high volumes of BFRP macrofibers can provide superior post-crack performance in FRC products (Adhikari 2013). Patnaik et al. (2013) found that BFRP macrofibers controlled crack widths better than high-tenacity PP macrofibers in beams subjected to accelerated corrosion and then tested in flexure. This was attributed to the fibers' increased stiffness and the superior bond properties between the impregnating resin and the concrete matrix (Patnaik et al. 2013). Patnaik et al. (2014) reported that increasing the dosage of BFRP macrofibers in concrete further increased the post-crack residual strength of FRC (Patnaik et al. 2014). Furthermore, Patnaik et al. (2017) investigated the addition of low volumes of BFRP macrofibers and high-tenacity PP macrofibers to concrete used in bridge decks. The study found that BFRP macrofibers were more effective than high-tenacity PP macrofibers in controlling crack widths and increasing ductility (Patnaik et al. 2017).

Branston et al. (2016) tested the effects of filament dispersion and bundle dispersion of basalt fibers (up to 0.3% volume fraction) on controlling free and restrained plastic shrinkage. The study reported that basalt fibers were highly effective in improving the concrete's ability to withstand plastic shrinkage by decreasing shrinkage-induced strains and limiting crack growth. It was found that, regardless of the type, the addition of 0.1% volume fraction of basalt glass fibers can eliminate plastic shrinkage-induced cracks. It was reported that this volume fraction could be further reduced by utilizing lower diameter filaments. In particular, filament dispersion was determined to deliver the best performance compared to bundle dispersion and BFRP minibars (Branston et al. 2016). Consistent with other reported results, Saradar et al. (2018) evaluated the early-age restrained shrinkage of various FRC mixtures and reported that concretes containing PP and steel fibers had the lowest crack widths in comparison to concretes containing basalt and silica glass fibers. As for the initiation of the first crack, it was found that concrete with basalt glass fibers had the earliest crack initiation time. Additionally, it was reported that as the stiffness of the fibers increased, their flexural strength increased while their ability to limit restrained shrinkage declined (Saradar et al. 2018).

Synthetic Fibers

Synthetic fibers refer to several types of fibers that are composed of man-made material other than metal or glass. The range of chemical and physical properties among the different types of synthetic fiber reinforcement provides an array of behaviors and optimal applications for the various types of synthetic fiber reinforcement. An obstacle common to most synthetic fibers is their low stiffness when compared to materials like steel. The synthetic fibers discussed in this study are PP, nylon, PVA, PO, carbon, PE, polyester, acrylic, and aramid.

Polypropylene Fibers

Polypropylene, with a chemical formula of $(C_3H_6)_n$, is a common type of concrete fiber, owing to its chemical stability in the alkalinity of concrete, wide availability, and low cost. In contrast to steel fibers, PP fibers have a relatively low tensile strength and modulus of elasticity. Although

new types of high-tenacity PP fibers have been developed with much higher strengths and elastic moduli compared to traditional PP fibers, they are still low in strength and elastic modulus compared to other high-strength concrete fibers. Despite the low strength of PP fiber, it is highly ductile; therefore, it can increase the toughness and impact resistance of concrete, especially at high strains. PP fiber is one of the most cost-effective concrete fibers available from almost all concrete fiber suppliers.

The hydrophobic nature and chemical stability of PP fibers often result in an overall weak fiber-matrix bond strength, leading to a mode of failure governed by the fibers' pull-out under external loads. However, if the concrete matrix's strength is increased sufficiently, or an appropriate mechanical anchorage is provided to the fibers (with geometric modifications), the mode of failure can change to the rupture of individual fibers, utilizing their full capacity. Cifuentes et al. (2013) confirmed this assessment by reporting that PP fibers failed due to pull-out in low- and normal-strength concrete while they failed due to rupture in high-strength concrete. To increase the fiber-matrix bond strength, the PP fibers' bond can be improved by splitting a PP fiber into fibrillated bundles during the mixing process.

Monofilament PP fibers, on the other hand, can have their bond strengths improved by shape variations. Oh et al. (2007) tested straight, crimped, hooked, button end, twisted, sinusoidal, and partially sinusoidal shape synthetic macrofibers for their bond strengths. The study concluded that the crimped and sinusoidal shape monofilament PP fibers exhibited the highest improvement in bond properties compared to straight monofilament PP fibers (Oh et al. 2007). Another common way to increase the fiber-matrix bond strength of monofilament PP fibers is by twisting the straight fibers along their longitudinal axes or indenting their surfaces. Yin et al. found that diamond surface indentations were more effective than line indentations in increasing the bond of PP macrofibers (Yin et al. 2015).

Chemical pre-treatments can also be adopted to increase the fiber-matrix bond for PP fibers. López-Buendía et al. (2013) used an alkaline surface treatment and found that the adhesion of PP macrofibers to the concrete matrix increased as a result of longitudinal roughness. In addition, the study showed how chemical adhesion between the individual fibers and concrete matrix contributed to increasing the flexural strength of the FRC product (López-Buendía et al. 2013). In a study by Hao et al. (2018), the microbially induced calcite precipitation pre-treatment method was investigated. The outcome showed the success of this method in improving the bond between the treated PP fiber and the mortar matrix. This improvement was explained by noting that the calcium carbonate produced as a result of microbial activities increases the surface roughness of the PP macrofiber (Hao et al. 2018). In addition, high-tenacity PP fibers can be utilized to develop a sufficient bond, providing significant post-crack residual strength and toughness. In a recent development, a new type of PP fiber has been produced with the ability to chemically bond with the concrete matrix. When this new type of PP macrofiber was compared to a traditional type of PP macrofiber, with both fiber types in monofilament form, it was determined that the fiber pull-out capacity improved by more than 30% (Attiogbe et al. 2014).

Mohod (2015) reported that PP fibers tend to form undispersed clumps and significantly reduce slump at volumes above 1.0%. However, this was found to be highly dependent on fiber

dimensions and mixture design (Mohod 2015). Dopko et al. (2018) similarly observed that PP macrofiber additions above a fiber volume of 1.0% greatly reduced the workability of FRC. In a comparison between PP and nylon fibers (at similar dosages in concrete), Heo et al. (2011) reported that the addition of PP fibers had a notable effect on the workability of FRC. Moreover, the study reported that using longer PP fibers further decreased workability (Heo et al. 2011).

There are some inconsistencies in the literature as to whether PP fibers notably affect the strength parameters of FRC prior to crack propagation. Some studies have reported that the compressive strength of FRC increased or was not affected by the addition of PP macrofibers, but the tensile strength was significantly improved at volumes below 0.55% (Choi and Yuan 2005, Hasan et al. 2011). On the other hand, Cifuentes et al. (2013) found that PP fibers increased both the compressive and splitting tensile strengths of FRC. Some other studies found that low volumes (i.e., 1.2 kg/m^3) of PP macrofibers had a negligible impact on the flexural strength of concrete (Soroushian et al. 2003). Ramezanianpour et al. (2013) reported that the addition of PP fibers reduced the concrete's compressive strength but increased both its splitting tensile and flexural strengths up to 40% and 10%, respectively. This trend was reported to be maintained until a fiber dosage of 0.7 kg/m^3 was reached (Ramezanianpour et al. 2013).

The inconsistences among studies regarding the ability of PP fibers to increase pre-peak strength parameters can be attributed to variations in fiber dosage, geometry, and mechanical properties, as well as the characteristics of the concrete matrix. Studies have found that recycled PP fibers can give FRC mechanical properties similar to those provided by other PP fibers while avoiding degradation in the concrete environment (Yin et al. 2015, Yin et al. 2016).

Several studies have reported a significant increase in the post-crack residual strength and toughness of FRC as a result of PP macrofiber addition (Swamy and Barr 1989, Hsie et al. 2008, Fraternali et al. 2011, Dopko et al. 2018). Cengiz and Turanli (2004) tested the toughness, energy absorption, and flexural ductility of shotcrete panels reinforced with steel mesh, steel fibers, and high-performance PP fibers (with a low modulus). In that study, the fiber contents were reported to be 0.45% and 0.64% for the steel fibers (with a 30 mm length and 0.6 mm diameter) and 0.78% and 1.1% for the PP fibers. The contribution of the high-performance PP fibers was promising for all of the measured properties. However, increasing the PP fiber dosage beyond 1.1% decreased the ultimate load bearing capacity of the concrete while negligibly increasing its energy absorption and flexural toughness characteristics (Cengiz and Turanli 2004). In general, a higher PP macrofiber content leads to better post-crack performance, although due to the low stiffness of PP fibers, residual strengths tend to be more positively influenced at larger deflections or wider crack openings. Based on the outcomes of past studies, it can be stated that while there is some evidence that the pre-crack mechanical properties of FRC can be modestly improved by PP fibers, the main advantages of adding PP macrofibers are realized after cracks are formed.

PP fibers can greatly reduce the drying shrinkage cracking of concrete by increasing the capacity of FRC to resist shrinkage-induced strains (Aly et al. 2008). Studies have also shown that plastic shrinkage in concrete can be limited by using PP fibers (Banthia and Gupta 2006, Islam and Gupta 2016). Furthermore, it has been reported that increasing the fiber dosage can help reduce

(or even eliminate) shrinkage-induced effects by minimizing the number of cracks and their widths. It has also been found that longer fibers with smaller diameters have a greater potential to reduce plastic shrinkage. Fibrillated PP microfibers have a relatively small diameter and high aspect ratio after opening, making them more effective than PP monofilaments in controlling plastic shrinkage cracking in fresh concrete (Bayasi and Zeng 1993, Banthia and Gupta 2006).

Nylon Fibers

Nylon is a synthetic fiber with a chemical formula of $(C_{12}H_{22}N_2O_2)_n$ that can have a range of strength properties dependent on the base polymer, manufacturing technique, and additives used to make the fiber. Although chemically different, nylon and PP fibers often deliver similar benefits when used in FRC because, in general, they have similar fiber-matrix bond strengths, tensile strengths, and elastic moduli. Nylon fibers are, however, more expensive than PP fibers. Recent interest in recycled nylon fibers is expected to help decrease the cost of this type of fiber. Nylon fibers can be readily purchased from most concrete fiber suppliers.

The pull-out behavior of nylon fibers from the concrete matrix is known to be very similar to that of PP fibers (Wang et al. 1987). However, the amide group (-CO-NH-) in nylon fibers reacts with water, which absorbs moisture into the fibers and causes them to swell (Giles et al. 2004). Examining the surface of nylon fibers during pull-out tests revealed that the pull-out capacity increases during the loading process because the concrete matrix scars the outside surface of the nylon fiber, effectively increasing the friction between the fiber and concrete matrix. A similar observation was made for PP microfibers (Wang et al. 1987). According to Yap et al. (2013), nylon fibers outperformed fibrillated PP fibers in compressive strength tests due to the hydrolysis of the amide group of the nylon and the consequent swelling of the fibers, which increased the bond between the nylon fibers and the concrete matrix. The overall bond behavior of nylon fibers has been documented by Khan and Ali (2016). In that study, when 50 mm long nylon fibers were tested in a normal-strength concrete under flexural loads, about 70% of the nylon fibers were found to fail due to pull-out while the remaining 30% failed due to rupture.

Nylon fibers are hydrophilic and can absorb a small amount of water during the mixing process. Several studies have found this feature beneficial to the dispersion of nylon fibers compared to PP fibers. However, at higher volume dosages, the water absorption capacity of the nylon fibers may negatively affect the mixture's workability due to the excessive absorption of mixing water. Yap et al. (2013) noted that the workability of nylon FRC was less than that of PP FRC at the same fiber content in lightweight concrete. This could be due to the fact that the fiber volume tested in the study, up to 0.75%, allowed the nylon fibers to absorb a significant amount of water, decreasing the workability of the mixture (Yap et al. 2013). Khan and Ali (2016) reported that 50 mm long nylon fibers dispersed at volumes close to 1.5% reduced the slump of the mixture to almost 30% of the slump obtained for the control mixtures that contained no fiber.

Song et al. (2005) observed that the addition of nylon and PP fibers increased the compressive strength and splitting tensile strength of FRC, with the nylon fibers providing better performance than the PP fibers owing to the nylon fibers' higher tensile strength and elastic modulus (Song et al. 2005). Yap et al. (2013) also compared nylon and PP fibers in terms of the compressive,

splitting tensile, and flexural strength of FRC and reported that although multifilament PP fibers provided a higher flexural strength, the addition of nylon fibers improved the compressive and tensile strengths further. On the other hand, Zia and Ali (2017) found that a 5.0% addition of nylon fibers (by weight of cement) decreased the compressive and splitting tensile strengths of FRC by more than 30% and 10%, respectively. Ozsar et al. (2017) reported that nylon microfibers are more effective in increasing the splitting tensile strength of mixtures with low water-to-cement ratios. This trend was reversed for nylon macrofibers (Ozsar et al. 2017).

Nylon fibers are used to enhance the post-peak failure characteristics of FRC. When dispersed in low volumes, nylon microfibers have minimal effects on the pre-crack mechanical properties of FRC. However, a higher toughness and a more ductile failure mode can be achieved with the addition of nylon fibers (Lee et al. 2012, Ozger et al. 2013, Song et al. 2015).

Zia and Ali (2017) investigated the effects of a 5% addition of jute, nylon, and PP fibers (by weight of cement) on controlling the cracking of concrete used in canals, with the ultimate goal of limiting water loss due to seepage. It was found that the addition of fibers increased the compressive strength, splitting tensile strength, and flexural toughness of FRC. However, the PP fibers outperformed the nylon fibers. The PP fibers also showed superior performance to the nylon fibers in total absorbed flexural energy; the PP fibers caused a 100% increase while the nylon fibers caused a 68% increase. This trend was much more significant in the total absorbed energy observed during the splitting tensile strength tests, which showed a 21% decrease in nylon FRC and an 11% increase in PP FRC. Furthermore, it can be understood from the study that PP FRC has superior post-peak properties than nylon or jute FRC (Zia and Ali 2017).

Ozsar et al. (2017) investigated the use of both monofilament nylon macrofibers and microfibers in two concrete matrices of different strengths. Comparing the nylon microfibers and macrofibers, the study found that the nylon microfibers increased the compressive strength of the composite and were most effective in decreasing plastic shrinkage cracking, while the nylon macrofibers increased the fracture energy and improved the post-crack performance of the tested mixtures (Ozsar et al. 2017).

Nylon fibers have been shown to be effective in restricting the propagation of drying and plastic shrinkage cracks in concrete. Nam et al. (2016) substituted natural fine aggregates with recycled aggregates and observed an increase in drying shrinkage. To resolve the issue, low volumes of nylon fibers (in the range of 0.1% to 0.5%) were added. The addition of nylon fibers was found to increase the resistance of the recycled aggregate concrete to shrinkage, even above the resistance of the natural aggregate concrete, which had no fibers (Nam et al. 2016).

Polyvinyl Alcohol Fibers

Polyvinyl alcohol, with a chemical formula of $(C_2H_4O)_n$, is a relatively high-strength synthetic fiber that was originally developed to replace asbestos in asbestos cement. The use of PVA fibers has been expanded to FRC applications, owing to their satisfactory mechanical properties and ability to bond chemically with the cement matrix. However, PVA fibers are less common in

practice because they are more expensive than most other concrete fibers. Although they are not widely available in the concrete fiber market, they can still be purchased from certain suppliers.

PVA fibers are hydrophilic, have a noncircular cross section, and form hydrogen bonds with the concrete matrix. These characteristics give PVA fibers the ability to form a strong bond in FRC applications (Zheng and Feldman 1995), which is estimated to be eight times stronger than the bond strength of PP fibers (Wongtanakitcharoen and Naaman 2007). Although PVA fibers are hydrophilic, they have a very low water absorption. PVA fibers are also very compatible with the chemical environment of the concrete matrix, retaining nearly their entire strength after accelerated aging tests equivalent to 100 years (Ogawa and Hoshiro 2011). Despite excellent resistance to acidic and alkaline environments, Roque et al. (2009) reported that PVA fibers can show degradation in seawater environments, especially after repeated wetting and drying cycles. It has been found in several studies that PVA fibers form both chemical and mechanical bonds with the matrix. Through SEM investigations, Zhao and He (2014) demonstrated the precipitation of the C-S-H gel on PVA fibers. Furthermore, Li et al. (2018) showed that pulled-out PVA fibers undergo a notable diameter loss, which reflects the strong bond between the PVA fibers and the cementitious matrix (Li et al. 2018).

Due to the ability of PVA fibers to chemically bond with the concrete matrix, there is no need to alter the geometric shape of this type of fiber. Therefore, PVA fibers are often manufactured in a monofilament form at both the macro and micro sizes. PVA fibers tend to fail by rupture, rather than pull-out, much faster than other fiber types. This has been attributed to a slip-hardening response, originating from strong fiber-matrix bond properties (Betterman et al. 1995, Hamoush et al. 2010). Additionally, it has been reported that the response of PVA fibers shifts from ductile to brittle as the fiber-matrix bond increases over time. The fiber failure mode can also shift from pull-out to rupture, depending on the concrete matrix properties (Li et al. 2004).

When PVA fibers are used in concrete, the workability of the concrete decreases due to the PVA fibers' water absorption. Hossain et al. (2012) evaluated the effect of the addition of PVA on the fresh and rheological properties of self-consolidating concrete. The authors observed that PVA microfibers greatly reduce the flowability and passing ability of self-consolidating concrete. In particular, it was reported that the addition of PVA fibers decreased the plastic viscosity of self-consolidating concrete. Also, as the fiber content was increased, the viscosity exhibited a greater reduction. PVA fibers were found to have a more pronounced effect on reducing the flowability and passing ability of self-consolidating concrete than steel microfibers and macrofibers (Hossain et al. 2012). Shafiq et al. (2016) reported the need for an increased water-to-cement ratio and a sufficient dosage of superplasticizer to meet the target slump for PVA macrofiber mixtures. The authors were able to achieve satisfactory workability characteristics with PVA fiber volume of 3.0% (Shafiq et al. 2016). Dopko et al. (2018) reported difficulties mixing PVA macrofibers in concrete at volumes over 1.0%, indicating that the fibers tend to re-aggregate and form clumps once a critical volume is reached. The study also found that PVA fibers caused decreased workability and dispersion issues compared to PP fibers at the same fiber volume, even though the PP fibers had a higher aspect ratio than the PVA fibers (Dopko et al. 2018).

Studies have reported different results regarding the effects of PVA fibers on the mechanical properties of FRC. In particular, it has been shown that even low volumes of PVA microfibers can reduce the compressive strength of FRC significantly (Yeganeh et al. 2019). On the other hand, Ahmad and Umar (2018) reported that a PVA fiber addition of up to 0.3% of self-consolidating concrete volume increased the compressive strength. Noushini et al. (2013) showed that a 0.25% addition of PVA fibers increased the compressive and splitting tensile strengths of FRC, while any further increase in the fiber content had the opposite effect on strength. The splitting tensile and flexural strengths of FRC have been reported by several studies to remain the same or increase with the addition of PVA fibers (Hossain et al. 2012, Shafiq et al. 2016, Ahmad and Umar 2018, Dopko et al. 2018). However, Yeganeh et al. (2019) reported a decrease in the flexural strength of FRC, although an increase in the splitting tensile strength was noted. In the absence of any explanation for this observation, it is believed that the low water-to-cement ratio of 0.3 hindered the dispersion of PVA fibers in the mixture, especially given the water absorption characteristics of PVA fibers.

PVA fibers have tensile strengths in the same range as steel fibers. However, the elastic modulus of PVA fibers is less than 25% that of steel. As a result, PVA fibers can only modestly increase the tensile and flexural strengths of hardened concrete but can more effectively increase the toughness and ductility (Shafiq et al. 2016). Many studies have reported that the addition of PVA microfibers and macrofibers increases the flexural toughness, flexural residual strength, tensile and compressive strength, energy absorption, ductility, and impact resistance of concrete. Furthermore, it has been stated that increasing the fiber volume has often made a positive contribution to the aforementioned properties (Hossain et al. 2012, Zhao and He 2014, Shafiq et al. 2016, Yeganeh et al. 2019). Shafiq et al. (2016) compared the pre-peak and post-peak mechanical properties of FRC containing 1.0% to 3.0% of PVA and basalt glass fibers. Additionally, 10% of cement was replaced with metakaolin and silica fume, and the same tests were completed. It was found that although basalt glass FRC delivers a marginally higher flexural strength compared to PVA FRC, the latter provides a superior post-peak flexural strength to the extent that FRC with a 3% PVA fiber addition provides deflection hardening properties (Shafiq et al. 2016). Hossain et al. (2013) investigated the performance of PVA and metallic microfibers and macrofibers in self-consolidating concrete. It was reported that the incorporation of both fiber types can greatly enhance the fracture energy of self-consolidating concrete mixtures. This enhancement exceeded a 300% increase in the fracture energy of self-consolidating concrete made with PVA fibers, which was attributed to the molecular bond formed between the individual PVA fibers and the self-consolidating concrete matrix (Hossain et al. 2013).

Both PVA macrofibers and microfibers are reported to be effective in controlling drying shrinkage cracks in concrete. It has been found that PVA fibers added to concrete at relatively low volumes (below 0.5%) decrease the widths of shrinkage-induced cracks by 90% for microfibers and 70% for macrofibers. The addition of PVA fibers did not affect the development rate of restrained drying shrinkage stress or the time of first crack generation. However, the fibers controlled the crack widths once cracks initiated. This observation indicates that pre-crack strength was not greatly influenced but the residual strength was positively impacted by the addition of PVA fibers (Passuello et al. 2009). Wongtanakitcharoen and Naaman (2007) investigated unrestrained early-age shrinkage in FRC made with a 0.1% to 0.4% addition of PVA

fibers. The study concluded that PVA fibers controlled unrestrained early-age shrinkage by 34% (on average) and thus providing improved performance compared to carbon and PP fibers with the same volume fractions (Wongtanakitcharoen and Naaman 2007).

Polyolefin Fibers

Polyolefin is a type of polymer fiber formed by the polymerization of olefin monomer units (C_nH_{2n}) that encompass polypropylene and polyethylene as subgroups. In the present study, PO fibers are discussed separately due to the distinction between PO and other polymeric fibers in the FRC literature. PO concrete fibers share similar properties with high-tenacity PP fibers. Because of the similarities between PO and PP fibers, namely low tensile strength, low elastic modulus, and high ultimate strain, the performance of FRC products made with these two types of fibers tends to be similar. It is also common for blended PP/PO copolymer resins to be manufactured into concrete macrofibers. PO fibers are sold by most concrete fiber suppliers and have a relatively low price.

PO fibers are very compatible with the concrete matrix and do not degrade in the concrete environment. The PO fiber-matrix bond is mechanical in nature (Yan et al. 1998). Depending on the manufacturing technique, PO macrofibers can be made with surface indentations to enhance their mechanical bond properties (Bentur and Mindess 2006). It has been suggested that since PO fibers have a low superficial hardness, their mechanical bond can be increased as a result of microscale surface imperfections that form because of damage to the fibers at the time of mixing. As expected, the bond properties between the PO fibers and the concrete matrix improve with the progress of cement hydration (Tagnit-Hamou et al. 2005). In particular, through SEM investigations, Han et al. (2012) found silica fume helpful in improving the bond between the PO fibers and the concrete matrix. Relatively low-modulus PO fibers were observed to be most effective when used with silica fume in concrete when 25 mm fibers were used in place of 50 mm fibers for improving strength, ductility, and absorption characteristics (Han et al. 2012).

Limitations in the fresh state as a result of adding PO fibers are similar to those previously discussed for PP fibers. PO fibers with surface indentations may further decrease workability compared to smooth PO fibers, mainly because of the increased surface area per fiber. Several studies have shown that PO fibers can be used in SCC mixtures (Alberti et al. 2014, Zaroudi et al. 2020). No significant detrimental effects to workability, however, have been reported in the literature for PO fibers when added in low volumes. Alberti et al. (2014) indicated that PO macrofibers with a length of 50 mm can mix well in SCC at volumes up to 1.0%. However, it should be noted that the study utilized a high water-to-cement ratio (i.e., 0.5) to improve workability. Zaroudi et al. (2020) reported that the addition of PO fibers at more than 1.0% volume fraction significantly reduced the slump of SCC. Smirnova et al. (2017) compared two methods of adding PO to a mixture and concluded that adding PO fibers to fresh concrete and further mixing it for 5 minutes led to insufficient dispersion and agglomeration of fibers. The proposed solution was to mix fibers with the dry constituents (aggregates and cement) for one minute prior to the addition of water and superplasticizer. Noting that macrofibers are often better dispersed than microfibers in the concrete matrix, the maximum volume fraction of PO macrofibers in concrete can be higher than that of PO microfibers (Smirnova et al. 2017).

Similar to other low-strength synthetic fibers, the addition of low volumes of PO fibers to concrete does not have a significant effect on the mechanical properties of FRC. Alberti et al. (2014) reported that for low PO fiber volumes, only tensile strength increased slightly, while for high PO fiber volumes, compressive strength decreased slightly and tensile strength increased substantially. Zaroudi et al. (2020) observed that by increasing the fiber content to 1.25%, both compressive and splitting tensile strengths experienced improvements. However, both strengths started to decrease when the fiber content increased beyond 1.25% (Zaroudi et al. 2020). Furthermore, the flexural strength of FRC was reported to increase when the fiber content increased (Adhikary et al. 2019).

Alani and Beckett (2013) investigated the performance of PO fibers in comparison to hooked-end steel fibers for slab-on-ground reinforcement applications. It was found that surface-embossed PO macrofibers can provide benefits similar to those provided by steel fibers. Equivalent performance between the PO and steel fibers was observed when the volumetric dosage of the PO fibers was about one-third higher than that of the steel fibers. The study, however, showed that high-tenacity synthetic macrofibers have the potential to be used as the primary reinforcement in certain slab-on-ground applications (Alani and Beckett 2013). Similarly, Alberti et al. (2014) described a case study in which the conventional reinforcing bars in a concrete water pipeline casing were completely replaced with 5 kg/m^3 of PO macrofibers. This approach was found to be satisfactory because only small tensile stresses were anticipated in the concrete. Eliminating conventional rebars reduced the cost and time of construction significantly (Alberti et al. 2014).

PO macrofibers are typically used to increase the post-crack residual strength of concrete. They can improve post-crack ductility and limit crack growth, but due to their low modulus they are often not as effective for low deflections or small crack widths as other fibers with higher elastic moduli (Alberti et al. 2014). Ramakrishnan (1999) described the use of PO macrofibers in bridge decks and barrier rails. It was reported that the addition of fibers at a volume of 1.5% not only improved the impact resistance and toughness of the concrete but also exhibited a synergistic effect with the rebar, shifting the cracking pattern from a smaller number of wider cracks to a larger number of narrower cracks, which would effectively limit the ingress of corrosive agents into the concrete (Ramakrishnan 1999). Alberti et al. (2014) compared the post-peak properties of FRC made with 3.0, 4.5, 6.0, and 10.0 kg/m^3 of PO macrofibers to FRC made with 26 kg/m^3 of steel fibers. The study found that regardless of fiber volume, toughness and ductility increased with the addition of PO fibers, providing improved residual strength. The results of fracture energy tests showed that the addition of PO fibers increased the fracture energy of the concrete up to 75% that of steel FRC after a 1 mm deflection, i.e., 1/300 of the span length. However, when the deflection increased to 5 mm, i.e., 1/60 of the span length, the PO fibers outperformed the steel fibers by 40%, proving the higher efficiency of PO fibers at high deflections. It should be noted that an admixture for improving the fiber-matrix bond had been used in the study for high-volume fiber mixtures (Alberti et al. 2014).

PO fibers of different lengths and aspect ratios have been reported to be effective in controlling plastic shrinkage and thermal cracking in concrete overlays. Shorter fibers have proved to be most effective for such applications at the same volume dosage as longer fibers (Banthia and Yan 2000). Yousefieh et al. (2017) found that controlling drying shrinkage in FRC made with a

PO fiber content of 1.0% was not as effective as when steel fibers were used, mainly due to the steel's higher modulus of elasticity. However, the PO fibers were found to perform better than PP fibers. Furthermore, the addition of fibers was found to delay crack initiation time (Yousefieh et al. 2017).

Carbon Fibers

Carbon fiber has historically been one of the most popular types of fiber for reinforcing brittle matrix composites to improve their tensile properties. The effectiveness of carbon fiber reinforcement in other types of matrices has sparked interest in using carbon fibers in FRC. Carbon fibers can have a wide range of mechanical properties depending on the materials used to make the fibers. For example, polyacrylonitrile (PAN)-based carbon fibers have a very high tensile strength and elastic modulus (up to the twice those of steel fibers), while pitch carbon fibers that are made from petroleum and coal tar pitch have a relatively lower tensile strength and elastic modulus. Pitch carbon fibers often exhibit a wide range of tensile strengths and elastic moduli depending on the nature of the pitch used to make them (Johnston 2014). The properties of carbon fibers can vary considerably depending on the manufacturing process as well. Both types of carbon fiber are made from varying degrees of heat treatment, stretching, and oxidation (Bentur and Mindess 2006). Carbon fibers are expensive compared to other fiber choices, which unavoidably limits their use in civil infrastructure projects.

Carbon fibers are chemically inert and, as a result, do not undergo strength deterioration in the concrete environment (Ali et al. 1972, Chand 2000, Bentur and Mindess 2006, Girgle et al. 2016). Therefore, carbon fibers can only form mechanical bonds with the concrete matrix. Fibers with a high modulus of elasticity, such as carbon fibers, tend to pull out rather than rupture under external loads applied to FRC. This behavior, however, also depends on the matrix strength and fiber dimensions, as well as the contact surface area between the fibers and the concrete matrix. Pitch carbon fibers in mortar have been found to have sufficient strength to fail by pull-out unless latex is used to enhance the fiber-matrix bond, in which case the failure mode shifts to fiber rupture (Larson et al. 1990).

Carbon macrofibers are uncommon because carbon fibers tend to break into shorter lengths during the mixing process due to their brittle nature (Nishioka et al. 1986). In particular, the presence of coarse aggregates can increase the level of damage to carbon fibers while mixing. However, such damage can be lessened by using appropriate mixing procedures and additives, such as methyl cellulose and superplasticizer, to better disperse the fibers with minimal mixing (Balaguru 1994). The upper limit of carbon fiber content for conventional mixing has been found to be 1.0% by volume due to the fiber's high aspect ratio and specific surface (Johnston 2014), although higher volumes can be accommodated with modified mixing procedures and the inclusion of admixtures (Akihama et al. 1984). Dopko et al. (2020) reported adequate workability and dispersion of carbon microfibers in FRC mixtures that contained carbon fiber volumes of up to 0.5%. This was achieved by the addition of superplasticizer and a modified mixing procedure using a gravity-based drum mixer to increase the mixing energy (Dopko et al. 2020).

Carbon fibers can improve the mechanical properties of cementitious composites if a sufficient volume of them is included. The extent of improvement is proportional to the strength and modulus of elasticity of the carbon fibers used. Stronger and stiffer carbon fibers more effectively increase the strength parameters, while weaker ones more likely contribute to enhancing toughness. Among the limited studies available, Yao et al. (2003) tested FRC with a high-strength carbon microfiber volume of 0.5% and found that the addition of fiber increased the compressive strength, splitting tensile strength, and modulus of rupture by 14%, 19%, and 9%, respectively. Chen et al. (2017) reported that the addition of carbon fibers increased the compressive strength of concrete, with the best result achieved when the carbon fiber volume was 1.0% by weight of cement, although the study did not investigate the effect of higher fiber contents. Dopko et al. (2020) tested varying volumes of carbon microfiber, accelerating admixture, and SRAs for their effects on compressive and splitting tensile strengths. The study found that increasing the carbon microfiber volume generally increased the 24-hour compressive and splitting tensile strengths of FRC. The presence of 0.3% carbon microfiber also increased the 7-day compressive and splitting tensile strengths by an average of 9.6% and 22.8%, respectively (Dopko et al. 2020). On the other hand, Chen and Chung (1996) reported that although the addition of carbon fibers increased the flexural strength of concrete specimens, the compressive strength of the specimens decreased, most likely because of the increased air content resulting from the addition of fiber. It should be noted that the study used a relatively weak carbon fiber (with a 690 MPa tensile strength), which can explain the reported findings (Chen and Chung 1996).

FRC samples with 0.5% carbon, PP, and steel fibers were tested by Yao et al. (2003) for their effects on post-peak properties. The steel fibers drastically outperformed the carbon and PP fibers in residual flexural strength and flexural toughness. The carbon fibers were found to increase the residual strength of the concrete, especially at lower deflections. However, FRC with PP fibers showed a higher residual flexural strength at higher deflections (Yao et al. 2003). In addition, Chen and Chung (1996) found that the flexural toughness of FRC made with 0.19% carbon fibers increased more than 150%.

A limited number of studies have measured the effect of carbon fibers on the shrinkage of concrete. Carbon fibers have been shown to be effective in reducing the restrained shrinkage and drying shrinkage cracking potential of carbon FRC (Chen and Chung 1996). Dopko et al. (2020) tested the restrained drying shrinkage of FRC with 0.1%, 0.3%, and 0.5% carbon microfibers. The study concluded that although carbon microfibers showed negligible effects on the rate and magnitude of stress caused by restrained shrinkage, they can efficiently control the crack opening potential. It was also found that accelerating admixtures have an adverse effect on the restrained drying shrinkage of carbon FRC, as captured by the strains recorded during ring tests. On the other hand, SRAs were reported to show great potential for controlling drying shrinkage-induced strains. It was also noted in the study that SRAs can compensate for the negative effects of accelerating admixtures on the drying shrinkage of carbon FRC (Dopko et al. 2020).

Polyethylene Fibers

Polyethylene fiber, with a chemical formula of $(C_2H_4)_n$, can be produced to have a wide range of mechanical properties. In the past, PE fibers were characterized by low strength and elastic modulus, similar to PP and PO fibers. However, the development of ultra-high density PE has greatly increased the strength and stiffness of this type of fiber. From a performance perspective, it can be stated that the higher the fiber density and molecular weight, the higher the strength and stiffness potential. These fiber properties depend on the degree of molecular alignment achieved by advanced production processes involving heat pressure and catalysts (Lepoutre 2013). High-strength polyethylene (HSPE) is a type of PE fiber made from gel-spinning ultra-high molecular weight PE. The tensile strength and modulus of elasticity of HSPE are higher than those of other polymeric fibers. HSPE is a high-performance product, and therefore it is expensive to buy directly from the manufacturer. However, waste HSPE fibers can be obtained from third-party distributors for a low price.

HSPE fibers are chemically inert, providing high stability and degradation resistance in the concrete environment, in addition to high resistance against acids and seawater. Recycled PE fibers also adequately withstand the alkalinity of the concrete environment (Pešić et al. 2016). HSPE fibers have a low coefficient of friction, causing them to form a weak bond with the surrounding matrix (Zheng and Feldman 1995, Marissen 2011). The bond strength of HSPE fibers, however, can be improved by surface treatments. Wu and Li (1999) studied such treatments and reported that the fibers can form a bond with the concrete matrix at a strength up to 1.0 MPa if a surface finish is applied to the fibers to increase their friction coefficient. Additionally, it was found that plasma treatment of the fibers can considerably increase the fiber-matrix bond strength (Wu and Li 1999). In a separate study, He et al. (2017) showed that coating HSPE fibers with carbon nanofiber can increase the frictional bond strength of the fibers by more than 20%. As found by Pešic et al. (2016), recycled high-density PE fibers fail due to pull-out caused by mechanical friction, while they undergo high elongation before being pulled out of the concrete matrix. Through SEM investigations, the study confirmed that the fibers do not form a chemical bond with the concrete matrix (Pešic et al. 2016).

Zhang and Li (2013) reported that the addition of PE fibers decreases the workability of FRC that contains fly ash and silica fume by reducing both slump and slump flow. PE macrofibers with a lower strength and modulus of elasticity, similar to those of PP and PO, have been reported to mix sufficiently well into a normal FRC matrix at volumes up to 4.0%. This is a relatively high fiber volume, and it should be noted that a high water-to-cement ratio was utilized in the study to help with mixing (Zhang and Li 2013). High fiber volumes, in the range of 2.0% to 4.0%, of high-aspect ratio HSPE fibers were used by Yamaguchi et al. (2011). These fiber volumes did not cause any slump issues because of the use of a high superplasticizer dosage and a high-shear force double-axis mixer (Yamaguchi et al. 2011).

HSPE fibers have shown adequate reinforcing effects in concrete. In the limited number of studies available, mixtures with HSPE fibers (as low as 0.025%) have exhibited higher flexural strengths compared to those made with 0.1% fibrillated PP fibers (Soroushian et al. 1992). Yamaguchi et al. (2011) explored the use of HSPE fibers in volumes of 2% and 4% for their

compressive, splitting tensile, and flexural strengths and reported an increase in all strength values due to the addition of HSPE fiber. The possibility of using recycled PE fibers for concrete reinforcement has also been investigated. Pešić et al. (2016) studied FRC that contained PE fibers made from recycled consumer products. The fibers used in the study had a relatively low yield strength (12 MPa compared to 40 to 80 MPa common for regular HSPE fibers) and modulus of elasticity (0.5 GPa compared to 0.9 to 1.1 GPa common for regular HSPE fibers), mainly due to the recycling process. The study found that the FRC strength parameters were not significantly influenced by the addition of fibers compared to the control mixture that contained no fibers (Pešić et al. 2016).

Low-strength PE fibers are effective in increasing post-crack flexural ductility, especially at large deflections (Kobayashi and Cho 1981). Yamaguchi et al. (2011) showed that the addition of high volumes of HSPE microfibers to concrete significantly increased its toughness and extreme load resistance. Moreover, Soroushian et al. (1992) reported that HSPE fibers provided an impact resistance comparable to that of fibrillated PP fibers at low volumes in a concrete mixture. Pešić et al. (2016) investigated the pre-peak and post-peak mechanical properties of FRC with 0.4%, 0.75%, and 1.25% volume fractions of recycled high-density PE fibers. For this purpose, two series of fibers (with 23 and 30 mm lengths and 0.25 and 0.40 mm diameters, respectively) were used. The study reported that a satisfactory flexural toughness and residual strength could be achieved by adding recycled high-density PE fibers. The residual flexural strength was found to be higher for FRC samples with shorter fibers (i.e., from 25% to 45% of the flexural peak value) and lower for FRC samples with longer fibers (i.e., from 13% to 32% of the flexural peak value). Furthermore, it was found that recycled high-density PE fibers can be effectively used in structural concrete because they exhibit post-peak properties similar to those of PP fibers (Pešić et al. 2016).

Pešić et al. (2016) investigated FRC made with recycled PE fibers and found that the total number and width of plastic shrinkage-induced cracks were significantly decreased by the presence of fibers, even at low volumes. The study reported that the crack reduction ratio ranged from 34% to 84% for samples containing 0.40% to 1.25% recycled PE fibers, respectively. The unrestrained drying shrinkage of concrete was also investigated in the study. With a 10% to 15% decrease in the strains recorded, the reduction achieved was in the same range as that provided by PP and other synthetic fibers (Pešić et al. 2016). Auchey and Dutta (1996) investigated recycled high-density PE fibers and concluded that FRC containing this type of fiber performed equal to or better than that containing PP fibers in freeze-thaw conditions, suggesting that recycled high-density PE fibers can be a secondary reinforcement alternative for resisting shrinkage and temperature gradients.

Polyester Fibers

Polyester fibers generally fall under two categories: polyethylene terephthalate (PET) and poly(1,4-cyclohexylene dimethylene terephthalate) (PCDT). PET and PCDT fibers are made using different processes and have different chemical and mechanical properties. PET fibers generally have a higher strength and stiffness than PCDT fibers, which are often characterized as more ductile. Only PET fibers have been subject to a sufficient amount of research regarding

their use in concrete, mostly as recycled fibers from consumer products, to warrant their inclusion in this study. Henceforth, all discussion of polyester fibers refers specifically to the PET variety. It should be noted that although PE and PET share the polyethylene name, they are chemically completely different, in that PET is a polyester, not a type of polyethylene. PET fibers can have variable chemical and mechanical properties, depending on the fibers' manufacturing technique. Similar to other polymeric fibers, the fiber-matrix bond of polyester fibers is reported to be only mechanical in nature.

Despite showing promise overall, the main concern with the use of polyester fibers in cementitious composites is the uncertainty regarding their stability in the highly alkaline environment of concrete. Most studies have reported some level of degradation after a prolonged exposure of this type of fiber to extreme environments. Kim et al. (2010) studied recycled PET FRC for strength retention after exposure to alkaline and acidic solutions. It was found that exposure to such solutions not only reduced the strength of the PET fibers but also significantly deteriorated the physical and mechanical properties of the entire concrete matrix (Kim et al. 2010). These observations were further supported by Fraternali et al. (2014), who reported that after 12 months in an aggressive seawater curing environment, the toughness of recycled PET FRC decreased by more than half. Rostami et al. (2019) confirmed past findings and reported a tensile strength loss that increased over time. Additionally, Silva et al. (2005) showed that PET FRC can suffer from decreased toughness over time. The study used SEM to characterize fiber degradation under prolonged exposure to an alkaline environment. This degradation was observed as surface irregularities, while in some regions complete degradation of the fibers was evident (Silva et al. 2005).

Contrary to studies that confirmed the degradation of PET fibers over time in alkaline environments, Ochi et al. (2007) found that recycled PET fibers underwent negligible degradation after 120 hours in an alkaline environment at 60°C. This was quantified through direct tensile tests on individual fibers (Ochi et al. 2007). This finding should be considered with caution because the fibers were subjected to only 120 hours of alkaline exposure, which may not have been long enough to allow sufficient exposure to relate the results to long-term durability. Regardless, there is sufficient evidence in the literature to conclude that PET fibers can undergo some level of degradation in the concrete environment, which is a major limitation to the fiber's reinforcing potential.

Although the majority of past studies used PET fiber volumes of 1.0% or lower in FRC, PET macrofibers have been reported to mix well in concrete at 1.5% or even up to 3.0% (Ochi et al. 2007, Borg et al. 2016). It must be noted that these studies utilized water-to-cement ratios equal to or greater than 0.55, leading to more workable mixtures.

Research has shown that polyester fibers are capable of improving the mechanical properties of concrete. Most research conducted on PET fibers has involved monofilament macrofibers made from recycled plastics. However, a limited number of studies have also investigated nonrecycled PET fibers. Swamy and Barr (1989) tested 20 mm long polyester fibers with a high aspect ratio at volumes up to 1.0%. The study found that the addition of these fibers increased the compressive, flexural, and splitting tensile strengths of the hardened composite by 5%, 7%, and

27%, respectively (Swamy and Barr 1989). Sivakumar and Santhanam (2007) investigated polyester microfibers dispersed at a volume of 0.5% in a high-strength concrete matrix and determined that while compressive strength was not significantly affected by the addition of polyester fibers, elastic modulus and splitting tensile and flexural strengths were all improved.

Recycled PET fibers have been shown to have different effects on concrete compressive strength based on their tensile strength, shape, length, and diameter. Kim et al. (2010) compared the performance of recycled PET fibers made from extruding shredded bottles with that of nonrecycled PP fibers. Both synthetic macrofibers were 50 mm long and had similar aspect ratios, but the PET fibers were surface embossed while the PP fibers were crimped. The study found that for both the PP and PET fibers, compressive strength and elastic modulus slightly decreased with an increase in fiber volume. However, the ultimate strength of FRC increased as the fiber volume increased (Kim et al. 2010). Similarly, Borg et al. (2016) investigated FRC with recycled PET fibers at volumes of 0.5%, 1.0%, and 1.5% that had been hand cut from waste bottles to two different lengths: 30 mm and 50 mm. The fibers of both lengths were either deformed or straight. The study found that compressive strength decreased in mixtures where PET fibers were present, with the largest reductions occurring when longer fibers were added at higher volumes (Borg et al. 2016).

Fraternali et al. (2014) studied FRC containing a constant 1.0% fiber volume made with recycled PET macrofibers that had been extruded from resins obtained from melting recycled bottle flakes. Three different recycled PET fibers were obtained, each with different geometries and parent resins, giving them different mechanical properties. These three fibers were compared to nonrecycled PP macrofibers with an embossed surface texture. The findings indicated that all of the PET and PP fibers improved the compressive strength of FRC and that straight macrofibers were provided a greater increase in compressive strength than embossed PP fibers (Fraternali et al. 2014). Additionally, recycled PET fibers have been found to be effective in increasing the flexural strength of FRC, with the fibers' effectiveness decreasing as their lengths increased (Fraternali et al. 2011, Fraternali et al. 2014). When comparing FRC products made with recycled PET fibers to those made with PP fibers, it has been found that both fibers similarly increase the mechanical properties of FRC (Kim et al. 2010, Fraternali et al. 2011), although Rostami et al. (2019) reported that PP fibers further enhance the flexural strength of FRC in comparison to PET fibers.

Only a few studies have been conducted on the post-peak properties of nonrecycled polyester fibers, while several studies have been conducted on recycled PET fibers. Swamy and Barr (1989) used 20 mm long nonrecycled polyester fibers with a high aspect ratio at volumes up to 1.0% and reported a 100% increase in the impact strength of FRC compared to that of plain concrete. The incorporation of recycled PET fibers into concrete was also found to enhance its post-peak properties (Swamy and Barr 1989). In particular, it has been reported that PET FRC benefits from high toughness and ductility (Kim et al. 2010, Fraternali et al. 2011, Borg et al. 2016). Kim et al. (2010) compared the ductility and ultimate flexural strength capacity of FRC containing 0.5%, 0.75%, and 1.0% recycled PET and crimped PP fibers with a length of 50 mm. The study showed that recycled PET and PP fibers have similar performance characteristics and that the addition of fibers increased the ductility and ultimate flexural strength capacity of concrete significantly (Kim et al. 2010). According to Fraternali et al. (2011), PET fibers with a

higher tensile strength can deliver a higher flexural ductility. Kim et al. (2010) reported that the ductility of a full-scale beam made with PET FRC increased up to 10 times that of a reference beam with no fibers. The toughness of the PET FRC increased as the fiber volume increased. Additionally, longer fibers were determined to further improve the toughness characteristics of FRC compared to shorter fibers, mainly because of the increased fiber-matrix bond strength (Borg et al. 2016).

Recycled PET fibers have been reported to be effective in controlling shrinkage-induced cracks. According to Borg et al. (2016), recycled PET fibers can reduce plastic shrinkage cracking under accelerated drying conditions and can reduce and delay crack opening under restrained drying shrinkage. Kim et al. (2010) added that the time to crack formation under restrained drying shrinkage increased with increasing fiber volumes. Pelisser et al. (2010) indicated that among short PP, recycled PET, glass, and nylon fibers, the short PP fibers were best at controlling crack initiation caused by plastic shrinkage, while the recycled PET and glass fibers showed similar performance and the nylon fibers had the weakest performance. This led the authors to recommend short recycled PET fibers as a promising substitute for PP fibers in limiting plastic shrinkage (Pelisser et al. 2010).

Acrylic Fibers

Acrylic is a polymer that contains at least 85% acrylonitrile by weight with a chemical formula of $(C_3H_3N)_n$. The name "acrylic" is the short form of, and essentially interchangeable with, polyacrylonitrile. As previously mentioned, PAN fiber is also the precursor material used to manufacture PAN-based carbon fiber. Acrylic fibers with a high tensile strength and elastic modulus were developed in the 1980s to replace carcinogenic asbestos in asbestos cement and have been used successfully as small-diameter short-cut fibers at high volumes for asbestos replacement in hollow circular and sheet cement products made with the Hatschek process. PAN fibers can possess a wide range of strength and stiffness parameters. Due to this variation, the properties of FRC with this type of fiber can also vary substantially. The research pertaining to the performance of PAN fibers in cementitious composites containing coarse aggregates has been rather limited. However, more research has been conducted on the use of acrylic fibers in paste or mortar, likely because PAN fibers are predominantly micro in form. Despite a relatively wide availability, acrylic microfibers have a higher price compared to other low-strength synthetic fibers.

Early forms of acrylic fibers exhibited low strength and elastic modulus, as well as poor resistance to acids and alkalis, which limited their application in concrete (Bentur and Mindess 2006). However, the new generation of acrylic fibers has shown little to no sensitivity to the alkalinity of concrete. Some studies have reported a small amount of long-term sensitivity to alkaline environments, especially at higher temperatures (Wang et al. 1987), while others have reported that acrylic fibers are not sensitive to chemical degradation (Amat et al. 1994, Jamshidi and Karimi 2010). Hahne et al. (1987) studied the performance of FRC made with high-strength PAN fibers. The study explored high-strength acrylic fibers of different lengths (6 to 24 mm), diameters (18 to 104 micrometers), strengths (up to 1,000 MPa), and elastic moduli (up to 19.5 GPa) for their fiber-matrix bond properties. It was reported that acrylic fibers form a satisfactory

bond with the concrete matrix due to their irregular cross-sectional shape (Hahne et al. 1987). Confirming this assessment, Jamshidi and Karimi (2010) investigated 3 to 4 mm fibers and found that acrylic fibers, similar to nylon fibers, form a stronger bond than PP fibers with the concrete matrix, partly due to the formation of cement hydration products on the fibers' surface.

The addition of PAN fibers in volumes of up to 2.5% has been reported to decrease the workability of FRC to the extent that the water-to-cement ratio must be increased substantially. Superplasticizers may also be needed to accommodate the addition of the fiber, especially when using low-diameter fibers (Hahne et al. 1987, Fan 2015, Mo et al. 2015).

PAN fibers with different tensile strengths, lengths, and volumes have been reported to have a negligible or negative effect on the compressive strength of FRC (Hahne et al. 1987, Mo et al. 2015). Mo et al. (2015) used 12 mm long acrylic fibers in volumes up to 0.2% and reported a 7% to 13% decrease in compressive strength. Furthermore, the study reported that the addition of PAN fibers increased both the tensile and flexural strength of FRC, especially at a 0.1% dosage (Mo et al. 2015). This is in line with the results of Hahne et al. (1987), which indicated that PAN fibers of greater length can further increase the mechanical properties of PAN FRC.

The ductility and post-crack residual strength of concrete are known to increase with the incorporation of PAN fibers (Hahne et al. 1987, Jamshidi and Karimi 2010). Among the limited number of studies available, Fan (2015) investigated the contribution of PAN microfibers to the post-peak mechanical properties of FRC. Fiber volumes between 0.5% and 2.0% were tested for their influence on impact toughness. The study concluded that the addition of PAN fibers enhanced the impact toughness of concrete by up to 250%, with a volume of PAN fibers of 1.0% providing the greatest improvement (Fan 2015).

The addition of PAN fibers minimizes the potential for drying shrinkage cracking, regardless of the volume fraction of the fiber, with higher volumes leading to better performance (Hahne et al. 1987, Mo et al. 2015). Fan (2015) investigated the effects of PAN fibers on the autogenous shrinkage of FRC and reported that a 21.7%, 39.1%, 26.1%, and 17.4% reduction in autogenous shrinkage-induced strains can be achieved in FRC made with 0.1%, 0.5%, 1.5%, and 2.0% PAN microfibers, respectively. This improvement in the autogenous shrinkage performance of FRC was attributed to the PAN fibers' modification of the FRC's pore structure, which was verified through mercury intrusion porosimetry analyses (Fan 2015).

Aramid Fibers

Aromatic polyamide is a polymer in which at least 85% of the amide group is bound directly to two aromatic rings. Known in short as "aramid," this fiber has many high-performance applications due to its high strength and elastic modulus relative to most other synthetic fibers. Aramid fibers are 2.5 times stronger than silica glass fibers and 5 times stronger than steel fibers per unit weight. These unique qualities have drawn attention to the use of aramid fibers for reinforcement in cementitious matrices. The two most common types of aramid fibers are marketed under the trade names Kevlar and Technora. These two fibers possess different properties, mainly due to differences in their production methods. Kevlar is produced by dry and

wet spinning of a sulfuric acid solution of aromatic polyamide, while Technora fiber production does not utilize acid spinning (Uomoto et al. 2002). Aramid fibers are expensive and not easily found in the concrete fiber market.

A limitation of aramid fibers for use as a concrete fiber is the lack of clarity in the literature about the level of strength degradation of this type of fiber in the concrete environment (Johnston 2014). Uomoto and Nishimura (1999) found that the sensitivity of aramid fibers to chemical deterioration has a correlation to the method used for manufacturing the fibers. The study reported that aramid fibers that were acid spun (i.e., Kevlar) underwent degradation at high temperatures (80°C and above) in acidic, alkaline, and distilled water solutions. Aramid fibers that were not acid spun (i.e., Technora) had much better chemical durability in similar solutions. Degradation of the Technora aramid was only an issue at high temperatures; however, such temperatures are not expected to be encountered in most concrete applications (Uomoto and Nishimura 1999). Derombise et al. (2009) studied the alkali resistance of Technora aramid fibers and reported that although small amounts of chain degradation and finish rearrangements can occur after alkali exposure, the fibers retain nearly all of their mechanical properties. It is important to note that the tests were performed with pH values up to 11 while the concrete environment has higher pH values, which can exacerbate the alkali deterioration of the fibers (Derombise et al. 2009). Uomoto and Nishimura (1999) reported that aramid fibers were capable of retaining 90%, 60% to 85%, and 45% of their strength after long-term aging in alkaline, acidic, and ultraviolet exposure environments, respectively. Additionally, aramid fiber-reinforced polymer (AFRP) showed increased alkali resistance compared to monofilament aramid fibers (Uomoto and Nishimura 1999). Overall, studies suggest that aramid fibers can be sensitive to alkali degradation. However, if the fibers are not acid spun and high temperatures are not anticipated through the service life of the FRC product, alkali degradation of the aramid fibers in concrete is not expected to be an issue.

Kevlar fibers are reported to have a weak bond with the concrete matrix due to their smooth surface, inert nature, and high crystallinity (Lin et al. 2000). However, Zhang et al. (2011) chemically treated Kevlar fibers and observed that treated fibers can have a more roughened surface (and a better fiber-matrix bond) than untreated fibers.

Nanni (1992) investigated different volumes of AFRP macrofibers dispersed in concrete. AFRP fibers include hundreds of aramid microfibers bound together by resin to form a single macrofiber. The study found that AFRP fibers significantly decrease the apparent workability and slump of concrete. Therefore, 2.5% was recommended as the maximum volume fraction of AFRP fibers that can be incorporated into FRC with conventional mixing procedures, a volume fraction similar to that of steel fibers (Nanni 1992).

Zhang et al. (2017) investigated aramid microfibers at volumes up to 1.5% in concrete. The study found that a fiber volume of 0.5% slightly increased the compressive strength and elastic modulus of the composite. However, mixtures with fiber volumes of 1.0% and 1.5% showed a decreased compressive strength and elastic modulus (Zhang et al. 2017). Nanni (1992) reported that AFRP fibers, similar to steel fibers, marginally increased the pre-crack flexural and splitting tensile strengths of FRC, while PP fibers decreased the flexural strength of FRC due to their

relatively high volume. The use of twisted Technora aramid macrofibers with a 0.5 mm diameter and cut lengths of 30 to 40 mm was investigated by Chan et al. (2016) and Zhao et al. (2018). The studies found satisfactory results with the twisted aramid macrofibers. Chan et al. (2016) tested 30 mm and 40 mm long Technora aramid twisted macrofibers dispersed in concrete at a volume of 1.0% for their effects on the flexural response of steel-reinforced concrete beams. The fibers did not significantly affect compressive strength, but the peak flexural load in the beams was found to increase by about 9%. The fiber length did not significantly improve the flexural test results. However, the crack widths in the beams were smaller for aramid fibers than for hooked-end steel fibers up to the yield point of the embedded steel bars (Chan et al. 2016).

Nanni (1992) found that a significant increase in the post-crack residual strength and toughness of concrete can be achieved by adding AFRP fibers. The study reported that the AFRP fibers greatly outperformed PP fibers while providing benefits similar to those of steel fibers (Nanni 1992). It is important to mention that steel fibers are prone to losing a portion of their capacity as corrosion progresses, while aramid fibers would not undergo any conventional corrosion. Abeysinghe et al. (2017) tested twisted Technora fibers with a 40 mm length to investigate their contribution to the extreme load resistance of concrete panels. An aramid fiber volume of 1.0% was found to reduce crack widths and eliminate spalling due to exposure to extreme loads (Abeysinghe et al. 2017).

Zhao et al. (2018) investigated 30 mm long Technora aramid macrofibers at volumes between 0.2% and 1.2% for their contribution to limiting plastic shrinkage cracking and restrained drying shrinkage. The addition of aramid fiber volumes of 0.4% and higher was found to eliminate plastic shrinkage cracking. Furthermore, the study reported that the addition of aramid fiber volumes of 0.8% and higher can decrease drying shrinkage strain by 15% (Zhao et al. 2018).

Comparison Among Synthetic and Glass Fibers

The expected performance and service life of reinforced concrete structures can be significantly affected by the occurrence of deterioration, as investigated in several studies (Shafei 2011; Alipour et al. 2011, 2013; Shafei et al. 2012, 2013; Shafei and Alipour 2015a, 2015b; Cui et al. 2019; Khatami et al. 2021) at various length scales (Hajilar and Shafei 2014, 2015, 2016a, 2016b, 2018a, 2018b, 2019), with consequences that can go beyond an individual structure (Khatami et al. 2016, Kulkarni and Shafei 2018, Khatami and Shafei 2021). The addition of fibers can greatly alter many fresh and hardened properties of concrete, depending on the fibers' chemical and physical characteristics (Dopko et al. 2018, 2020; Karim et al. 2019; Karim and Shafei 2021b, 2021c; Veigas et al. 2022).

Based on several investigations reviewed for the present study with a focus on synthetic and glass fibers, this section provides a synthesis of the most common trends and observations regarding the performance of fibers in each of the following categories: stability and bond, workability, pre-peak mechanical properties, post-peak mechanical properties, and shrinkage (Shafei et al. 2021).

Stability and Bond

Portland cement concrete provides a highly alkaline environment with a pH value as high as 13.5, which protects steel rebars from corrosion. Such an environment has been proven to cause deterioration in some fiber types. Therefore, ensuring these fibers' long-term stability is of paramount importance. Among the fibers investigated, both silica and basalt glass fibers have been shown to degrade significantly in the concrete matrix, reflecting the need to employ methods to enhance the alkalinity tolerance of glass-based fibers. Such methods range from coating the individual fibers with alkali-resistant materials to covering the fibers with polymer resins. In addition, aramid fibers, especially the acid-spun type, have been reported to undergo notable degradation in concrete. Furthermore, PAN and PET fibers are susceptible to some level of degradation in alkaline environments. The other reviewed fibers, however, have shown great chemical stability in concrete.

When FRC is subjected to external loads, fibers tend to fail by pull-out and/or rupture. The distribution between these two modes of failure is a function of the fiber's elastic modulus and the fiber-matrix bond. As the modulus of elasticity decreases and the fiber-matrix bond increases, the majority of fibers tend to fail due to rupture. The bond between the individual fibers and the concrete matrix is often governed by the concrete's properties, such as water-to-cement ratio, and the fiber's characteristics, such as the material, length, and shape details. One of the main reasons for the addition of fibers to a concrete mixture is their ability to enhance the post-peak mechanical properties of the concrete by providing higher ductility and residual strength. Therefore, a high fiber-matrix bond that leads to sudden fiber ruptures is not favorable. On the other hand, a low fiber-matrix bond introduces other issues, particularly in limiting the capability of fibers to bridge cracks.

Therefore, an optimum bond is desired for fibers to have the best efficiency. PVA fibers form a hydrogenic bond with the concrete matrix, while the other fibers primarily have a mechanical bond. Thus, PVA fibers tend to fail due to rupture, and a high fiber-matrix bond is expected from them. Nylon, PAN, and PO fibers have been reported to form a relatively strong bond with the concrete due to the swelling and increase of friction during pull-out, irregular cross-sections, and damage during the mixing process, respectively. In contrast, PE fibers form a relatively weak bond with the concrete matrix, posing a challenge to its use in FRC. Several methods have been attempted to increase the strength of the fiber-matrix bond, with various degrees of success. Examples include using the fibrillated form of the fiber, changing the shape of the individual fibers, and using coating materials.

Workability

Regardless of the dosage and characteristics of fibers, the addition of fibers decreases the workability of concrete. This is further exacerbated when the fiber content is increased. Longer fibers can cause higher friction within fresh concrete, further reducing the workability of FRC mixtures. However, it should be noted that, for a fixed volume fraction, shorter fibers cause a greater decrease in workability due to their higher surface areas. Studies have shown that using proper admixtures, such as water reducers and pozzolans, and employing appropriate mixing

equipment can increase the maximum volume of fibers that can be included in FRC without causing workability issues.

PVA fibers can significantly decrease the workability of concrete due to their water absorption characteristics. Nylon fibers are also reported to have some water absorption characteristics. While this helps these types of fibers better disperse in the concrete at low volume fractions, a significant reduction in workability is anticipated at high volume fractions. Compared to other fiber types, basalt glass fibers are reported to mix well in concrete because they have a density similar to that of concrete.

Pre-Peak Mechanical Properties

Studies have reported sometimes contrary observations regarding the effects of fiber addition on the compressive strength of FRC. This can be attributed to the different properties of the concretes and fibers used in the experiments. When it comes to compressive strength, dense packing plays a key role in ensuring that the entrapped air is minimized. Therefore, regardless of fiber type, using short fibers at a low dosage can lead to an increase in compressive strength. This can be achieved rather easily, especially in concrete mixtures with a high water-to-cement ratio.

Moreover, the addition of fibers has been consistently reported to improve the splitting tensile and flexural strengths of concrete, with macrofibers resulting in more pronounced improvements in comparison to microfibers. Additionally, increasing the fiber content can result in higher splitting tensile and flexural strengths, as long as fibers are well dispersed. In general, the higher the fiber's modulus of elasticity, the better it can enhance the splitting tensile and flexural strengths of the concrete. Comparative studies have shown that glass fibers can better improve the flexural strength of concrete compared to PO fibers, high-tenacity PP fibers, and nylon fibers. It has also been found that high-modulus carbon and aramid fibers greatly help augment the splitting tensile and flexural strengths of concrete, as long as the minimum required fiber-matrix bond is provided.

Post-Peak Mechanical Properties

One of the main limitations of plain concrete is its brittle behavior after reaching its ultimate strength, which is captured in stress-strain curves as a peak and then a sharp drop. To overcome this drawback, fibers are incorporated into concrete mixtures to enhance the post-peak mechanical properties of concrete, such as ductility, toughness, and residual strength. Even low volumes of fibers have been proven effective in improving all of the post-peak mechanical properties of concrete, except for some reported cases involving compressive energy absorption. The reason for the overall positive contribution of fibers is their ability to bridge cracks, facilitating the transfer of residual stresses from one end of a crack to the other. Higher fiber contents provide more bridging pathways, which help convey more stresses and thus further increase the post-peak mechanical properties of FRC.

Studies have shown that microfibers are better in controlling microcracks, whereas macrofibers deliver better performance in limiting macrocracks. Because macrocracks are generated after the peak of the stress-strain curve is reached, macrofibers can be more efficient in enhancing the post-peak properties of concrete. High-modulus fibers, such as carbon and aramid, followed by glass fibers, have shown great potential to improve the post-peak mechanical properties of FRC. On the other hand, the contribution of nylon fibers to the post-peak mechanical properties of concrete is expected to be less than that contributed by PP, PVA, and HSPE fibers.

Shrinkage

Because concrete has a low tensile strength, shrinkage-induced cracks due to water consumption and/or loss can be a great concern for long-term durability. This is because when concrete loses water as a result of excessive evaporation, internal tensile stresses are generated that may exceed the concrete's tensile strength, leading to the formation and propagation of cracks.

To address the issue of shrinkage-induced cracks, several studies have investigated the effects of adding fibers to concrete. Regardless of their material and characteristics, fibers can greatly reduce the width and number of cracks while delaying the time of the first crack. Additionally, it has been found that the higher the fiber content, the fewer and narrower the shrinkage-induced cracks, to the extent that such cracks can be eliminated entirely. The fiber aspect ratio is a key factor affecting the performance of FRC in terms of shrinkage-induced cracking. Fibers with a higher aspect ratio have been shown to perform better in controlling shrinkage, and therefore microfibers can be more efficient than macrofibers in this regard. As a case in point, fibrillated PP fibers have shown great potential in limiting shrinkage-induced cracks due to their high aspect ratio.

CHAPTER 5. EXPERIMENTAL PROGRAM

In this research, a comprehensive study was carried out to investigate multiple crack mitigation strategies in concrete, including the use of supplementary and alternative cementitious materials and the addition of fiber to concrete mixtures. Additionally, the mechanical and durability properties of the concrete mixtures created for this study were determined. To fulfil these objectives, a three-stage investigation was performed.

In this chapter, the properties of the materials used in this project and the procedure used to mix the materials are discussed first, followed by an outline of the three stages of the investigation. In Stage 1, the best performing binder composition was identified. Stage 2 was designed to identify the effect of microfibers on the crack resistance, mechanical properties, and chloride resistance of FRC. In Stage 3, the mechanical properties of hybrid fiber-reinforced concrete (i.e., FRC with both microfibers and macrofibers) were investigated.

Material Properties

In this research, multiple SCMs and fibers were investigated. The replacement levels of the SCMs and the fiber volumes used in each stage of the study are described in the sections corresponding to the different stages below. The base mixture proportions are listed in Table 1, and the w/b ratio was selected to be 0.42.

Table 1. Base mixture proportions (lb/yd^3)

Ingredients	Water	Portland Cement	Coarse aggregate	Fine aggregate
Weight (lb/yd^3)	294	700.0	1,565.9	1,548.4

Ordinary portland cement Type I/II with a specific gravity of 3.1 was used as the primary binder following the requirements of ASTM C150. Type K cement, Class F fly ash, and silica fume were used as SCMs. The chemical composition of the binders is summarized in Table 2.

Table 2. Chemical composition of the binders used in the study (% weight)

Binder type	CaO	SiO_2	SO_3	Fe_2O_3	Al_2O_3	MgO	K_2O	Na_2O	TiO_2	Ye'elimite	Gypsum
Portland cement	62.94	20.10	3.18	3.09	4.44	2.88	0.61	0.10	0.24	-	1.40
Type K cement	65.40	1.80	25.10	1.20	4.80	1.40	0.10	-	-	19.30	15.00
Class F fly ash	15.78	50.87	0.61	5.27	20.17	3.19	1.09	0.69	1.29	-	-
Silica fume	0.30	94.30	-	0.09	0.09	0.43	0.83	0.27	-	-	-

PP, AR glass, and PVA were used as the macrofibers (see Figure 2a), while PP was the only microfiber type used (see Figure 2b).

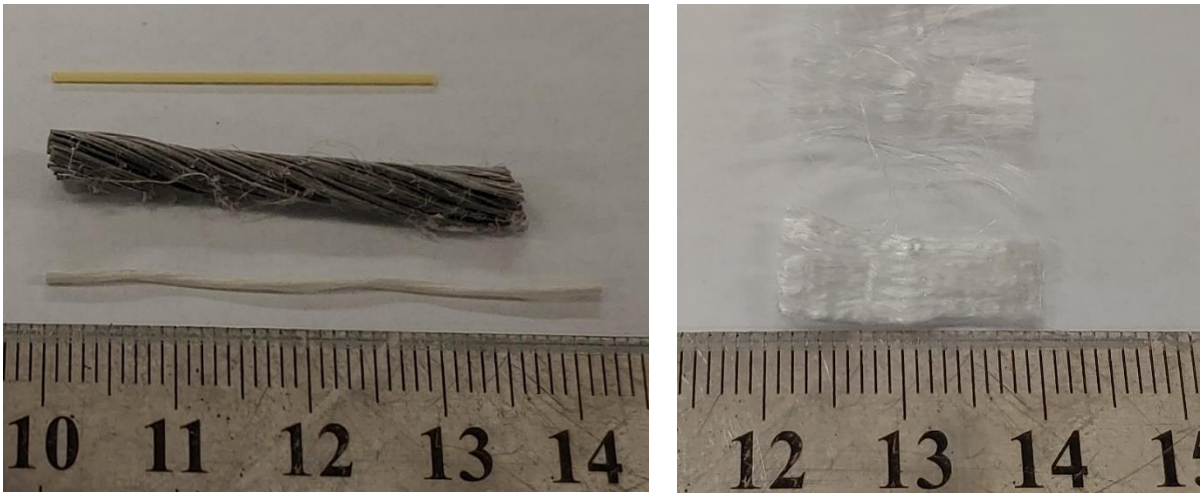

(a) (b)

Figure 2. Fibers used in the study: (a) from top to bottom, PVA, PP, and AR glass macrofibers and (b) PP microfibers

Table 3 presents the physical and mechanical properties of the fibers used in this study.

Table 3. Physical and mechanical properties of the fibers used in the study

Fiber type	Classification	Length (in.)	Tensile strength (ksi)	Shape	Density (lb/yd^3)
PP	Microfiber	0.75	83–96	Fibrillated	1,517
PP	Macrofiber	1.5	83–96	Twisted bundle	1,517
AR glass	Macrofiber	1.69	131	Twisted monofilament	4,382
PVA	Macrofiber	1.25	120	Straight monofilament	2,191

River sand and crushed aggregate with a maximum size of 1 in. were used as the fine and coarse aggregates, respectively. Additionally, regular water reducer was used to obtain the desired workability.

Mixing Procedure

A drum mixer was used to mix the ingredients. Initially, the coarse aggregates and one-third of water were mixed for 2 minutes. Then, the fine aggregates and another one-third of the water were added to the mixture, which was mixed for 2 additional minutes. Finally, portland cement, any SCMs, and the remaining water were added to the mixture, which was mixed for an additional 5 minutes. If any water reducer or fibers were needed, they were added during the final stage. After mixing, the concrete was cast in different molds (discussed in more detail in the

following sections) and tightly covered with a plastic sheet for 24±1 hours at room temperature. After that, the specimens were demolded and cured in a moist room until their testing age.

Stage 1. Binder Investigation

Plastic Shrinkage Cracking in Restrained Concrete Slabs

The procedure used to evaluate plastic shrinkage cracking in a restrained concrete slab followed the general procedure specified in ASTM C1579, Standard Test Method for Evaluating Plastic Shrinkage Cracking of Restrained Fiber-Reinforced Concrete (Using a Steel Form Insert). While this standard provided the foundation for the testing procedure, the actual procedure deviated slightly to best adapt the test to the research goals.

Test Matrix

In total, nine specimens were used to evaluate plastic shrinkage cracking in restrained slabs, as shown in Table 4.

Table 4. Test matrix for plastic shrinkage cracking in restrained concrete slabs

Specimen	% Type K	% Fly Ash (F)	% Silica Fume
0-0	0	0	0
7.5K-0	7.5	0	0
15K-0	15	0	0
0-15FA	0	15	0
7.5K-15FA	7.5	15	0
15K-15FA	15	15	0
0-7.5SF	0	0	7.5
7.5K-7.5SF	7.5	0	7.5
15K-7.5SF	15	0	7.5

Percent values are mass percentages.

The concrete mixes were chosen to evaluate and compare the plastic shrinkage behavior of concrete containing various types and proportions of SCMs. The nine slabs tested were categorized into three major groups, with each major group containing three individual slabs. The specimens were categorized into the major groups based on the type of pozzolanic SCM (if any) included in the concrete mix. Both Class F fly ash as well as silica fume were added as pozzolanic SCMs. The three major groups included Control (no pozzolanic SCM), Fly Ash (Class F), and Silica Fume. The three individual specimens in each of the three major groups varied in their proportion of Type K expansive cement. The mass percentages of Type K cement included in each of the three individual specimens were 0.0%, 7.5%, and 15.0%.

The goal of the test matrix was to evaluate the effects of various proportions of Type K expansive cement in the various concrete mixes. The specimens were separated into three major

groups in order to evaluate the influence of pozzolanic SCMs on the effectiveness of plastic shrinkage mitigation for a given percentage of Type K cement. Within each major group, the amount of pozzolanic SCM was held constant so that the effects of Type K cement on plastic shrinkage cracking could be evaluated.

Testing Equipment

Performing a restrained slab test involves mixing the concrete, casting it into a slab mold containing a steel insert, and placing the slab into an environment with the appropriate environmental conditions. The following equipment was used to perform these tasks:

- Concrete mixer – The type of concrete mixer is not specified in ASTM C1579; any mixer that provides an adequately hydrated and incorporated concrete mix will suffice. A drum mixer with a capacity of 3 ft^3 was utilized for this project.

- Mold – A rectangular plywood slab mold was used, with inside plan dimensions of 22 in. long by 15 in. wide by 4 in. high. The standard specifies the minimum mold height based on maximum aggregate size. For this project, the maximum aggregate size was 1 in.

- Internal restraint – An internal restraint serves two purposes in this test. First, the restraint limits the free shrinkage of the concrete, which in turn promotes plastic shrinkage cracking. In addition, the restraint creates thin portions in the slab that act as planes of weakness and ensure that plastic shrinkage cracking occurs in a consistent location between tests. The restraint dimensions are specified in ASTM C1579.

- Vibrating platform and finishing tools – A vibrating device is necessary to adequately consolidate the aggregate within the concrete. For this project, a vibrating platform was used, though a stick vibrator would also have sufficed as long as it met the frequency requirements in ASTM C1579. Once consolidated, the slab must be screeded, by trowel or other means, to create a surface on which plastic shrinkage cracks may be observed.

- Environmental chamber – To ensure the appropriate environmental conditions, the restrained slabs are placed in an environmental chamber. The environmental chamber used for this project allowed for the monitoring and control of temperature, humidity, and airflow. The sensors contained in the environmental chamber eliminated the need for additional sensors to monitor environmental conditions. ASTM C1579 outlines the necessary drying conditions.

- Variable-speed fan – Within the environmental chamber, a fan is required to create a constant source of airflow over the specimen. A constant source of wind promotes evaporation of bleed water and subsequent plastic shrinkage cracking.

- Sensors/instrumentation – As the concrete slab hydrates, the appropriate instrumentation must be set up to collect the desired data. For this project, a capillary pressure sensor system (CPSS) was used to record pore water pressure in the concrete specimens.

- Crack measurement system – To measure plastic shrinkage cracking, a system must be in place to capture images of the cracks and measure their widths. For this project, a handheld microscopic camera was used to collect images of cracks, with a scale bar included in every image to determine crack width.

Test Procedure

The first step in performing a restrained slab test is to design a concrete mix with the desired strength and slump characteristics. Mix proportions vary with the objectives of each research project. After mix design, the materials must be weighed, adequately mixed, and cast into the mold. The internal restraint is fixed to the inside of the mold to create planes of weakness in the concrete slab. The slab is cast and vibrated in two layers to achieve relatively even consolidation of the slab and avoid excess vibration and subsequent settlement in the concrete.

The appropriate slab depth was found through trial and error to be 1/4 in. below the top of the mold. Larger slab depths did not readily crack through the entire slab, and smaller slab depths resulted in excessive cracking of specimens even with large proportions of Type K expansive cement. Once the slabs were vibrated and screeded to an adequately smooth surface, they were carefully transported to the environmental chamber. If a slab experienced a disturbance while being moved, the surface was screeded upon placement in the environmental chamber.

Once the concrete slabs were placed in the environmental chamber, the necessary instrumentation was applied. For this project, the only instrumentation required was the placement of a CPSS in each freshly poured slab. The procedure for CPSS installation described below is not included in ASTM C1579 and is specific to this project. Note that certain instrumentation, such as an embedded strain gauge, may require installation prior to casting and screeding a slab.

Each CPSS was prepared prior to concrete mixing to allow adequate time for sensor preparation. Measuring pore water pressure through a CPSS requires a hydraulic connection between the drying concrete and the pressure transducer housed in the sensor. The entrance of air would disrupt the hydraulic connection and cause the sensor to record zero-gauge pressure. As a result, it was critical to degas the water used in the CPSS. The following procedure was used:

1. To prepare the sensors, water was first injected into the sensors themselves to ensure hydraulic contact with the pressure transducer.

2. Next, plastic sensor tips were filled with distilled water and securely connected to the sensor.

3. Once the sensors and tips were full of water, a syringe was used to place the water under vacuum at a pressure between 60 and 80 kPa for a minimum of 5 minutes, or until the sensor was adequately degassed. Based on testing experience, to ensure thorough degassing it is recommended to keep the vacuum applied for at least 15 minutes.

4. After applying the vacuum and agitating the sensor tip to remove air bubbles, the vacuum was removed and the sensor tips topped off with distilled water, if needed.

5. Once the sensor tips were degassed and filled completely, the sensors were temporarily set aside until applied to the slab.

This process was performed for as many sensors as needed for adequate capillary pressure monitoring. This project utilized four sensors per slab until one sensor became unusable, after which each test used three sensors. An instrumented slab inside the environmental chamber is shown in Figure 3.

Figure 3. Restrained slab instrumented with CPSS sensors

After instrumenting the fresh slabs with CPSS and beginning data collection, the fan in the environmental chamber was turned on and the test began. Capillary pressure data were collected for six hours as the slab dried in the environmental chamber. Throughout the drying process, the slab was checked intermittently for the formation of plastic shrinkage cracks. For this project, checks were performed every 30 minutes throughout the duration of the test. Once plastic shrinkage cracking was observed, a picture was taken of the crack with a 0.1 mm scale bar visible in the picture. This process was repeated until 6 hours had elapsed and the test was complete. Upon completion of the test, CPSS data were processed using spreadsheet software, and plastic shrinkage cracks were measured using photo processing software. To process the CPSS data and crack images, this project utilized Microsoft Excel and ImageJ, respectively.

The test procedure outlined above differs in some respects from the procedure specified in ASTM C1579. First, the procedure used in this project investigated the plastic shrinkage behavior of Type K cement concrete rather than FRC, as described in the standard. The test setup outlined in the standard provides a general scenario in which plastic shrinkage cracking may be investigated. The deviation for this project was only in the method used for plastic shrinkage cracking mitigation. The test procedure and observations are still valid when using Type K cement as opposed to fiber reinforcement. Second, slightly underfilling the mold promotes crack formation because the planes of weakness in the slab become even thinner. To accentuate the cracks formed in the first six hours, the mold was underfilled by 1/4 in. in this study, which differed from the standard in which the mold is filled completely. Finally, for this project evaporation was not monitored directly with a monitoring pan. Instead, water loss due to cement hydration as well as evaporation was derived from the CPSS results, specifically in the rate of capillary pressure development.

Testing Parameters

In this project, the restrained slab tests were primarily used to measure two parameters: capillary pressure and plastic shrinkage crack width. This section discusses how capillary pressure and plastic shrinkage crack width were measured during the restrained slab tests.

Capillary Pressure. Capillary pressure was measured through the CPSS mentioned above. As noted in the test procedure, a hydraulic connection between the concrete pore water and the CPSS pressure transducer was established. As free water in concrete is consumed either by cement and SCM hydration or bleeding and evaporation, a negative pressure develops within the water. This pressure development is described in the literature review above regarding the formation of plastic shrinkage cracks.

The negative pore water pressure in the drying concrete specimen was recorded by the CPSS. Processing the raw CPSS data showed the rate and magnitude of capillary pressure development in the concrete. However, care must be taken not to overestimate the importance of the pressure magnitude recorded by the CPSS. Due to the unpredictable nature of air entry into the concrete pore system or stray air bubbles in the sensor tip itself, the magnitude of capillary pressure is often highly variable. Potentially more meaningful is the rate of capillary pressure development in concrete. The rate of pressure development provides insight into the rate at which free water is consumed, and consequently the potential rate and severity of plastic shrinkage cracking. One would expect a specimen with a very slow rate of pressure development (i.e., a slow rate of water consumption) to experience delayed or less severe cracking than a specimen with a comparatively higher rate of pressure development. Adherence to or deviation from this expectation provides insight into the effectiveness of Type K cement as a means of plastic shrinkage cracking mitigation.

Plastic Shrinkage Crack Width. The widths of plastic shrinkage cracks were measured to quantify the magnitude of plastic shrinkage cracking that the concrete specimens experienced. As previously described, a handheld microscopic camera was used to collect images of plastic shrinkage cracks as they occurred and widened over the duration of the test. At the onset of

cracking, the crack was inspected using the camera to visually determine the approximate widest point in the crack. This point was chosen as the representative crack location because the widest location would allow for the most accurate measurement. Crack measurements are made with computer software, and a single pixel of error would more drastically affect a narrow crack than a wider crack because each pixel constitutes a larger percentage of the total crack width if the crack is relatively narrow.

When recording subsequent crack measurements, it was very important to ensure that the same location within the crack was observed for each measurement. Provided that the crack did not occur near the edge of the slab, it was assumed that each point in the crack expanded at the same rate. Therefore, while crack magnitude is undoubtedly important, the possibility for human error in selecting the widest point in the crack must be considered. Equally important to crack magnitude is the rate at which plastic shrinkage cracks expand, which was assumed to remain constant throughout the slab, excluding the edge portions. Similar to capillary pressure measurement, the rate of plastic shrinkage crack growth may be a more reliable metric than the observed crack magnitude, although both should be considered.

Digital Image Correlation

Unlike the test procedure discussed above, the use of digital image correlation (DIC) to measure strain in restrained concrete slabs does not adhere to a specific standard established by a testing organization. While DIC is a well-established tool for measuring displacement and strain, a specific test standard for using DIC to measure strain in restrained concrete slabs is not available. As a result, past experiments were used to determine the best approach for utilizing DIC to measure strain in restrained concrete slabs.

Test Matrix

For this project, DIC was used in conjunction with capillary pressure in restrained concrete slabs to investigate the plastic shrinkage behavior of Type K expansive cement. In total, four restrained concrete slabs were tested using DIC. Each slab contained an increasing proportion of Type K expansive cement. The mass percentages of Type K cement investigated in this project were 0.0%, 7.5%, 15.0%, and 22.5%, as shown in Table 5.

Table 5. Test matrix for strain measurement by digital image correlation

Specimen	% Type K
0K	0
7.5K	7.5
15K	15
22.5K	22.5

Percent values are mass percentages.

The goal of performing DIC testing was to determine the strain resulting from plastic shrinkage cracking in restrained concrete slabs. The strain within a restrained concrete slab as plastic

shrinkage cracking occurs is an indicator of potential crack development. Strain in restrained slabs undergoing plastic shrinkage cracking may be measured and compared by correlating capillary pressure and crack width results to determine the plastic shrinkage cracking behavior of concrete containing various proportions of Type K cement, as well as the relationships between strain, capillary pressure, and cracking.

Testing Equipment

Measuring strain though DIC testing involves casting restrained concrete slabs, taking a series of images as the slab dries, and processing the images using computer software. The mixing and casting of restrained concrete slabs used the same equipment as listed in the previous section on plastic shrinkage cracking. The additional equipment used to perform DIC testing was as follows:

- Chalk-based spray paint – DIC software requires an easily distinguishable pattern to be applied to the concrete surface in order to detect surface movements. Black and white chalk-based spray paint allowed for the application of a pattern to the concrete surface while minimizing the effects on evaporation rate (Bertelsen et al. 2019, Niu et al. 2019).

- Digital camera and tripod – A digital camera is required to record high-quality images of the concrete surface, which are then be uploaded to a computer for processing. For this project, a Canon T7 was used to capture images for DIC. A tripod was necessary to hold the camera steady for the duration of testing.

- Intervalometer – To capture images automatically at a set time interval, an intervalometer is required to engage the camera shutter. Some cameras contain this function internally, or external intervalometers are available for this purpose. Alternatively, a graphing calculator may be programmed to act as an intervalometer.

- DIC software – A software package is required to process the images of the concrete surface. Programs may be written for processing images for DIC, or readily available software may be used. For this project, MATLAB code was used for image processing.

Test Procedure

The first step in DIC testing is the casting of restrained concrete slabs. The procedure for casting restrained slabs is detailed in the previous section on plastic shrinkage cracking. The slabs cast for DIC testing were exactly the same as those used for the capillary pressure investigation described above, with the exception of the CPSS instrumentation. Once cast, the concrete slabs were prepared for drying and image collection following the procedure described in Bertelsen et al. (2019). The slabs were cast and subsequently left to begin drying at an ambient temperature for 45 minutes. At this time, the slabs were painted with black and white chalk-based spray paint. First, a base layer of white paint was applied to the slab, followed by a light, uniformly speckled coating of black paint. A speckled pattern was achieved by spraying the black paint roughly

horizontally and allowing it to fall downwards onto the white base layer. Once the paint was applied, 55 minutes after casting, the slab was transferred to the environmental chamber where image collection would take place.

At one hour after initial casting, image collection began as the slabs dried (Bertelsen et al. 2019). It is important to note that, unlike CPSS testing, a fan should not be applied to the slabs used for DIC testing because as this could affect the freshly painted surface. Testing proceeded for 6 hours after image collection began. Images were collected every 10 minutes throughout the testing period, for a total of 36 images for each test. Because cracks form and propagate relatively slowly, it was not necessary to collect images at shorter time intervals. Once the images were collected, they were processed with the help of DIC software to determine changes in the surface pattern relative to a physical scale placed next to the slab. The software was then able to output a strain map of the surface in question.

The use of chalk-based spray paint, as opposed to acrylic-based spray paint, is critical for allowing the concrete slab to adequately dry during the test period. Acrylic paint contains oil, which acts as a barrier to the water attempting to evaporate from the concrete surface. The use of a white acrylic base layer severely reduces the evaporation rate of concrete (Bertelsen et al. 2019, Niu et al. 2019). Evaporation and subsequent capillary pressure development result in plastic shrinkage cracking, and therefore a drastic reduction in evaporation would delay or eliminate the formation of plastic shrinkage cracks during the testing period. As a result, it is imperative that evaporation occurs during DIC testing (Bertelsen et al. 2019, Okeil et al. 2020). Bertelsen et al. (2019) showed that a concrete slab to which chalk-based spray paint has been applied results in a nearly identical rate of evaporation compared to a concrete slab with no paint applied to the surface (Bertelsen et al. 2019). As a result, the evaporation rate for restrained slabs painted with chalk-based spray paint is assumed to be equal to that of nonpainted slabs, such as those used for capillary pressure monitoring.

Testing Parameters

For this project, DIC was used to measure strain in restrained concrete slabs. As described above, the application of an even, white base layer followed by a uniform layer of black speckle pattern created a uniform pattern that was easily recognized by the DIC software, GOM Correlate. As restrained slabs dry, plastic shrinkage cracking takes place. Throughout the duration of plastic shrinkage cracking, images were collected of the surface of the concrete slab. Although invisible to the naked eye, tiny changes in the surface pattern occur as the slab shrinks and deforms. The uniform pattern created by the black and white spray paint provided a reference point against which the DIC software could easily recognize changes. In addition, the black speckle pattern overlaying the white base provided a relatively high-contrast surface, which helped the software detect the surface pattern.

The mechanism of strain calculation was fairly straightforward. Strain was determined using DIC software by measuring changes in the concrete surface pattern relative to the scale established prior to measurement. A scale was set by placing a ruler next to each restrained slab or by placing marks at a known distance apart next to the slab and within the frame of each

image. Once a scale was set in the software, changes in the surface pattern measured in pixels were converted to physical lengths using the scale. Dividing deformation by known length provided the surface strain for each restrained concrete slab.

Stage 2. Microfiber Investigation

Cracking Age of Concrete Under Restrained Shrinkage

The procedure used to determine the cracking age of concrete subject to restrained shrinkage followed the general procedure specified in ASTM C1581, Standard Test Method for Determining Age at Cracking and Induced Tensile Stress Characteristics of Mortar and Concrete under Restrained Shrinkage. This standard provided the general outline of the testing procedure, but slight modifications were made to best accomplish the research goals.

Test Matrix

For the investigation of cracking age under restrained shrinkage, eight specimens were examined. The goal of testing was to evaluate the effects of the proportion of PP microfiber reinforcement on the cracking age of concrete. Four different mix designs were considered, each with an increasing volume percentage of PP microfiber reinforcement. For each mix, two identical specimens were cast and tested in order to determine an average strain and compare cracking behavior between them.

Among the four mix designs tested under restrained shrinkage, the only differences were the proportions of PP microfibers and superplasticizer. While the percentage of PP microfiber reinforcement was changed to observe the effects on strain and cracking age, the dose of superplasticizer was adjusted according to fiber percentage simply to maintain workability for each mix. As noted in the previous chapter, proportions of PP microfiber exceeding approximately 1.0% may drastically reduce workability. Therefore, it was important to scale the superplasticizer percentage in proportion to the PP microfiber percentage in order to ensure adequate workability. The goal of testing was to determine the effect of PP microfiber percentage on drying strain and cracking age. The mix designs tested contained fiber volume percentages of 0.0%, 0.25%, 0.50%, and 1.0%. For each mix design, two specimens were tested. Table 6 presents the test matrix for determining the cracking age of FRC under restrained shrinkage.

Table 6. Test matrix for cracking age of concrete under restrained shrinkage

Specimen	% PP Microfiber
1a/b	0.00
2a/b	0.25
3a/b	0.50
4a/b	1.00

Percent values are volume percentages.
The “a/b” designation denotes two identical specimens for a given fiber proportion.

Testing Equipment

Performing a test of cracking age under restrained shrinkage, also called a ring test, involves mixing concrete, casting concrete into ring molds, and allowing the concrete to hydrate for 28 days in an appropriate environment. The following equipment was used to carry out testing:

- Concrete mixer – The type of concrete mixer is not specified in ASTM C1581; any mixer that provides an adequately hydrated and incorporated concrete mix will suffice. A drum mixer with a capacity of 3 ft^3 was utilized for this project.

- Vibrating platform and finishing tools – A vibrating device is necessary to adequately consolidate the aggregate within the concrete. For this project, a vibrating platform was used, though a stick vibrator would also have sufficed as long as it met the frequency requirements in ASTM C1581. Once consolidated, the slab must be screeded, by trowel or other means, to create a uniform surface.

- Steel inner ring – The steel inner ring provides shape to the concrete ring, as well as a surface against which the concrete ring may compress as the concrete hydrates. Compressive strain was measured by placing strain gauges on the inside face of the steel inner ring. The dimensions of the steel inner ring are provided in ASTM C1581.

- Strain gauges – As noted above, electrical resistance strain gauges were placed on the inside face of the steel inner ring to record the compressive strain caused by concrete drying. A minimum of two strain gauges is required by ASTM C1581.

- Outer ring – The outer ring serves to shape the concrete as it dries. No instrumentation was required on the outer ring because it was removed once the concrete could hold its shape. Dimensions of the outer ring are noted in ASTM C1581 to ensure an appropriate size for the concrete ring. Various nonabsorptive, nonreactive materials such as polyvinylchloride (PVC) or steel may be used for the outer ring, as noted in ASTM C1581.

- Base – The base that holds the concrete ring may be any nonabsorptive, nonreactive surface such as epoxy-coated plywood.

- Data acquisition system – A system compatible with the strain gauges must be in place to collect and store strain data. Details of the system requirements may be found in ASTM C1581.

Test Procedure

To perform a ring test, the first steps are to design the appropriate concrete mix and prepare the materials for mixing. It is important to set up the ring mold prior to mixing the materials to expedite the casting process. If necessary, a minimum of two electrical resistance strain gauges

can be mounted to the inside face of the steel inner ring. Strain gauges are mounted at mid-height and are oriented in the circumferential direction of the steel ring in order to measure hoop strain. Once instrumented, the steel inner ring and outer ring are coated with a release agent to prevent concrete adherence and are placed on the base. The rings are then secured in such a way that a 1.5 in. clear space is maintained between all points of the rings. In ASTM C1581, the rings are secured to the base. However, the inner and outer rings may be secured to each other using c-clamps and simply placed on top of the base.

Once the rings are securely in place with a 1.5 in. clear space, concrete mixing may begin. Next, the concrete is cast into the ring mold in accordance with the procedure outlined in ASTM C1581. For this project, two rings were cast for each mix design instead of the three recommended in ASTM C1581. Two rings were cast so that a sufficient amount of each mix could be allocated for use as cylinders to complete additional testing. As discussed in the results section, the use of two rings for each mix design appeared to provide adequate insight into the cracking behavior of the FRC mixes.

After casting, the concrete rings are transferred to the drying environment, and the outer ring is immediately loosened, either from the base or from the inner ring. Strain gauges are then attached to the data acquisition system. For this project, strain data were collected every 10 minutes. As per ASTM C1581, strain data should be collected at intervals of no more than 30 minutes.

For the first 24 hours of the drying process, the specimens are covered with polyethylene film to allow for moist curing. Once 24 hours have passed, the polyethylene film and the outer ring are removed from the concrete ring. The top of the surface of the concrete ring is then sealed with soft paraffin wax (i.e., petroleum jelly) and covered with aluminum foil to ensure that the outer face of the concrete ring is the only exposed surface, and consequently the only surface from which the ring may dry (see Figure 4). Each specimen is left in this state to hydrate for 28 days.

Figure 4. Concrete ring undergoing restrained shrinkage

Testing Parameters

Ring tests were performed for this project to investigate the compressive strain development of the drying specimens and the cracking age of FRC compared with plain concrete. This section discusses how strain and cracking age were determined from restrained shrinkage tests.

Compressive Strain. Compressive strain due to drying of the concrete ring was measured, as previously mentioned, using electrical resistance strain gauges. The electrical resistance resulting from the change in gauge wire diameter was converted by a computer program into a microstrain measurement. The drying of the concrete ring causes shrinkage and subsequent inward contraction of the concrete ring. The contraction of the concrete ring as it dries applies a compressive stress to the inner steel ring, which results in a compressive strain in the steel.

The rate of compressive strain development is a useful metric for comparing the relative rates at which different mixes experience drying and subsequently experience shrinkage. The only variable between mixes in this study was PP microfiber percentage. Because the fibers do not chemically react with water and workability is achieved through superplasticizer to keep water demand constant for each mix, the rate of drying was expected to be very similar for each mix. The magnitude of compressive strain provides insight into the extent of drying and shrinkage experienced by a given specimen. Due to the similar rates of strain development, constant environmental conditions, and fixed drying time for each specimen tested, compressive strain magnitudes were expected to be similar for each specimen.

Cracking Age. The cracking age of a concrete ring under restrained shrinkage was determined by examining the compressive strain data. Crack formation was evidenced by a sudden jump in negative (i.e., compressive) strain to approximately zero strain in the steel inner ring. As shrinkage occurs, tensile stress accumulates in the uncracked concrete ring. In the event that the shrinkage-induced tensile stress exceeds the tensile strength of the concrete, shrinkage cracking occurs in the concrete ring. The sudden cracking of the concrete ring renders it unable to resist tensile stress. In other words, the concrete ring no longer has the tensile capacity to constrict around the steel inner ring, causing the strain in the steel ring to suddenly return to zero. A specimen that does not experience cracking during the 28-day drying time would show a continuous decline in strain (i.e., increasing magnitude of compressive strain) for the entire testing period with no sudden jumps to zero strain.

Splitting Tensile Strength of Concrete

The procedure used to determine the splitting tensile strength of concrete cylinders followed the general procedure specified in ASTM C496, Standard Test Method for Splitting Tensile Strength of Cylindrical Concrete Specimens. The test procedure outlined in the standard did not require modification to better suit the research goals (Shi and Shafei 2021).

Test Matrix

Splitting tensile tests are performed on concrete cylinders to determine tensile strength and concrete cracking potential when used in conjunction with ring test results. As such, the test matrix for splitting tensile testing looks very similar to that used for determining cracking age under restrained shrinkage. The same mixing precautions used for mixing FRC rings, particularly the use of superplasticizer in proportion to PP microfiber percentage, applied to the splitting tensile test specimens because both specimens were taken from the same mix. Like the test matrix shown in Table 6, the concrete mixes were differentiated by PP microfiber proportion, with volumes of 0.0%, 0.25%, 0.50%, and 1.0%. However, for each mix design, three specimens were tested for splitting tensile strength at 7, 14, and 28 days. Testing three specimens at three different ages called for nine cylindrical specimens in total for each mix design. Table 7 illustrates the test matrix for determining the splitting tensile strength of concrete.

Table 7. Test matrix for splitting tensile strength

Specimen	Age (days)	% PP Microfiber
1-7a/b/c	7	0.00
2-7a/b/c	7	0.25
3-7a/b/c	7	0.50
4-7a/b/c	7	1.00
1-14a/b/c	14	0.00
2-14a/b/c	14	0.25
3-14a/b/c	14	0.50
4-14a/b/c	14	1.00
1-28a/b/c	28	0.00
2-28a/b/c	28	0.25
3-28a/b/c	28	0.50
4-28a/b/c	28	1.00

Percent values are mass percentages.
The “a/b/c” designation denotes three identical specimens for a given age and fiber proportion.

Testing Equipment

Performing splitting tensile strength tests, otherwise known as split cylinder tests, involves mixing concrete, casting concrete into cylindrical molds, and allowing the concrete to cure for various time periods in a moist curing environment. The following equipment was used to carry out testing:

- Concrete mixer – The type of concrete mixer is not specified in ASTM C496; any mixer that provides an adequately hydrated and incorporated concrete mix will suffice. A drum mixer with a capacity of 3 ft^3 was utilized for this project.

- Cylindrical molds – For this project, the inside length and diameter of the cylindrical molds were 8 and 4 in., respectively. Possible specimen dimensions are available in ASTM C192.

- Vibrating platform and finishing tools – A vibrating device is necessary to adequately consolidate the aggregate within the concrete. For this project, a vibrating platform was used, though a stick vibrator would also have sufficed as long as it met the frequency requirements in ASTM C496. Once consolidated, the slab must be screeded, by trowel or other means, to create a uniform surface.

- Testing machine and bearing device – A testing machine is required for loading the specimens to create diametric tension. To hold the specimens in place and ensure even bearing, each specimen was placed inside a bearing device. The bearing device must be able to withstand the specimen loading as well as evenly distribute pressure to the specimen. Details on the device materials and geometry are provided in ASTM C496.

Test Procedure

The first steps in performing a splitting tensile test are designing and mixing the concrete to be tested. Note that the plastic cylindrical molds used for this project need not be coated in a release agent because they are simply cut away from the specimen. After mixing, the concrete is cast into the cylindrical molds in two layers, vibrating on a platform to consolidate. Once full, the concrete cylinders are screeded to minimize the surface roughness of the top face. The cylinders are then tightly closed and set to cure in a nonmoist curing environment for 24 hours. Once 24 hours have passed, the concrete cylinders are extracted from the molds and placed into a moist curing chamber to continue curing.

Splitting tensile tests were performed on the PP FRC samples at 7, 14, and 28 days. Each round of testing followed the same procedure. Three specimens were removed from the moist curing chamber and allowed to air dry for 5 to 10 minutes. Once surface dry, the specimens were loaded into the bearing device, which itself was loaded into the testing machine. The bearing device used in this study consisted of a steel base, vertical steel arms, and a steel bearing bar. The specimens were placed on a 1/8 in. strip of plywood that rested on the steel base. The concrete specimens were then placed against the vertical steel arms to prevent the cylinders from rolling. Finally, a second strip of plywood was placed on top of the specimens and underneath the steel bearing bar that makes contact with the testing machine actuator. A concrete cylinder set up in the testing machine is shown in Figure 5.

Figure 5. Concrete cylinder and bearing device loaded into the testing machine

For this project, the cylinders were loaded at 150 psi/min, which is the middle of the range specified in ASTM C496, 100 to 200 psi/min. The testing machine was set to cease loading once a 10% strength reduction was recorded in the specimen.

Testing Parameters

Splitting tensile tests were performed in this project to compare the tensile strength and cracking potential of FRC specimens at different stages of the curing process. This section discusses how tensile strength and cracking potential were determined using split cylinder tests.

Tensile Strength. The tensile strength of concrete was determined indirectly from split cylinder testing. For this project, only peak compressive load data were directly obtained through split cylinder testing. To provide useful information regarding tensile strength, this compressive load was used in the calculation of splitting (i.e., peak) tensile stress. Calculating the tensile stress at which the cylinder split diametrically provides the tensile strength of concrete for a given mix and age.

Cracking Potential. Similar to tensile strength, cracking potential is a parameter that was obtained indirectly from both the split cylinder and ring tests. As outlined by Dopko (2018), essentially the strain development graph obtained through ring testing may be compared with the tensile strength development profile obtained through splitting tensile testing to determine the cracking potential of a concrete specimen. Through a series of calculations that are explored further in the results section, the cracking potential of a concrete specimen at a given age was taken as the ratio of the actual maximum stress caused by shrinkage over the tensile strength of the concrete. Determining cracking potential allows for the comparison of cracking likelihood between two specimens that may not show any cracking.

Compressive Strength of Concrete

The procedure used to determine the compressive strength of concrete cylinders followed the general procedure specified in ASTM C39, Standard Test Method for Compressive Strength of Cylindrical Concrete Specimens. The test procedure outlined in the standard did not require modification to better suit the research goals.

Test Matrix

Compressive strength tests were used in this project as an overall assessment and comparison of the 28-day strength development of FRC mixes. Similar to the splitting tensile test specimens, the specimens tested for 28-day compressive strength were cast from the same FRC mixes used in the ring tests. As a result, compressive strength testing was performed on PP FRC specimens with fiber volumes of 0.0%, 0.25%, 0.50%, and 1.0%. In contrast to split cylinder testing, compressive tests are only carried out on concrete cylinders once they have reached 28 days of moist curing and are assumed to be fully cured. This project was not concerned with compressive strength development over time, but instead aimed to compare the fully cured 28-day compressive strength among various FRC mixes in conjunction with the cracking behavior of the FRC. For each of the four FRC mix designs tested, three cylindrical specimens were tested for 28-day compressive strength. Table 8 illustrates the test matrix for determining the 28-day compressive strength of concrete.

Table 8. Test matrix for compressive strength of concrete

Specimen	% PP Microfiber
1a/b/c	0.00
2a/b/c	0.25
3a/b/c	0.50
4a/b/c	1.00

Percent values are volume percentages.
The “a/b/c” designation denotes three identical specimens for a given fiber proportion.

Testing Equipment

Performing compressive strength tests involves mixing concrete, casting the concrete into cylindrical molds, and allowing the concrete to cure for 28 days in a moist curing environment. Note that the mixing and casting of cylindrical specimens for compressive strength testing follows the same procedure as that used to cast cylinders for split cylinder testing. The following equipment is unique to compressive strength testing:

- Testing machine and bearing blocks – A testing machine with a sufficient loading capacity and loading rates is required to ensure compressive failure of the specimens. In addition, steel bearing plates are required at the top and bottom of the concrete cylinder to ensure even pressure distribution throughout the specimen and protect the testing machine actuator.

Test Procedure

The initial steps in compressive strength testing, from concrete mix design to beginning the moist curing of the cylinders, are identical to those in split cylinder testing. For this project, specimens were cast from the same FRC mixes used for the split cylinder tests and were cured under identical conditions. Where the procedures begin to differ is the curing times for the concrete cylinders. This project investigated the 28-day compressive strength of concrete cylinders, meaning that no specimens were tested prior to reaching their 28-day compressive strength. At 28 days, the concrete cylinders were removed from the curing chamber to air dry for 5 to 10 minutes. After drying, the specimens were placed into the testing machine with bearing blocks above and below the cylinder. Using an appropriate rate of loading as outlined in ASTM C39, each specimen was then loaded under axial compression until the load was reduced to at most 95% of the peak compressive load. For this project, a loading rate of 35 psi/sec was used in accordance with ASTM C39, and failure was indicated by a reduction in load to 90% of the peak load.

Testing Parameters

Compressive strength tests were performed for this project to determine and compare the 28-day compressive strengths of different FRC mixes. The compressive strength of concrete was calculated indirectly from the peak compressive loads and the geometries of the cylindrical specimens. Although not directly measured, compressive strength was calculated very intuitively simply by dividing the peak compressive load observed during testing by the cross-sectional area of the concrete cylinder. The calculation allowed the peak compressive force to be normalized into a compressive stress that could be used to compare concrete specimens of any geometry.

Chloride Penetration by Rapid Migration

The procedure used to predict chloride penetration into concrete followed the general procedure specified in AASHTO T 357-15, Standard Method of Test for Predicting Chloride Penetration of Hydraulic Cement Concrete by the Rapid Migration Procedure. This standard provided the general outline of the testing procedure, but slight modifications were made to best accomplish the research goals.

Test Matrix

The investigation of chloride penetration in this research involved testing 12 FRC specimens in total. The goal of rapid migration testing (RMT) is to investigate the effects of PP microfiber proportion on the rate of chloride penetration into concrete. Four FRC mix designs were examined in this project, and for each mix three identical FRC discs were tested for chloride penetration. The specimens used for RMT were produced from concrete cylinders, similar to those used in the other tests discussed above. However, for RMT the FRC cylinders were cut into discs 2 in. in length and 4 in. in diameter.

Similar to the other FRC test matrices, the mixes tested under RMT varied only in their proportion of PP microfibers. The fiber percentages used in this project were 0.0%, 0.25%, 0.50%, and 1.0% by volume. The concrete cylinders were moist cured and at 27 days were cut into discs and placed back into the curing chamber until 28 days. Because RMT is focused on chloride penetration in concrete that has been cured for 28 days, it is unnecessary to test samples at various stages of curing. As a result, only three discs were tested for each mix design. Table 9 illustrates the test matrix for determining chloride penetration in FRC.

Table 9. Test matrix for chloride penetration by rapid migration

Specimen	% PP Microfiber
1a/b/c	0.00
2a/b/c	0.25
3a/b/c	0.50
4a/b/c	1.00

Percent values are volume percentages.
The "a/b/c" designation denotes three identical specimens for a given fiber proportion.

Testing Equipment

Performing RMT involves cutting and conditioning concrete specimens and setting up an electrolytic cell to accelerate the penetration of chloride ions into concrete. The following equipment was used to perform the necessary tasks:

- Water-cooled diamond saw – To cut concrete cylinders into the discs required for RMT, a water-cooled diamond saw is necessary to achieve straight, accurate cuts without damaging the cut surfaces of the discs.

- Vacuum desiccator with pressure gauge – A vacuum desiccator is used to condition concrete discs for testing. The desiccator must be capable of fitting at least three specimens and allow for two valve-operated hose connections for regulating pressure and water flow. A pressure gauge is necessary to accurately pressurize the desiccator.

- Vacuum pump – A vacuum pump is required to pressurize the desiccator. The capacity of the pump must be adequate for proper conditioning of the specimens. For this project, a negative pressure of 25 psi was maintained for conditioning.

- Plastic reservoir – A plastic reservoir serves as the housing for the cathode portion of the electrolytic cell setup for RMT. The reservoir must be of sufficient size for the cathode to be submerged in solution.

- Cathode and plastic support – A section of steel mesh serves as the cathode submerged in solution. The cathode rests on a plastic support so that both are resting at approximately a 20° to 30° angle in the plastic reservoir.

- Rubber sleeve and metal clamps – The concrete discs are contained in rubber sleeves with an inner diameter matching the diameter of the specimens (2 in.). The sleeve is fixed tightly around each specimen by the use of two metal clamps, one near each end of the disc. Clamps should be sufficiently tight to ensure that sleeves are watertight around the discs.

- Anode – Steel mesh serves as the anode. The mesh is formed into circles that are placed on the top ends of the concrete discs inside their rubber sleeves and is submerged in solution. A portion of the anode extends out of the rubber sleeve so that it can be attached to the power supply.

- Power supply and ammeter – An external power supply is required to apply electricity to the electrolytic cell. The amperes delivered by the power supply must be monitored by an ammeter. The power supply used in this project contained an ammeter.

- Caliper – A caliper is necessary to accurately measure chloride penetration depth into the concrete specimens upon completion of testing.

- Sodium chloride – Sodium chloride is used to create a 10% by mass NaCl solution in which the cathode is submerged.

- Sodium hydroxide – Sodium hydroxide is used to create a 0.3 N NaOH solution in which the anode is submerged.

- Silver nitrate solution – A 0.1 M silver nitrate solution is sprayed on the specimens upon completion of testing. The solution reacts with the chloride and creates a clear profile of the chloride penetration depth.

Test Procedure

To perform RMT, concrete specimens are first cut from cured cylinders. Specimens are cut using a water-cooled diamond saw. To ensure uniformity among the cut faces of the test specimens, approximately 1 in. is cut away from each side of the concrete cylinder and discarded. The rest of the concrete cylinder is cut into three specimens, each with two cut faces. The concrete specimens are then conditioned in a desiccator prior to testing. Conditioning involves placing clean specimens into a dry desiccator while a negative pressure of 25 psi is maintained for 3 hours. While running the vacuum pump, a hose is placed over one of the desiccator valves, and the other end is submerged in water. The desiccator valve is then opened until the specimens are covered with degassed water. While the specimens are submerged, a negative pressure of 25 psi is maintained for an additional 1 hour. Once the hour has passed, the vacuum in the desiccator is released, and specimens are left submerged at atmospheric pressure for 18 hours.

After 18 hours, the specimens have been sufficiently conditioned for testing. Before testing, the NaCl and NaOH solutions are prepared. The NaCl solution must be able to submerge the cathode

in solution, and the exact volume required varies based on the plastic reservoir used. The NaOH solution is prepared by dissolving 12 grams of NaOH in one liter of distilled water to create a solution of 0.3 normality. For three test specimens, one liter of NaOH solution provides enough solution to submerge the disc portion of the steel anodes. If larger test setups are used, more NaOH solution may be required.

Once mixed, the NaCl solution is poured into the plastic reservoir to sufficiently cover the plastic support and steel mesh cathode. Next, the concrete specimens are removed from the desiccator and placed into rubber sleeves, with one face of the specimen flush with one end of the sleeve. Clamps are placed around the sleeves, near the top and bottom of each disc, to prevent solution from leaking past the specimens during testing. The sleeves are then placed, specimen side down, onto the steel cathode submerged in the NaCl solution. It is important to ensure that small rubber pads are placed between the specimen and the steel mesh to prevent direct contact; the current is meant to flow through the NaCl and NaOH solutions in contact with the concrete specimens. Next, the steel mesh anode is placed into the rubber sleeves on top of the specimens. Again, small rubber pads are placed between the specimen and the anode to prevent direct contact. The sleeves are then filled with enough NaOH solution to submerge the circular portion of the anode.

Once the specimens are placed into the sleeves and the specimens, cathode, and anode are in contact with the appropriate solutions, the cathode and anode are connected to the power supply. Because the cathode is a single piece of steel mesh, a single connection is made between the cathode and the negative terminal of the power supply. In contrast, one anode is placed for each individual specimen, and as many connections are required as the number of specimens (three for this project). Each anode is connected to the positive terminal of the power supply. The complete test setup is shown in Figure 6.

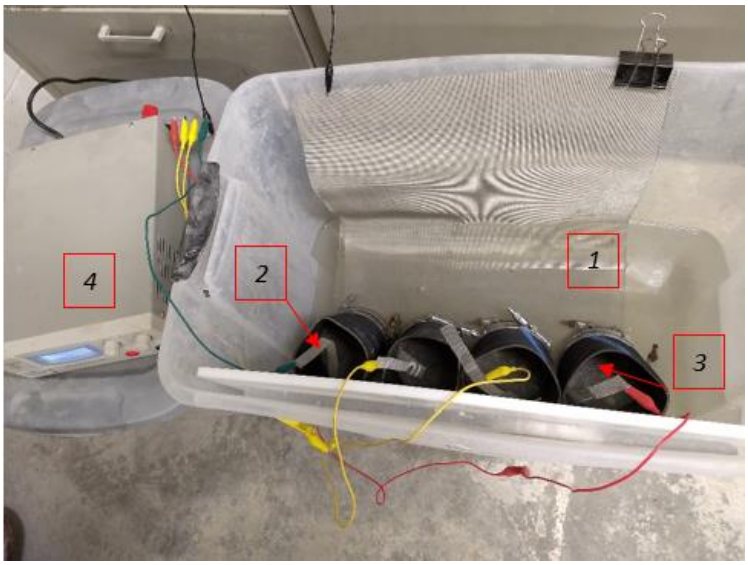

Figure 6. RMT setup: (1) cathode in NaCl solution, (2) anode in NaOH solution, (3) specimen in rubber sleeve, (4) power supply

The power supply is switched on and set to a potential of 30.0 V to begin the RMT. At this point, the temperature of the NaOH solution for each specimen is recorded. The power supply is turned off after 24 hours, at which point the chloride penetration is terminated.

After disassembling the electrolytic cell and removing each specimen from its rubber sleeve, the specimens are split diametrically in a loading machine to separate each disc into two equal halves, each 2 in. in length with a half-circular cross-section. The split face of each piece is then sprayed with silver nitrate solution. After 10 to 15 minutes, white silver chloride precipitate is easily visible on the split face of the specimen. A caliper is used at seven locations along the face of the specimen to measure the depth to which chloride has penetrated each specimen. This procedure is repeated for each FRC mix design to determine average chloride penetration depth.

Testing Parameters

For this project, RMT was performed to determine the effects of various PP microfiber percentages on chloride penetration depth. Chloride penetration depth was directly measured on the split face of each specimen. The silver chloride precipitate formed from the reaction between the silver nitrate applied to the split face of each specimen and the sodium chloride that penetrated into the specimens made the depth of chloride penetration easily visible with the naked eye. Once visible, the depth of chloride penetration was simply measured with a caliper at seven locations along the split face of each specimen.

The electrical potential applied across each concrete specimen creates an electrolytic cell that forces the chloride ions present in the NaCl solution to migrate into the concrete disc. Negatively charged chloride ions are driven towards the positively charged anode by the potential applied across the electrolytic cell. In this test setup, the steel mesh submerged in NaCl solution acted as the cathode. Electrons were applied from the power source to the cathode, resulting in a negative charge. Negative chloride ions, as a result, were driven through the concrete specimens towards the steel mesh submerged in the NaOH solution, which served as the positively charged anode. Establishing an electrolytic cell forced chloride ions into the concrete at an accelerated rate compared to what a concrete element experiences in service. The accelerated chloride penetration resulting from RMT allowed for a comparison of chloride penetration depths among different concrete mixes. By comparing the penetration depth with the test duration, the chloride penetration rates between mixes could also be compared.

Stage 3. Hybrid Fiber Investigation

In this stage, the mechanical properties of hybrid fiber-reinforced concrete were investigated. For this purpose, the compressive strength, splitting tensile strength, and flexural strength of hybrid FRC specimens were measured. The compressive strength tests were carried out after 7, 28, and 56 days following the same procedure used in Stage 2. The splitting tensile strength tests were conducted on the hybrid FRC specimens after 28 days of curing following the procedure used in Stage 2. For both of these tests, the binder content was selected based on the results of Stage 1, which are explained in detail in Chapter 6, and the fiber combinations were similar to those employed in the flexural strength tests, which are discussed in the following section.

Flexural Strength of Concrete

The procedure used to measure the flexural strength of fiber-reinforced concrete is discussed in ASTM C1609, Standard Method for Flexural Performance of Fiber-Reinforced Concrete (Using Beam with Third-Point Loading). This standard provided the general outline of the testing procedure, but slight modifications were made to best accomplish the research goals.

Test Matrix

Three-point bending tests are performed on concrete beams to determine the flexural strength and toughness of fiber-reinforced concretes. As shown in Table 10, PP microfibers were used as the only type of microfiber, while three types of macrofiber were employed: PP, AR glass, and PVA.

Table 10. Test matrix for flexural strength

Specimen	% PP Microfiber	% PP Macrofiber	% AR glass Macrofiber	% PVA Macrofiber
OPC	0	0	0	0
P0-125	0	0.125	0	0
P0-25	0	0.25	0	0
P0-50	0	0.50	0	0
P1-125	0.0625	0.125	0	0
P1-1875	0.0625	0.1875	0	0
P1-25	0.0625	0.25	0	0
P2-125	0.125	0.125	0	0
P2-25	0.125	0.25	0	0
G0-125	0	0	0.125	0
G0-25	0	0	0.25	0
G0-50	0	0	0.50	0
G1-125	0.0625	0	0.125	0
G1-1875	0.0625	0	0.1875	0
G1-25	0.0625	0	0.25	0
G2-125	0.125	0	0.125	0
G2-25	0.125	0	0.25	0
V0-125	0	0	0	0.125
V0-25	0	0	0	0.25
V0-50	0	0	0	0.50
V1-125	0.0625	0	0	0.125
V1-1875	0.0625	0	0	0.1875
V1-25	0.0625	0	0	0.25
V2-125	0.125	0	0	0.125
V2-25	0.125	0	0	0.25

Percent values are volume percentages.

In total, 25 mixes were made, and for each mixture three specimens were tested for flexural strength at 28 days. It can be seen in Table 10 that two levels of microfiber, 0.0625% (approximately 1 lb/yd^3) and 0.125% (approximately 2 lb/yd^3), were used along with four levels of macrofiber, 0.125%, 0.1875%, 0.25%, and 0.50%.

Testing Equipment

Performing three-point bending tests involves mixing concrete, casting concrete into beam molds, and allowing the concrete to cure in a moist curing environment. The following equipment was used to carry out testing:

- Concrete mixer – The type of concrete mixer is not specified in ASTM C1609; any mixer that provides an adequately hydrated and incorporated concrete mix will suffice. A drum mixer with a capacity of 3 ft^3 was utilized for this project.

- Beam molds – For this project, the inside length, width, and height of the beam molds were 14, 4, and 4 in., respectively. Possible specimen dimensions are available in ASTM C1609.

- Vibrating platform and finishing tools – A vibrating device is necessary to adequately consolidate the aggregate within the concrete. For this project, a vibrating platform was used, though a stick vibrator would also have sufficed as long as it met the frequency requirements in ASTM C1609. Once consolidated, the slab must be screeded, by trowel or other means, to create a uniform surface.

- Testing machine – A testing machine is required to load the specimens to create a pure bending moment in the midspan. To hold each specimen in place and ensure the symmetrical generation of the pure bending moment, the length of each beam was divided into three 4 in. sections. Two rods were used to load the edges of the middle section (see Figure 7), and a direct current differential transformer (DCDT) was installed to measure the deflection of the midspan at 0.1-second intervals. More details on the device settings and special provisions are provided in ASTM C1609.

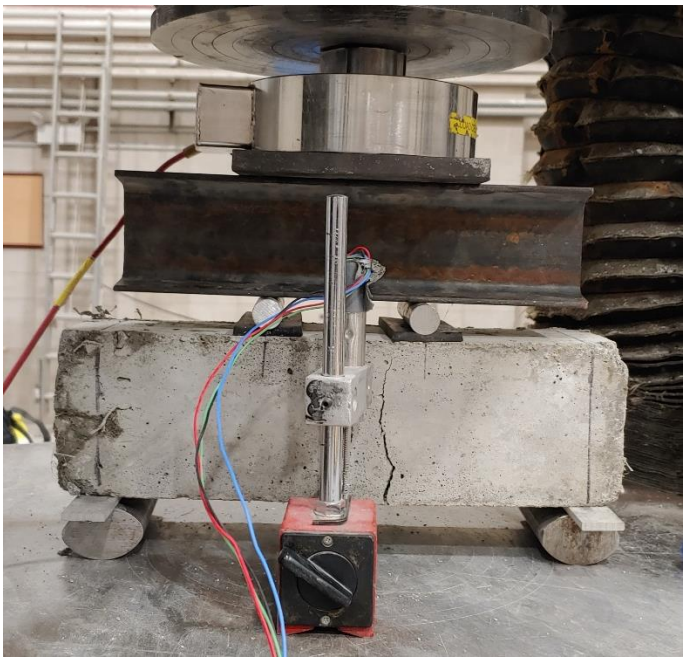

Figure 7. Three-point bending test setup

Test Procedure

The first steps in performing a three-point bending test are designing and mixing the concrete to be tested. After mixing, the concrete is cast into beam molds in two layers, vibrating on a platform to consolidate. (Note that the beam molds used for this project needed to be coated in a release agent.) Once the molds are full, the concrete beams are screeded to minimize the surface roughness of the top face. The beams are then tightly covered with a plastic sheet and set to cure in a nonmoist curing environment for 24 hours. Once 24 hours have passed, the concrete beams are demolded from the molds and placed into a moist curing chamber to continue curing.

In this study, flexural strength tests were performed on the hybrid FRC specimens at 28 days. Each round of testing followed the same procedure. Three specimens were removed from the moist curing chamber and mounted on the setup shown in Figure 13. For this purpose, the beams were mounted on two elliptical rods 12 in. apart from each other. Two additional rods were then placed on top of the specimen at a distance of 4 in. from each support. Finally, an L-shaped piece of metal was glued to the center of each beam and a DCDT was used to record the deflection of the midspan of the beam at 0.1-second intervals.

Testing Parameters

Three-point bending tests were performed in this project to compare the flexural strength and toughness of FRC specimens with different fiber combinations. This section discusses how flexural strength and toughness were determined using three-point bending tests.

Flexural Strength. The flexural strength of concrete was determined indirectly from the three-point bending tests. For this project, the load and deflection at the midspan were continuously recorded. The peak load was used to measure the flexural strength of the FRC, which can be calculated using Equation 1.

$$f = \frac{PL}{bd^2} \quad \textbf{(1)}$$

where:

f = flexural strength (psi)

P = peak load (lbf)

L = span length (in.)

b = average width of the specimen at the fracture (in.)

d = average depth of the specimen at the fracture (in.)

Toughness. The toughness of FRC was measured indirectly by calculating the total area under the load-deflection curve up to a net deflection of 1/150 of the span length.

CHAPTER 6. RESULTS AND DISCUSSION

Stage 1. Binder Investigation

This section describes the investigation of concretes with multiple binder compositions for their performance in terms of restrained plastic shrinkage. The best performing combination of binders was selected as the primary mix design, as discussed in the following sections.

Plastic Shrinkage Cracking in Restrained Concrete Slabs

The experimental results for the testing parameters investigated for restrained concrete slabs are discussed in the following sections. Data are presented for capillary pressure and plastic shrinkage crack width.

Capillary Pressure

The general capillary pressure behavior exhibited by the restrained slab specimens is illustrated in Figures 8 through 10.

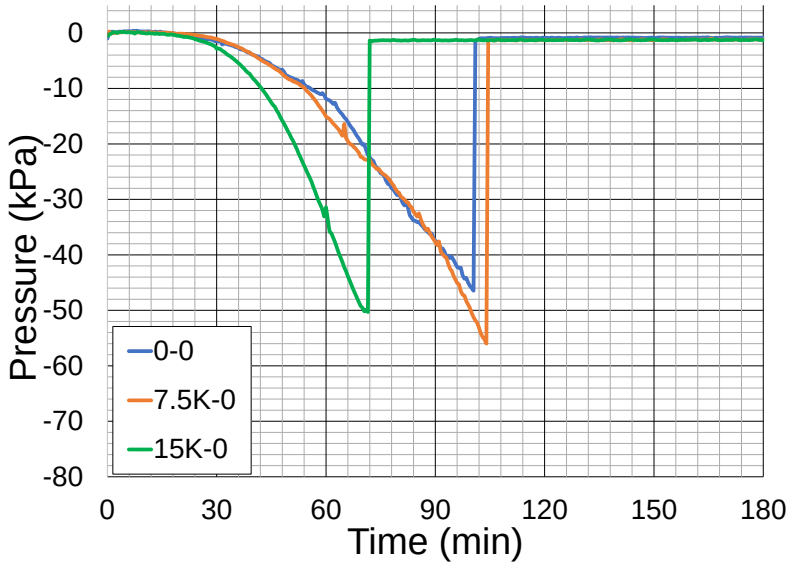

Figure 8. Capillary pressure development rates for Specimens 0-0 (Control), 7.5K-0, and 15K-0

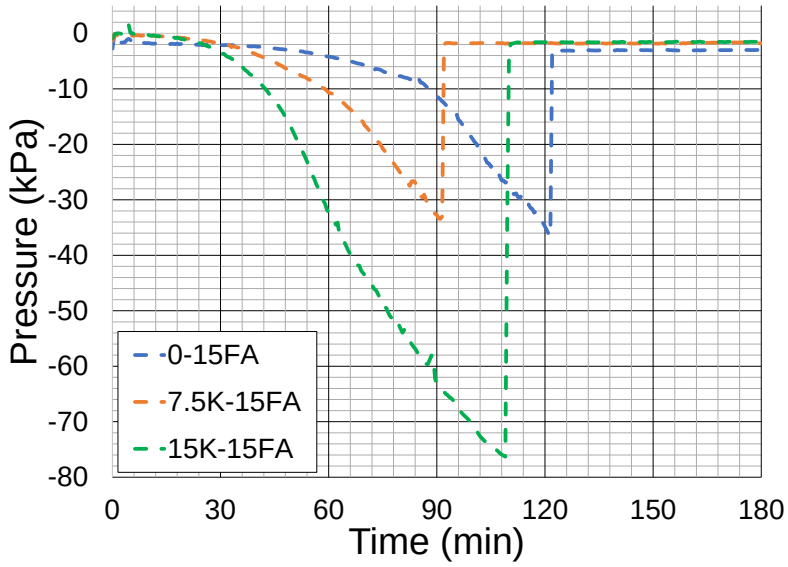

Figure 9. Capillary pressure development rates for Specimens 0-15FA, 7.5K-15FA, and 15K-15FA

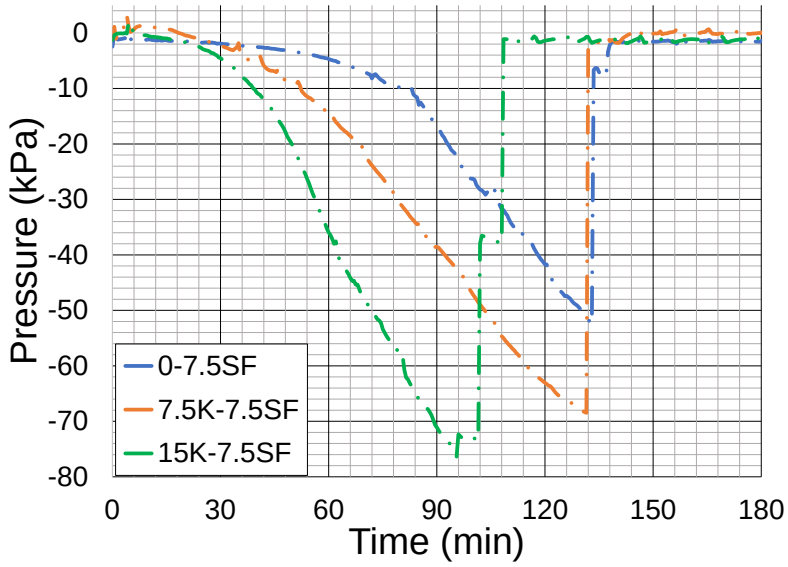

Figure 10. Capillary pressure development rates for Specimens 0-7.5SF, 7.5K-7.5SF, and 15K-7.5SF

The capillary pressure plots seem to verify certain expected behavior based on the literature review. For instance, when comparing mixes with 0% Type K cement, Figures 10 shows an increased rate of capillary pressure development compared with the control mixture in Figure 8. Such behavior agrees with the literature, in that silica fume increases the water demand of concrete. On the other hand, fly ash is shown to be effective in decreasing the rate of capillary pressure as a result of the reduction in water demand of concrete due to the spherical shape of the fly ash particles, which improves the workability of concrete.

In addition, Figure 8 shows a general trend of an increased rate of capillary pressure development with an increase in Type K cement content. When the SCM is limited to Type K cement only, the increase in the rate of pressure development is less pronounced at lower doses of Type K cement but becomes more evident as the Type K cement content increases (see Figure 8). For the mixes in Figures 9 and 10, which contain additional SCMs, the increased rate of capillary pressure development is much more drastic, even at lower proportions of Type K cement. Such behavior seems to suggest that when Type K cement is the sole SCM and is present in relatively low proportions, the result is a slightly increased rate of capillary pressure development compared to plain concrete. However, as the dose of Type K cement increases, or in the presence of additional SCMs, the increase in the rate of capillary pressure development is much more pronounced. The observed differences in the rate of capillary pressure development among mixes with only Type K cement and mixes with Type K cement plus additional SCMs are important to consider for special concrete mix designs. For example, a high-strength design utilizing silica fume may experience a significantly increased rate of capillary pressure development upon the addition of Type K cement.

Figures 8 through 10 show a wide range of maximum pressure magnitudes. Recall that the capillary pressure magnitude displayed in the plots indicates the air-entry time of the early-age concrete. As noted in the literature review, Sayahi (2019) asserts that the magnitude of capillary pressure seems to be a local property within concrete while the rate of pressure development seems to be a global property of the entire element. The results obtained for each individual slab in this project seem to show similar behavior, in that capillary pressure magnitude is highly variable between sensors for a given slab. The results obtained in this project also match the finding by Sayahi (2019) that the rate of capillary pressure development in a given slab is a global property as opposed to a local property. As a result, it is assumed that as long as a sufficient number of data points are collected to create a reliable profile of the rate of pressure development, the magnitude of capillary pressure for a given plot is not necessarily representative of the entire slab.

Further limiting the reliability of the pressure magnitudes shown in the plots is the sensitivity of the CPSS sensors. As discussed above, the entrance of air into a sensor disrupts the hydraulic connection and cause the pressure reading to return to gauge pressure. While the capillary pressure plots are intended to return to gauge pressure at the time of air entry into the cement matrix, the results may be skewed by the presence of air bubbles in the water that are invisible to the naked eye. Whether errant air bubbles remain in the water inserted into the sensor or sensor tip or in the concrete free water, the introduction of an air bubble into the CPSS sensor returns the sensor to gauge pressure and falsely implies air entry into the cement matrix. The highly sensitive nature of the sensors, in particular their maximum pressure magnitude readings, justifies the selection of a representative data set for a given specimen in order to eliminate erroneous readings caused by obvious outliers in the data. In addition, individual sensor results for a given slab show a pattern of relatively consistent pressure development rates, regardless of the magnitude of pressure observed or eventual outliers in the data as air is introduced into the sensors, further justifying the selection of a representative data set for each slab.

Plastic Shrinkage Crack Width

Figures 11 through 13 and Tables 11 through 13 illustrate the development and propagation of plastic shrinkage cracks in the nine restrained slab specimens.

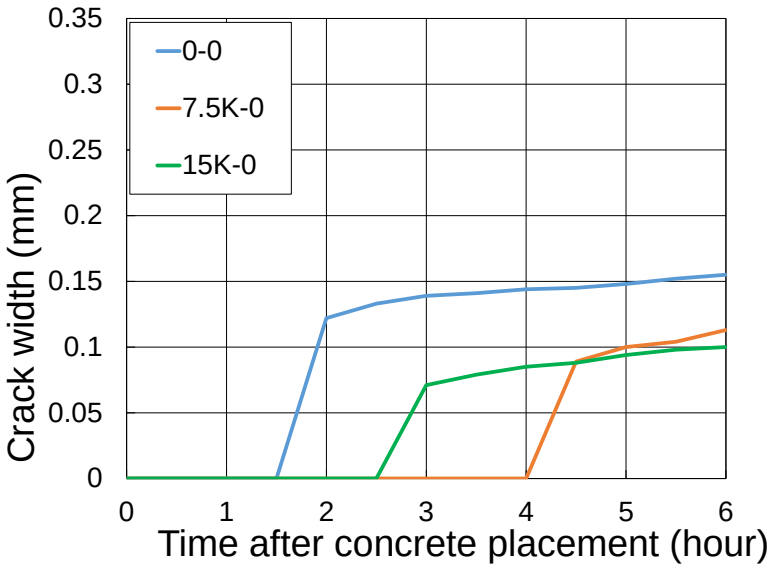

Figure 11. Onset and rate of plastic shrinkage cracking for Specimens 0-0, 7.5K-0, and 15K-0

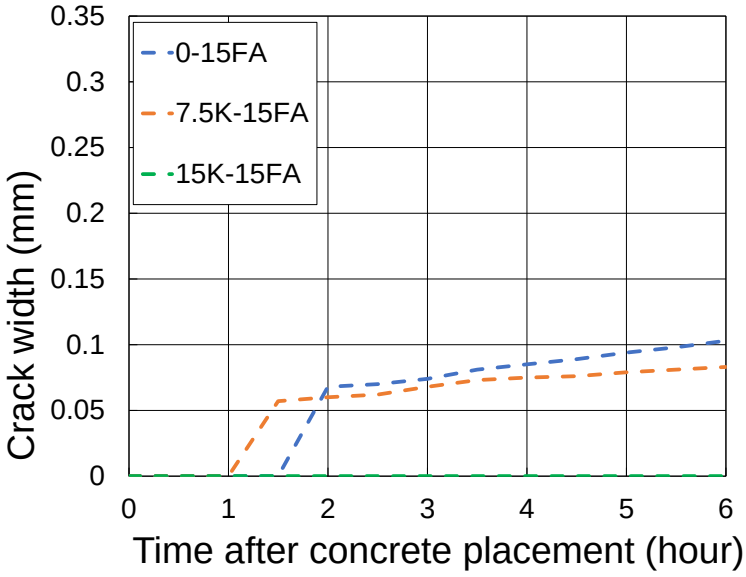

Figure 12. Onset and rate of plastic shrinkage cracking for Specimens 0-15FA, 7.5K-15FA, and 15K-15FA

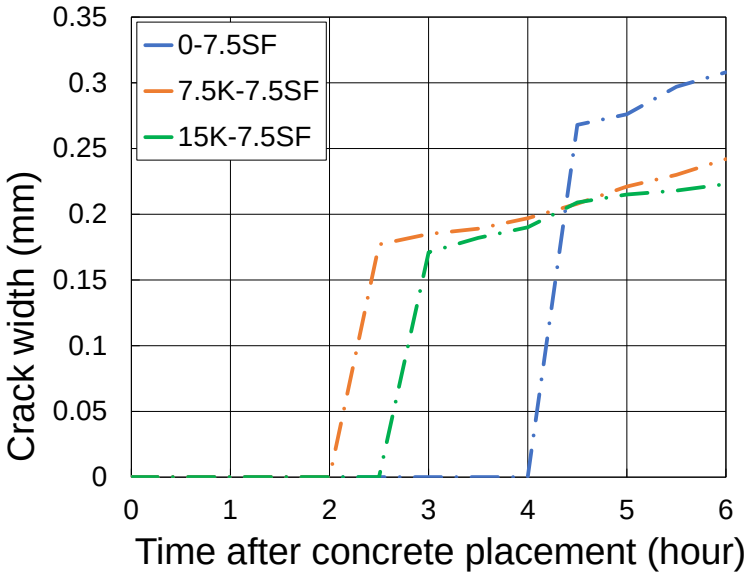

Figure 13. Onset and rate of plastic shrinkage cracking for Specimens 0-7.5SF, 7.5K-7.5SF, and 15K-7.5SF

Table 11. Plastic shrinkage cracking images for Type K concrete slabs

	Time (hours)												
Sample	**0.5**	**1.0**	**1.5**	**2.0**	**2.5**	**3.0**	**3.5**	**4.0**	**4.5**	**5.0**	**5.5**	**6.0**
0-0	-	-	-	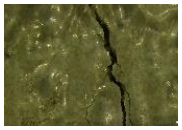	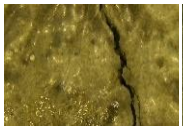	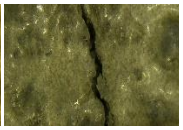	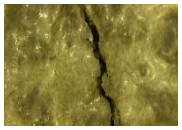	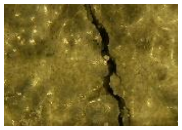	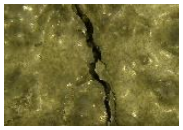	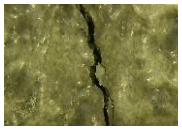	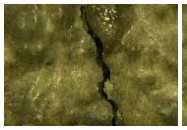	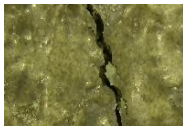
7.5K-0	-	-	-	-	-	-	-	-	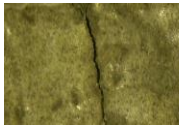	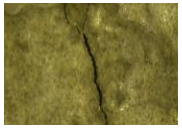	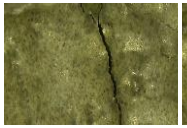	
15K-0	-	-	-	-	-	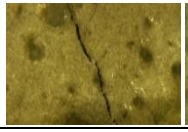	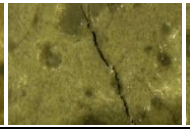	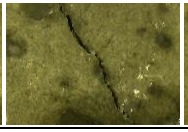	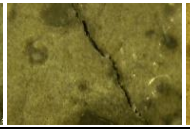	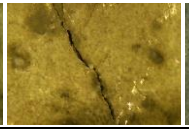		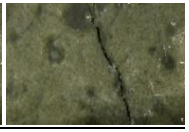

Table 12. Plastic shrinkage cracking images for fly ash concrete slabs

	Time (hours)											
Sample	**0.5**	**1.0**	**1.5**	**2.0**	**2.5**	**3.0**	**3.5**	**4.0**	**4.5**	**5.0**	**5.5**	**6.0**
0-15FA	-	-	-								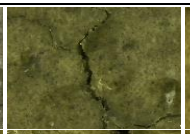	
7.5K-15FA	-	-	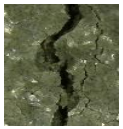	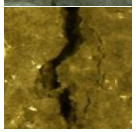	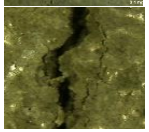	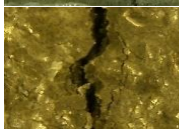	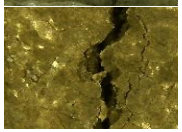		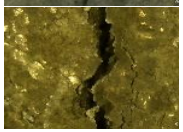		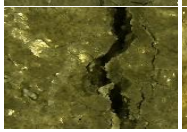	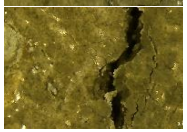
15K-15FA	-	-	-	-	-	-	-	-	-	-	-	-

Table 13. Plastic shrinkage cracking images for silica fume concrete slabs and control sample

Sample	Time (hours)											
	0.5	1.0	1.5	2.0	2.5	3.0	3.5	4.0	4.5	5.0	5.5	6.0
0-7.5SF	-	-	-	-	-	-	-	-		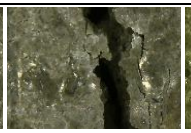	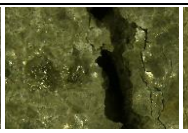	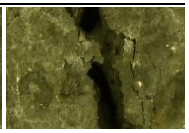
7.5K-4.5SF	-	-	-	-								
5K-7.5SF	-	-	-	-	-	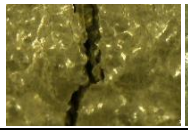	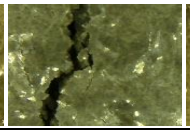	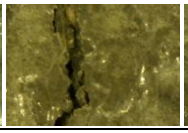	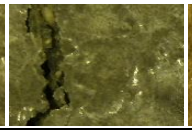	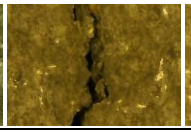	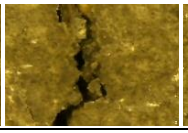	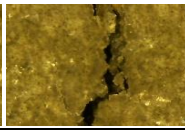

Figures 11 through 13 show crack development graphically, while Tables 11 through 13 show actual crack images taken throughout testing. In general, for each grouping of specimens (i.e., Type K only, Type K with fly ash, and Type K with silica fume), an increase in the proportion of Type K cement results in a reduction of plastic shrinkage crack width at the end of the testing period. Considering slabs with only Type K cement, the addition of 7.5% and 15% Type K cement leads to a 27% and 35% reduction in crack width, respectively, when compared to the control specimen composed of plain concrete. Among the fly ash slabs, the addition of 7.5% Type K cement results in a 19% reduction in crack width compared to Specimen 0-15FA, which contains no Type K cement and 15% fly ash. For Specimen 15K-15FA, no plastic shrinkage cracking was observed during the testing period. Finally, considering the silica fume slabs, the addition of 7.5% and 15% Type K cement results in a reduction in crack width of 21% and 28%, respectively, compared to Specimen 0-7.5SF.

The reduction in crack width with an increased percentage of Type K cement is expected based on the literature review and the expansive behavior of Type K cement. Less expected is the delay in crack development for Specimen 0-7.5SF when compared to the control specimen. Based on the literature review, silica fume is expected to increase the water demand of a concrete mix, potentially resulting in reduced bleed water and accelerated plastic shrinkage crack development. However, compared to the plain concrete slab, Specimen 0-7.5SF shows a delay in the onset of plastic shrinkage cracking. A possible explanation for this behavior is the dosage of superplasticizer utilized. To achieve adequate workability for the silica fume mixes, superplasticizer was included. It is possible that the proportion of superplasticizer exceeded what was required to achieve the necessary slump, thereby excessively mitigating the water-consuming behavior of silica fume, which would delay crack development.

Considering the rate of crack propagation, the general trend for the fly ash and silica fume mixes is a reduction in the rate of crack propagation with an increase in Type K cement. Beginning at the onset of plastic shrinkage cracking, Specimen 7.5K-15FA experiences a 0.3% reduction in crack propagation rate compared to Specimen 0-15FA. Specimen 15K-15FA does not experience cracking during the testing period. For the silica fume slabs, the addition of 7.5% and 15% Type K cement is accompanied by a 0.8% and 0.9% reduction in the cracking rate, respectively, relative to Specimen 0-7.5SF. This trend among the fly ash and silica fume specimens suggests that the addition of Type K cement may slow the rate of plastic shrinkage crack propagation once cracking begins, seemingly independent of the time at which cracking initiates. In contrast, Specimens 7.5K-0 and 15K-0 experience an increase of 0.8% and 0.1% in the crack propagation rate compared to the control specimen, which contains no Type K cement. The increased rate of crack propagation with increased percentages of Type K cement for specimens containing only Type K cement may be caused by the increase in water demand caused by the addition of Type K cement. The increased water demand due to Type K cement may result in higher rates of crack propagation compared to plain concrete. Specimens 0-15FA and 0-7.5SF both utilize superplasticizer to achieve adequate workability, which serves to reduce water demand, potentially freeing extra water for Type K cement, allowing the expansive behavior of Type K cement to outweigh the increase in water consumption.

Digital Image Correlation

The experimental results for the testing parameters investigated through DIC are discussed in this section. Data are presented for plastic shrinkage-induced strain in restrained concrete slabs.

Figures 14 through 21 illustrate the final tensile strain exhibited by each of the four slabs investigated through DIC.

Figure 14. Final tensile strain chart for Specimen 0K

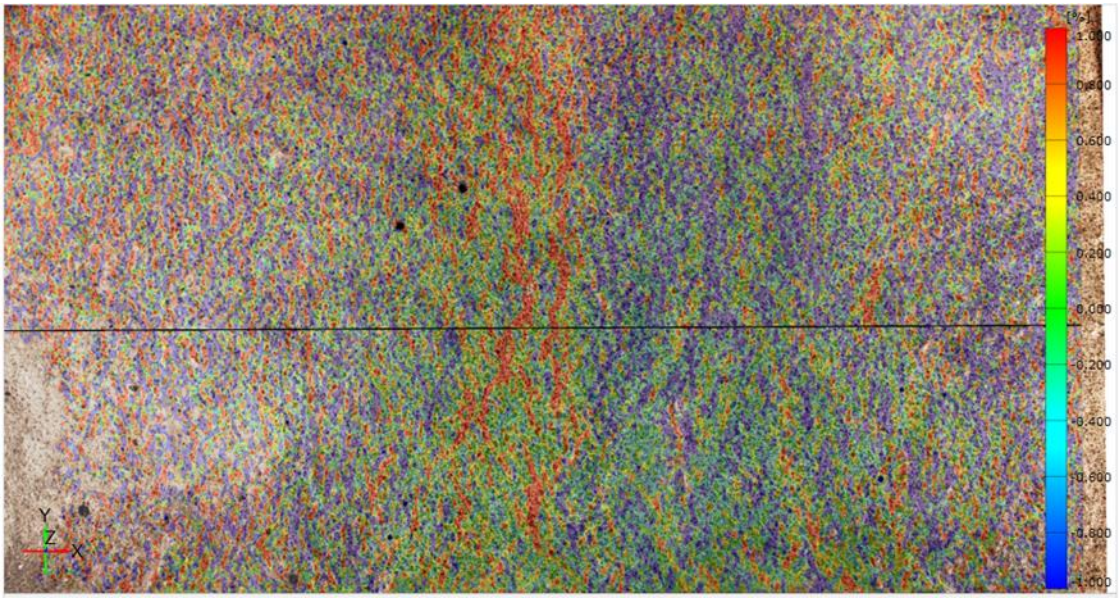

Figure 15. Final tensile strain map for Specimen 0K

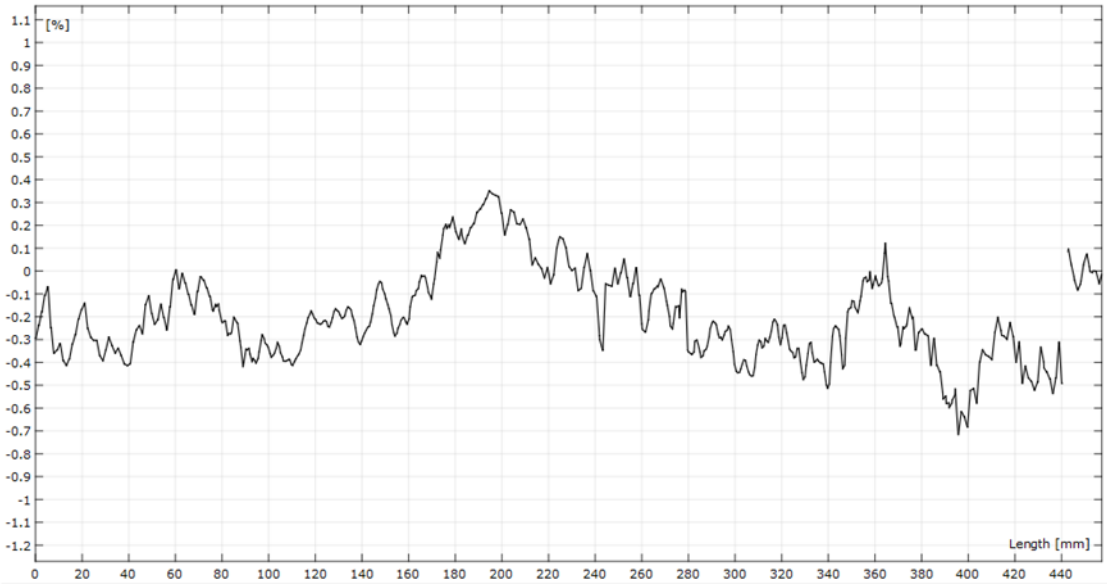

Figure 16. Final tensile strain chart for Specimen 7.5K

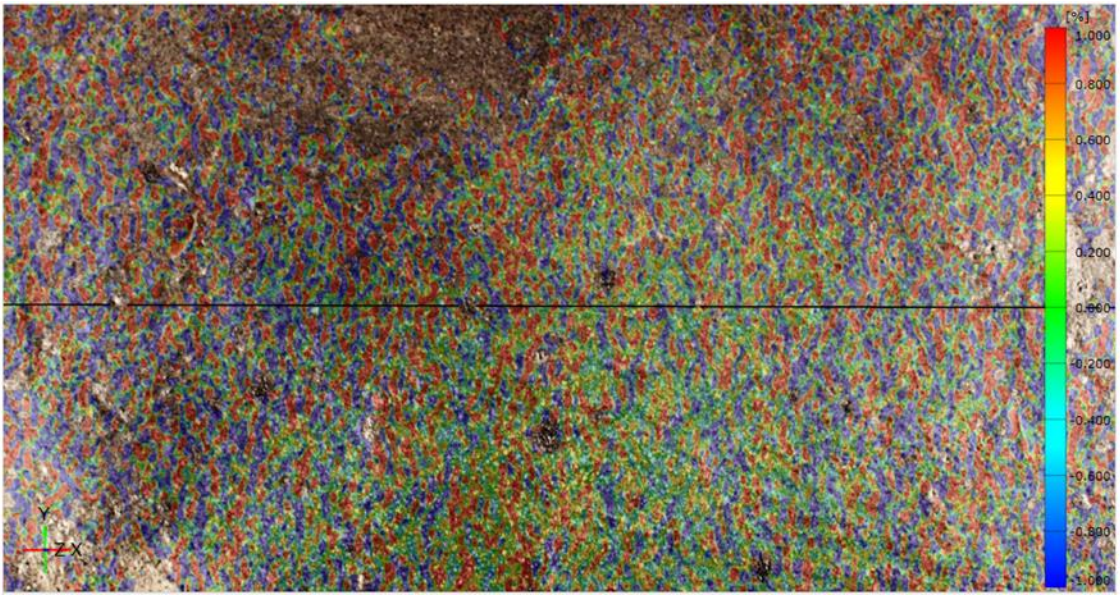

Figure 17. Final tensile strain map for Specimen 7.5K

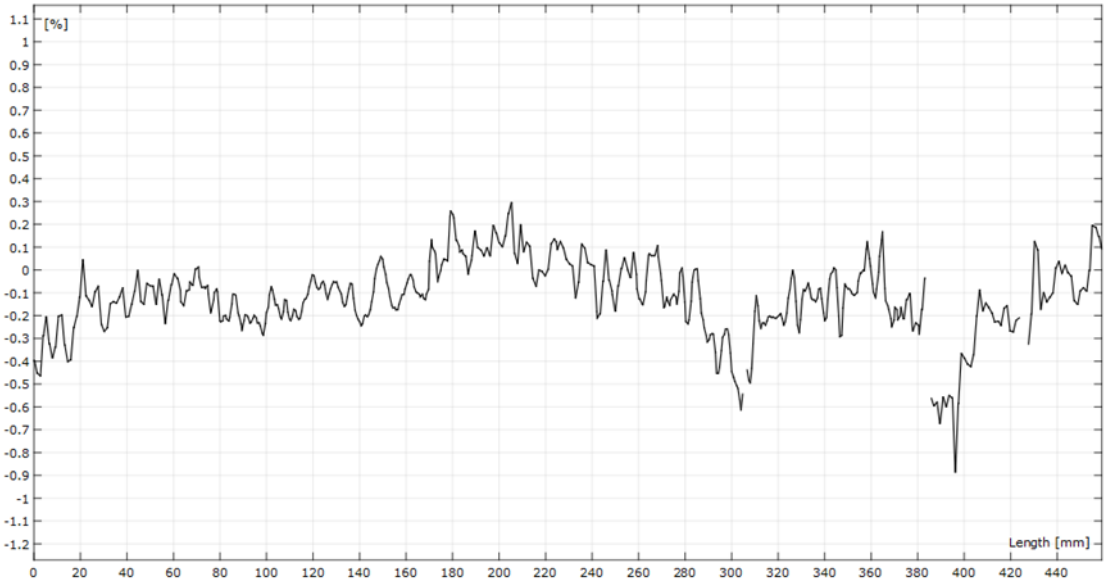

Figure 18. Final tensile strain chart for Specimen 15K

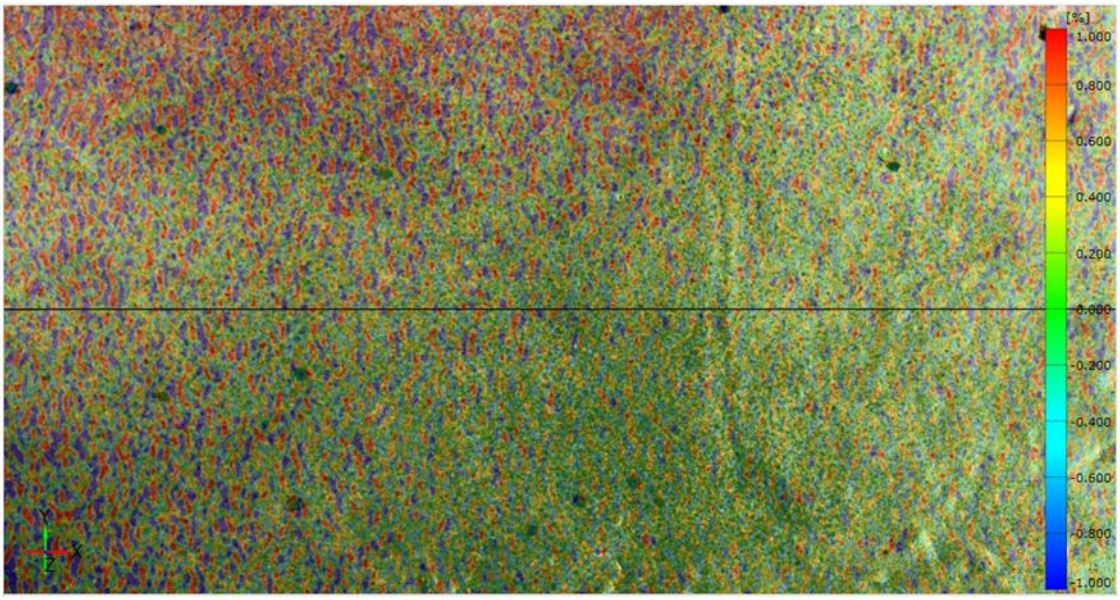

Figure 19. Final tensile strain map for Specimen 15K

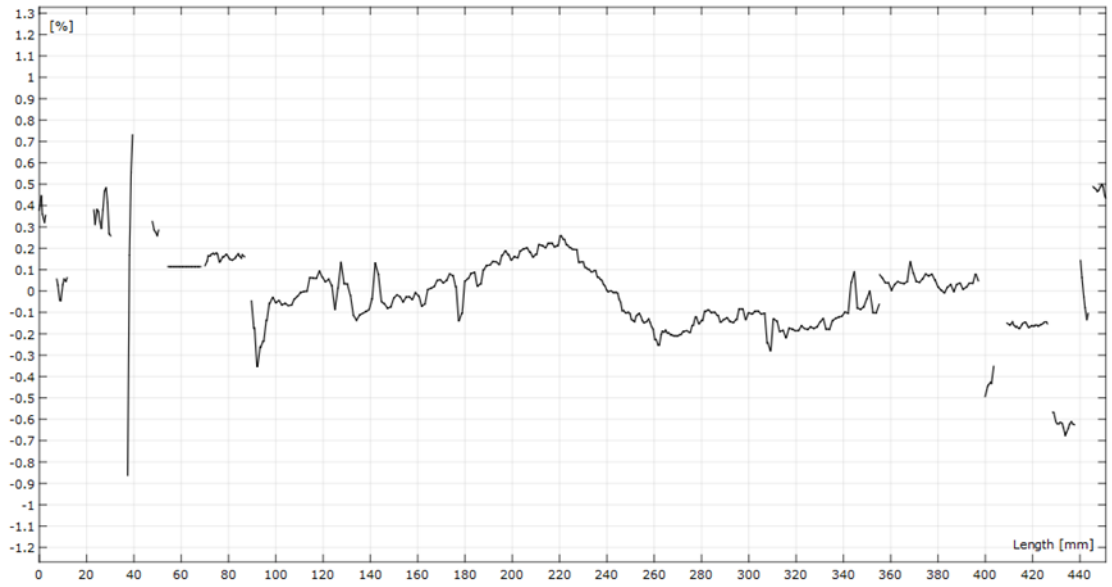

Figure 20. Final tensile strain chart for Specimen 22.5K

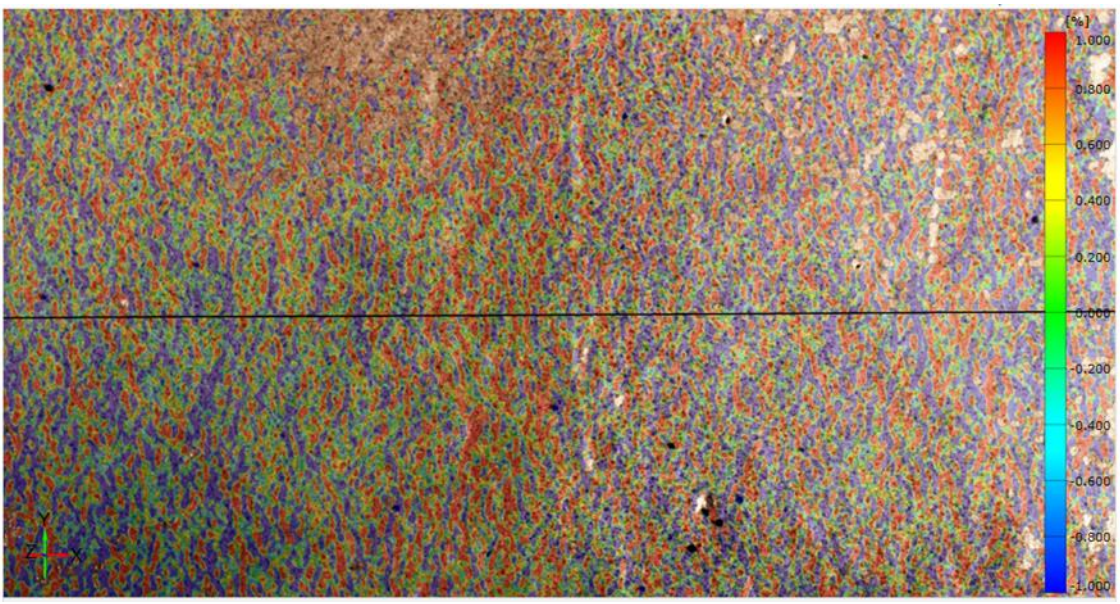

Figure 21. Final tensile strain map for Specimen 22.5K

For each slab and corresponding mix design, a pair of figures is presented. The first shows a tensile strain chart for a section taken at the midpoint of the y-axis in the x-direction of the slab, while the seconds provides a gradient-scale tensile strain map over the entire slab surface. Both the tensile strain maps and charts depict the final strain values observed over the testing period.

The general trend in tensile strain behavior among the specimens is a decrease in the magnitude of strain with an increase in Type K expansive cement. This relationship is most clearly shown in the charts of tensile strain along the x-axis. It is important to note that, for this project, consideration must be given to the location along the x-axis at which tensile strain values are

compared. The internal restraint present in the specimens results in slabs with the thinnest section directly in the center of slab, along the x-axis. The plane of weakness ensures that plastic shrinkage cracking takes place in the center of the slab, which facilitates the identification of cracks. In other words, the internal restraint should ensure the largest tensile strain directly in the center of the slab, along the x-axis. Therefore, the range of x-values over which strain is compared is approximately 200 to 240 mm, roughly the midpoint along the x-axis. Slight variations occur in the exact location of maximum strain, because the cracking location changes based on variations in each slab, such as the distribution of coarse aggregate. Despite minor variations, the strain charts appear to exhibit maximum values near the center of the x-axis.

On comparing the maximum strain values over the aforementioned range of x-values, an inverse relationship between Type K cement proportion and tensile strain is observed. This relationship suggests that the expansive behavior of Type K cement serves to counteract plastic shrinkage in early-age concrete specimens. From Specimen 0K to Specimen 7.5K, the addition of 7.5% Type K cement results in a reduction in maximum tensile strain of 29.0%. Each additional 7.5% increase in Type K cement dosage for Specimens 15K and 22.5K results in decreases in maximum tensile strain of 40.1% and 47.3%, respectively, compared to the control, Specimen 0K. In terms of relative decrease, Specimen 7.5K undergoes a 29.0% reduction in strain compared to Specimen 0K. Relative to Specimen 7.5K, Specimen 15K undergoes a 15.6% reduction in maximum tensile strain. Increasing the Type K cement percentage to 22.5% for Specimen 22.5K results in a 12.0% reduction in strain relative to Specimen 15K.

The absolute and relative percentages of strain decrease suggest that an increase in Type K expansive cement results in decreased tensile strain, at least up to 22.5% Type K cement. The most drastic relative decrease in strain occurs between Specimens 0K and 7.5K, in that Specimen 7.5K experiences roughly twice the relative reduction in strain as Specimens 15K and 22.5K. However, as Type K cement proportion increases from 15% to 22.5% for Specimen 22.5K, the relative reduction in strain is similar to that experienced between Specimens 7.5K and 15K. While it is apparent that the most efficient dose of Type K cement is that added in Specimen 7.5K, which results in a 29.0% reduction in strain, the trend in relative strain decrease is interesting because it suggests the possibility that even higher doses of Type K cement may be efficient in significantly reducing tensile strain. Further testing is required to identify the optimal dose of Type K cement in order to most efficiently reduce tensile strain.

Certain difficulties experienced during testing are evident in Figures 14 through 21. Both the strain maps and charts illustrate the difficulty in obtaining a consistent surface pattern and, consequently, a recognizable surface in the DIC software. As a result, some strain maps show sporadic strain, particularly near the edges. The same may be said for the strain charts, which sometimes feature gaps in the data near the extremes of the x-axis. Lighting may play a role in the surface inconsistencies as well, given that perfectly even lighting is difficult to achieve in the otherwise unlit environmental chamber. Despite the challenges in achieving a perfectly uniform surface, it appears that useable strain data are still collected from the testing process. For all specimens, the output of the DIC software indicates surfaces with an adequate pattern quality over the majority of the surface area. Also, each specimen features a surface that is relatively uniform near the section from which the strain charts are taken. Because the midpoint of the y-

axis, in the x-direction, is the section of interest regarding tensile strain, the data obtained through DIC are considered adequate.

Stage 2. Microfiber Investigation

Based on the results of Stage 1, fly ash was selected as the SCM in this project. The samples tested in Stages 2 and 3 followed the mixture proportions listed in Table 1. However, 20% of the portland cement was replaced with fly ash.

Cracking Age of FRC Under Restrained Shrinkage

The experimental results for the testing parameters investigated in the restrained shrinkage ring tests are discussed in the following sections. Data are presented for compressive strain and cracking age.

Compressive Strain and Cracking Age

Figures 22 through 26 show the development of compressive strain for each of the eight specimens subjected to ring tests, and Figure 32 shows the mean compressive strain development for all mixes.

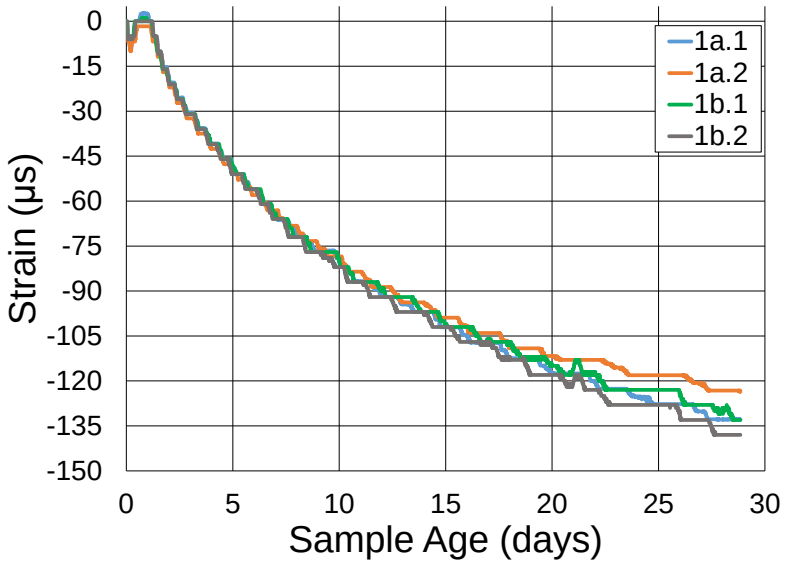

Figure 22. Compressive strain development for Mix 1 (0.0% fiber)

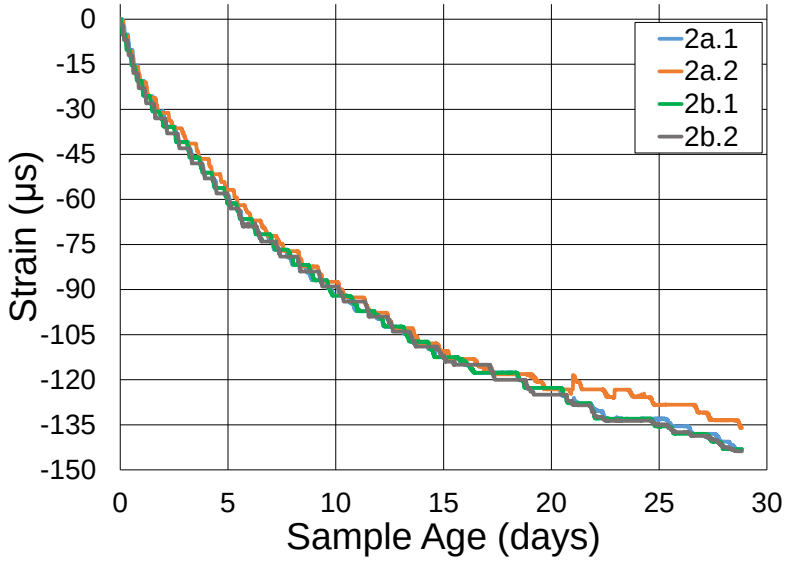

Figure 23. Compressive strain development for Mix 2 (0.25% fiber)

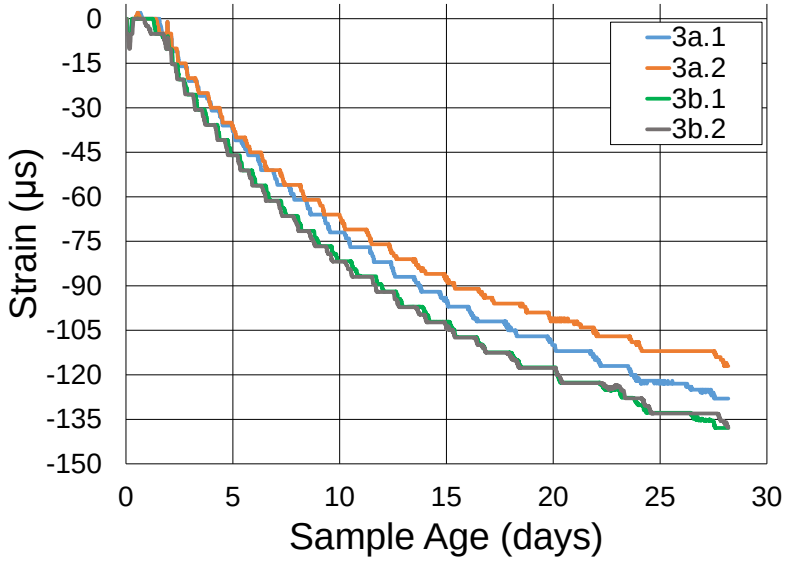

Figure 24. Compressive strain development for Mix 3 (0.50% fiber)

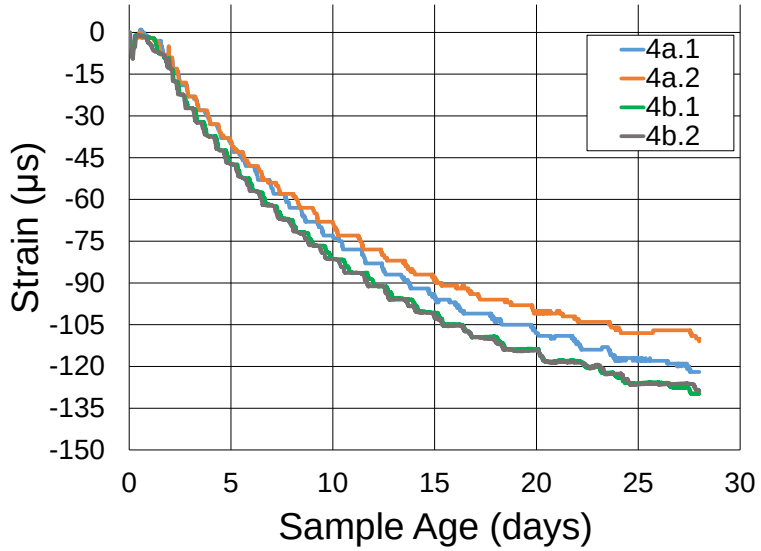

Figure 25. Compressive strain development for Mix 4 (1.0% fiber)

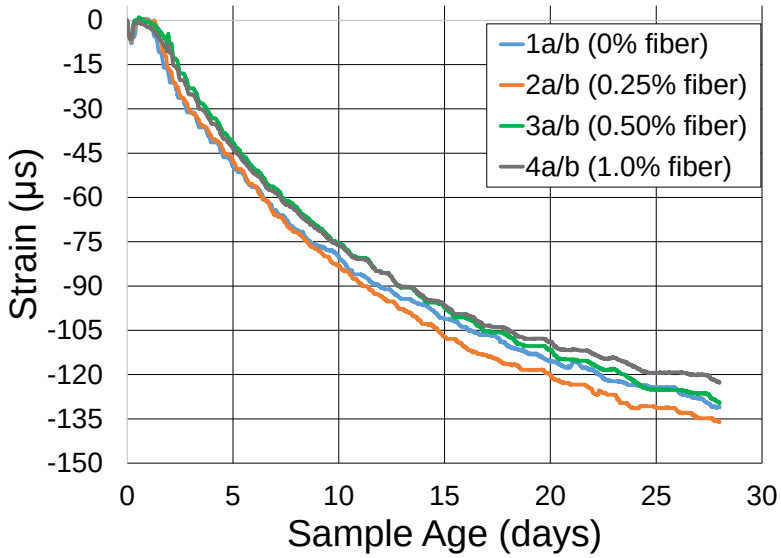

Figure 26. Mean compressive strain development for all FRC mixes

As each plot shows, the FRC specimens display similar strain development behavior for each proportion of PP microfibers. In addition, for each pair of FRC ring specimens tested, strain development occurs at similar rates between specimens. Specifically, each FRC specimen subjected to restrained shrinkage exhibits a magnitude of compressive strain that increases exponentially over the duration of the test.

Figure 26 shows an increase in the average rate of compressive strain development for the 0.25% PP microfiber mix compared to the control mix. However, the average rate of strain development decreases in mixes with PP microfiber percentages from 0.50% to 1.0%. The observation that,

relative to a control mixture, the average rate of strain development increases in mixes with PP microfiber percentages up to 0.25% and decreases in mixes with PP microfiber percentages of 0.50% and 1.0% is interesting. This finding has various potential causes. At first glance, it is tempting to attribute the reduced rate of strain development to the fibers' ability to bridge and mitigate cracking, assuming that the fibers act as a source of rigidity for concrete and thus reduce shrinkage and deformation. However, as discussed above, PP microfibers exhibit a relatively low elastic modulus, making them ineffective in improving early-age strength properties in concrete compared to other fibers with higher stiffness values. In addition, the average rate of compressive strain development exhibited by the mixtures containing 0.25%, 0.50%, and 1.00% PP microfibers increases 3.6%, decreases 1.2%, and decreases 6.5%, respectively, compared to the control mixture. Considering that larger discrepancies exist for all but one pair of identical specimens, and even between strain gauges for a single specimen, it is reasonable to conclude that PP microfiber percentage does not drastically affect the rate of compressive strain development. Such a conclusion agrees with the findings of Dopko (2018).

As Figures 22 through 26 show, none of the specimens investigated in the ring tests experienced cracking during the testing period. Cracking is indicated by a sudden jump to zero compressive strain in the steel ring as the surrounding concrete loses the tensile capacity to apply compression to the ring. While no specimen experienced cracking during testing, the compressive strain and tensile strength data were used to determine a metric for resistance to cracking.

Splitting Tensile Strength of FRC

The experimental results for the testing parameters investigated in the splitting tensile tests are discussed in the following sections. Data are presented for the tensile strength and cracking potential of FRC.

Tensile Strength

Figure 27 illustrates the development of tensile strength in each of the four FRC mixes over 28 days.

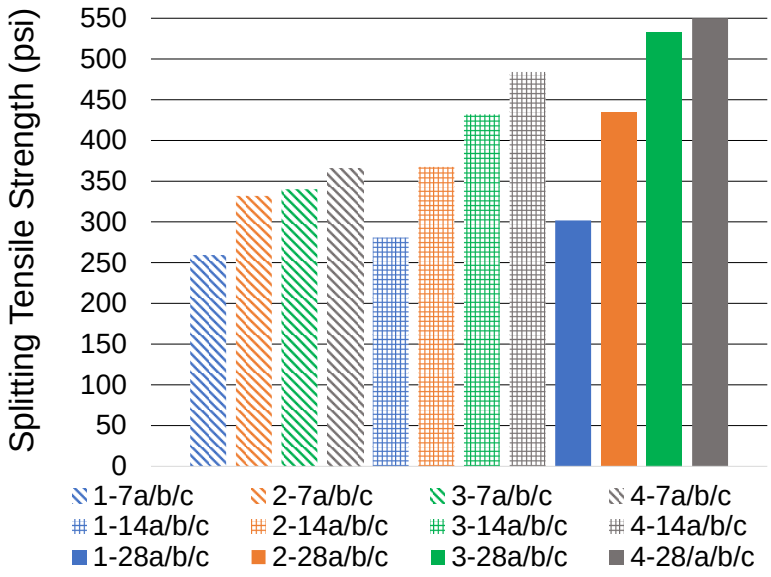

Figure 27. Tensile strength of FRC mixes at 7, 14, and 28 days

The general trends observed in the chart are increases in tensile strength with age and PP microfiber proportion. While a general trend is observed of increasing tensile strength with increasing fiber percentage, the data suggest that, above a certain fiber dose, fiber percentage reaches a point of diminishing returns in terms of increasing tensile strength. Considering the development of tensile strength over time, a fiber dose of 0.25% in Mix 2 results in a 30% increase in tensile strength between 7 and 28 days. This percentage is considerably higher than the 16% increase experienced by Mix 1, the control mixture. When comparing fiber doses of 0.50% and 1.0% (i.e., Mixes 3 and 4), the percent increase in tensile strength between 7 and 28 days is 56% and 51%, respectively. The relatively close increases in tensile strength over time for Mixes 3 and 4 suggest that, above a certain fiber percentage, the percent increase in tensile strength over time plateaus.

In addition to tensile strength development over time for individual FRC mixes, Figure 27 also suggests a point of diminishing returns for tensile strength between different mixes at the same age. Relative to Mix 1, the addition of 0.25% PP microfiber in Mix 2 results in a 44% increase in 28-day tensile strength. Comparing Mixes 2 and 3, the increase in fiber proportion from 0.25% to 0.50% results in an increase in 28-day tensile strength of 23%, or 77% above that of Mix 1. Finally, between Mixes 3 and 4, increasing the fiber dose from 0.50% to 1.0% results in an increase in 28-day tensile strength of 4%, or 84% above that of Mix 1.

Cracking Potential

As mentioned in the previous section, no specimen subjected to ring testing experienced cracking during the test. As discussed in Chapter 5, the compressive strain plots indicate the time of crack initiation by a sudden jump to zero strain when the cracked concrete no longer contains the tensile capacity to apply a compressive force to the inner steel ring. None of the strain charts in

Figures 22 through 26 exhibit a jump to zero strain, indicating that no mixes experienced drying shrinkage cracking during testing.

Although drying shrinkage cracking was not observed for any mix, the effect of PP microfiber percentage on drying shrinkage cracking was assessed by plotting cracking potential, the ratio of the actual maximum stress experienced during ring testing and the splitting tensile strength of a given concrete mix. As illustrated in Figure 28, cracking potential remains consistently lower in mixes with higher proportions of PP microfibers throughout the entire test period.

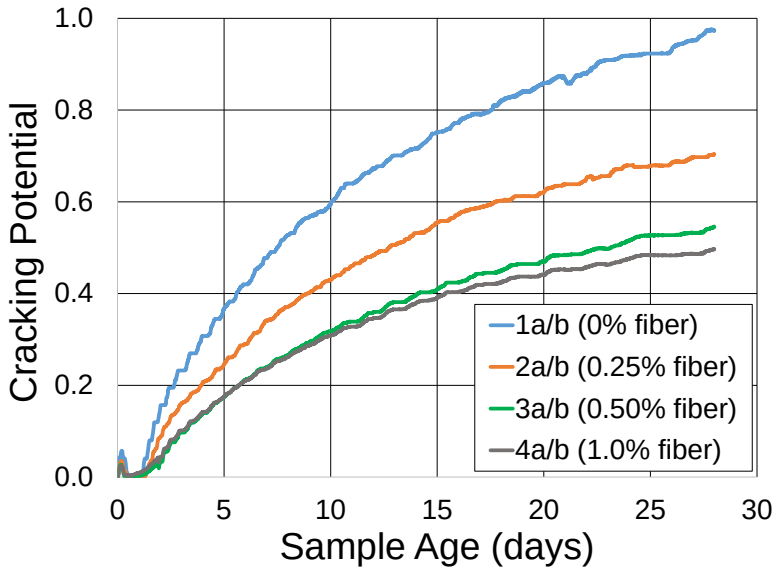

Figure 28. Cracking potential over time for all FRC mixes

The reduction in cracking potential with increasing fiber percentage points to improved resistance to drying shrinkage cracking for FRC mixes with higher fiber doses, despite no specimen experiencing drying shrinkage cracking under the experimental conditions. It should be noted that the cracking potential trendlines plotted in Figure 28 never exceed 1.0, the ratio at which the actual stress experienced during testing is greater than the tensile strength of a given mix. This observation is consistent with the lack of cracking observed during the testing period.

The method of calculating cracking potential was originally developed by Hossain and Weiss (2006) and refined by Wang et al. (2012). The general procedure involves determining the actual maximum shrinkage-induced stress in the concrete ring, σ_{actual_max}, and computing the ratio of σ_{actual_max} to the measured tensile strength of a given concrete mix. The actual maximum shrinkage-induced stress in concrete is calculated from the surface pressure on the outer face of the inner steel ring, which in turn is calculated using the recorded strain and other known values. The equations used to calculate cracking potential as follows:

$$p = \varepsilon_s E_s \frac{R_{so}^2 - R_{si}^2}{2R_{so}^2} \quad (2)$$

where:

p = surface pressure on outer face of inner steel ring (psi)

ε_s = strain recorded on inner face of inner steel ring (in./in.)

E_s = elastic modulus of steel = 29,000 ksi

R_{so} = outer radius of inner steel ring (in.)

R_{si} = inner radius of inner steel ring (in.)

$$\sigma_{actual\_max} = p\left(\frac{R_{so}^2+R_{co}^2}{R_{co}^2-R_{so}^2}+\nu\right) \quad (3)$$

where:

σ_{actual_max} = actual maximum shrinkage-induced stress in concrete (psi)

ν = Poisson's ratio of concrete (assumed to be 0.2)

R_{co} = outer radius of concrete ring (in.)

$$\theta_{cr} = \frac{\sigma_{actual\_max}}{f_{spt}} \quad (4)$$

where:

θ_{cr} = cracking potential of concrete

f_{spt} = splitting tensile strength of concrete at a given age (psi)

Compressive Strength of FRC

Figure 29 illustrates the change in the 28-day compressive strength of concrete as PP microfiber percentage increases.

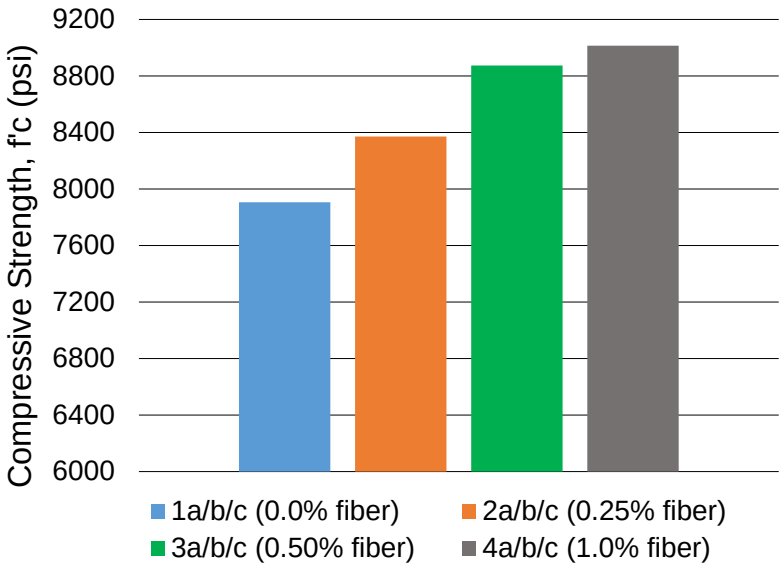

Figure 29. 28-day compressive strength of FRC mixes

The general trend observed is an increase in 28-day compressive strength as PP microfiber percentage increases. However, similar to tensile strength, compressive strength appears to reach a point of diminishing returns at which higher doses of PP microfibers result in a reduced relative strength increase. Figure 29 shows that the addition of 0.25%, 0.50%, and 1.0% PP microfibers to the concrete results in an increase in compressive strength of 5.9%, 12.2%, and 14.0%, respectively, compared to the control mixture. From Mix 1 to Mix 2, the relative increase in compressive strength is 5.9%. A similar relative strength increase of 6.4% is observed from Mix 2 to Mix 3. However, when the PP microfiber dosage increases from 0.50% to 1.0% between Mixes 3 and 4, the relative increase in compressive strength is 1.8%, approximately three times less than that observed between other mixes. The reduced relative increase in compressive strength between Mixes 3 and 4 indicates that a PP microfiber proportion of 1.0% provides a less efficient compressive strength gain compared to lower dosages.

Chloride Penetration by Rapid Migration

The general trend observed regarding mean chloride penetration depth within FRC specimens is a decrease in penetration depth with increasing PP microfiber percentage, as shown in Figure 30a.

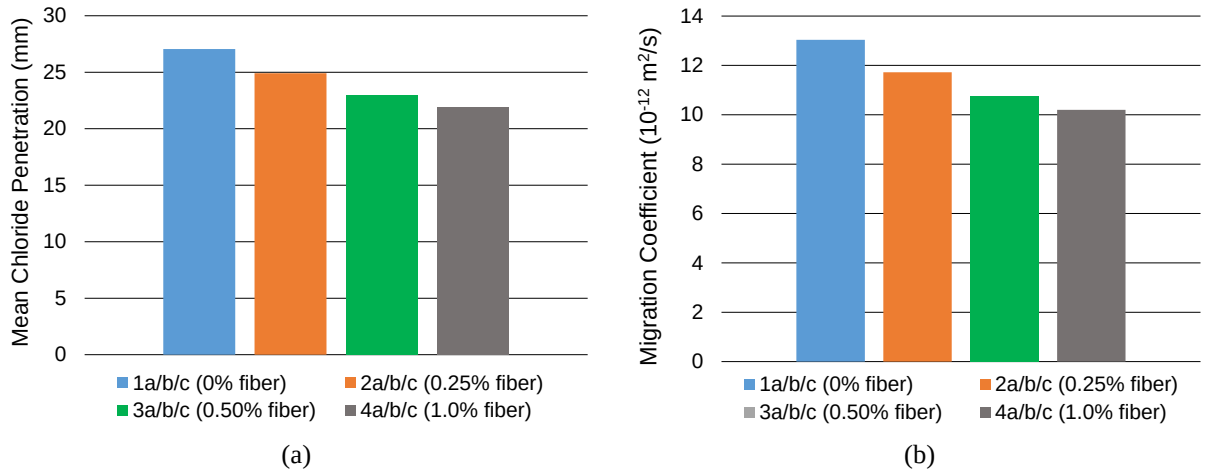

Figure 30. Rapid chloride migration test results for (a) mean chloride penetration depth and (b) migration coefficient

The chloride penetration results in the chart appear to show relatively consistent decreases as PP microfiber proportion increases from 0.0% to 1.0%. Relative to the control, mixes with PP microfiber proportions of 0.25%, 0.50%, and 1.0% exhibit decreases in mean chloride penetration depth of 7.9%, 15.2%, and 19.1%, respectively. The relative decrease in penetration depth from Mix 1 to Mix 2 is 7.9%, which happens to be equal to the relative decrease in penetration depth from Mix 2 to Mix 3. However, from Mix 3 to Mix 4, the relative decrease in penetration depth is 4.7%, approximately 40% less than that between Mixes 1 and 2 and between Mixes 2 and 3.

To more clearly observe the effects of PP microfiber percentage on chloride ion resistance, the migration coefficients calculated for the mixtures are shown in Figure 30b. The migration coefficients show a trend similar to that observed for chloride penetration depth, where the control sample evinces the lowest resistance against the migration of chloride ions. It can also be inferred from Figure 30b that increasing the microfiber content decreases the migration coefficient of a mix, endowing the concrete with a higher resistance against chloride.

Stage 3. Hybrid Fiber Investigation

Workability

Figure 31 shows the amount of water reducer needed for each of the hybrid FRC mixtures to reach a slump of 5 to 6 in.

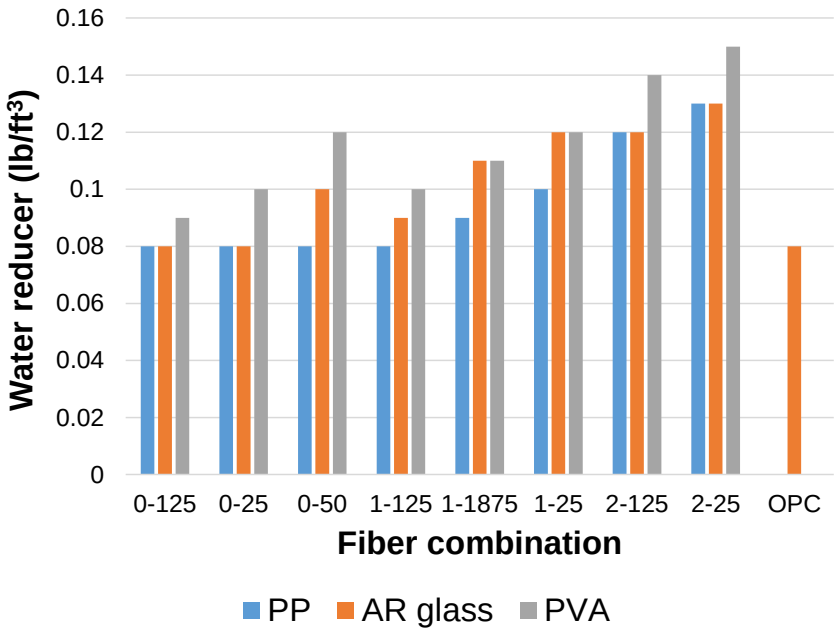

Figure 31. Water reducer demand of hybrid FRC mixes

It can be observed that regardless of fiber length and type, increasing the fiber content increases the demand for water reducer. The mixtures containing PVA macrofibers show a higher demand for water reducing admixtures compared to the mixtures with PP and AR glass macrofibers. The water absorption capability of the PVA macrofibers is likely responsible for this excessive demand for water reducer. The mixes with PP and AR glass macrofibers show similar performance, but the mixes with PP macrofibers show the lowest demand for water reducer overall.

Compressive Strength

The compressive strengths of the mixtures containing PP, AR glass, and PVA macrofibers are shown in Figures 32 through 34, respectively.

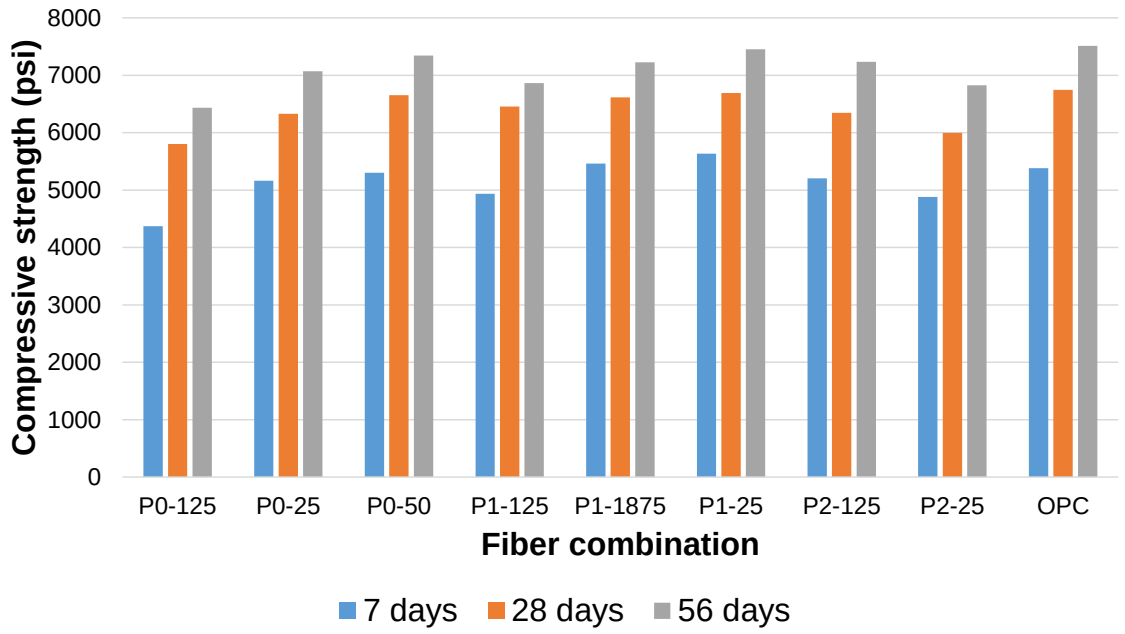

Figure 32. Compressive strength of hybrid FRC with PP macrofibers

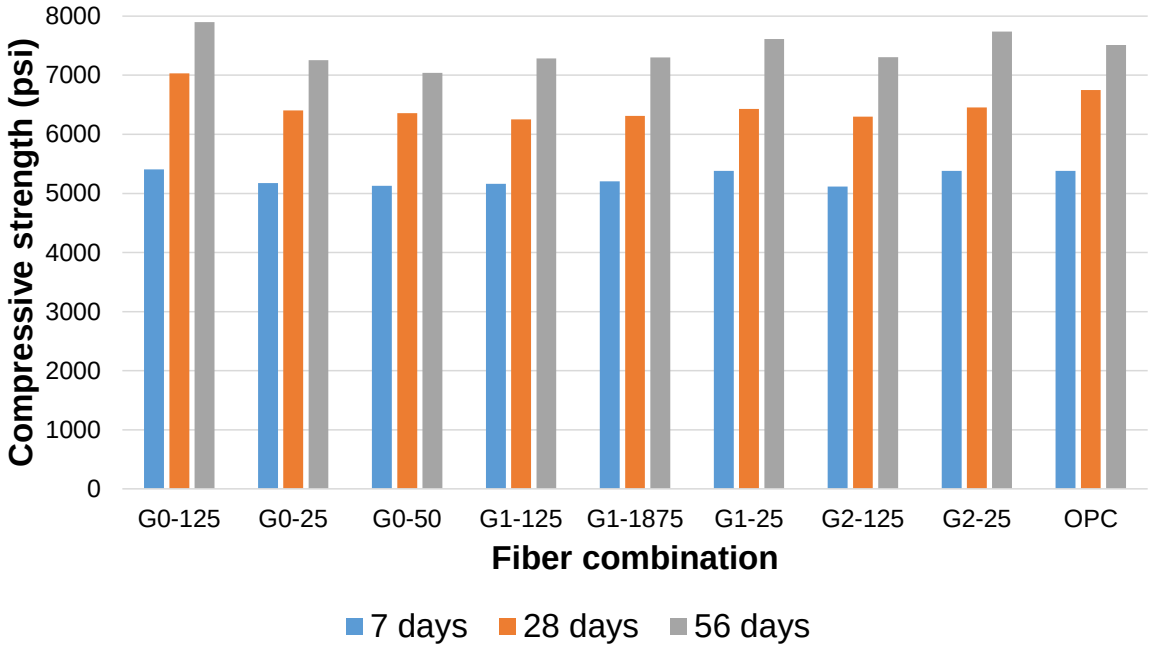

Figure 33. Compressive strength of hybrid FRC with AR glass macrofibers

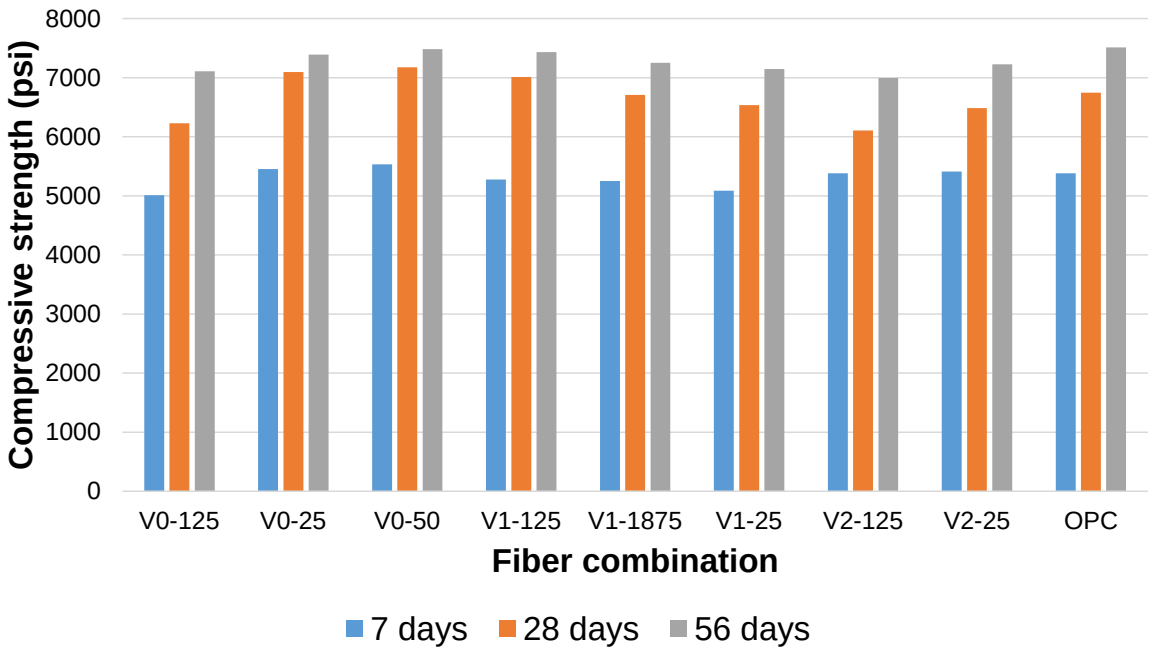

Figure 34. Compressive strength of hybrid FRC with PVA macrofibers

It can be observed in Figure 32 that, in general, PP macrofibers adversely affect the compressive strength of FRC. The addition of 0.125% PP macrofibers generally reduces the compressive strength of concrete. However, the amount of this reduction decreases when microfibers are incorporated into the mix. For instance, at the age of 56 days, P0-125 shows a 14% decrease in compressive strength compared to the control sample, while compressive strength decreases by 7% and 4% in P1-125 and P2-125, respectively. Increasing the macrofiber content augments the compressive strength of FRC mixes without microfibers or with 0.0625% microfibers, while this trend is reversed in mixtures containing 0.125% microfibers.

According to Figure 33, the AR glass mixtures show ranges of compressive strength values similar to that of the control sample. When no microfiber is present in the mixture, the addition of 0.125% AR glass macrofibers increases compressive strength by 5% at 56 days. However, increasing the volume of AR glass macrofibers has a negative effect on compressive strength, to the extent that the mixtures with 0.25% and 0.50% AR glass macrofibers experience a 3% and 6% decrease in compressive strength compared to the control sample. These observations can be explained by the packing potential of the fibers. The AR glass fibers employed in this research were long monofilaments, which are difficult to pack in the concrete matrix. Although at a very low dosage (i.e., 0.125%) AR glass macrofibers contribute to compressive strength due to their high stiffness, their packing difficulty seems to introduce air voids into the matrix and thus reduce compressive strength at higher dosages.

Furthermore, the incorporation of microfibers is shown to be effective in reducing the negative effect of the AR glass macrofibers because they enhance the grading of the macrofibers and help them pack better. To support this claim, the results for G0-25, G1-25, and G2-25 can be compared to those for G0-125. G0-25 undergoes an 8% drop in compressive strength compared

to G0-125, while G1-25 and G2-25 experience much lower decreases of 4% and 2%, respectively. Moreover, the results suggest that in mixtures containing microfibers, increasing the macrofiber dosage leads to an increase in compressive strength, which is in contrast to the trend observed in mixtures without microfibers.

Figure 34 shows the compressive strength results for the mixtures made with PVA macrofibers. The figure shows that addition of PVA macrofibers to the concrete marginally decreases the compressive strength, which can be a result of the water absorption of the PVA fibers as well as the rigid shape of the monofilaments. When no microfiber is incorporated into the mixture, the addition of PVA macrofibers is effective in enhancing the compressive strength of the FRC.

Overall, hybrid FRC with AR glass macrofibers shows better performance in terms of compressive strength than hybrid FRC with PP or PVA macrofibers.

Tensile Strength

The splitting tensile strengths of the FRC mixtures are illustrated in Figure 35.

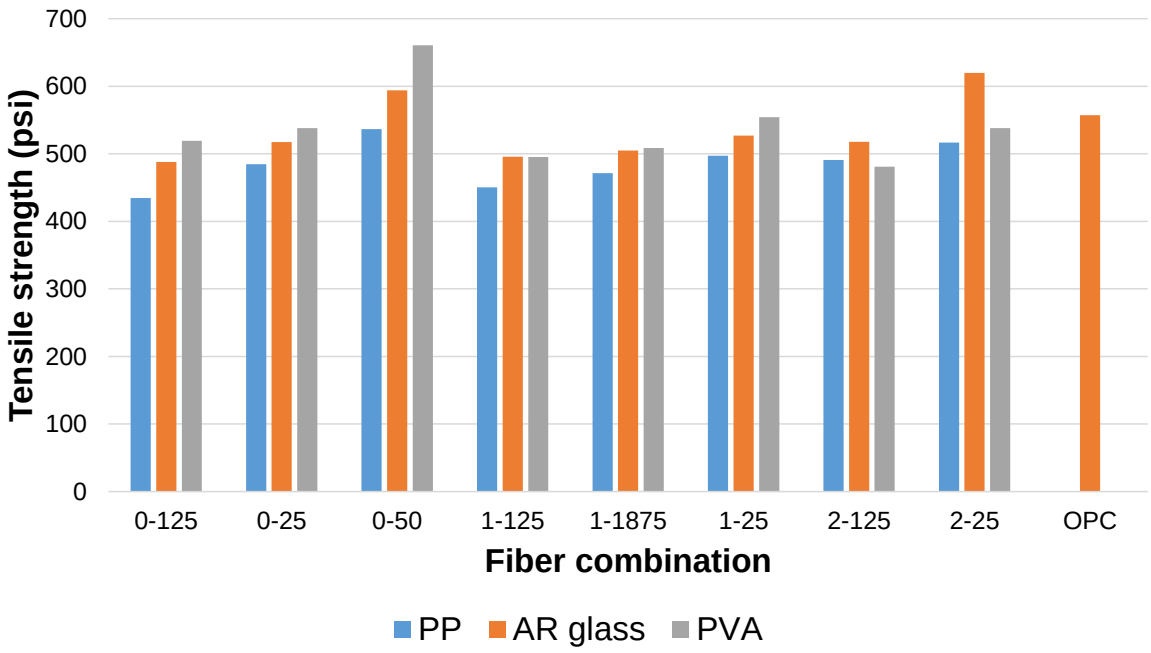

Figure 35. Splitting tensile strengths of hybrid FRC with PP, AR glass, and PVA macrofibers

It can be observed that a majority of the fiber combinations evince a lower tensile strength compared to the control sample, which can be attributed to the higher porosity of the FRC mixtures as well as the formation of a weak interfacial zone around the PP and AR glass macrofibers. It can also be seen that, in contrast to the control specimen, the samples with

macrofibers did not split, suggesting that macrofibers have the potential to provide residual tensile strength, which was not measured in this research.

According to Figure 35, regardless of macrofiber type, increasing the macrofiber dosage results in an increase in the tensile strength of the FRC at all microfiber contents due to an increase in the quantity of the fibers, which provide additional load-bearing conduits. When no microfiber is incorporated into the mixture, mixes with PVA show superior performance to mixes with AR glass, which in turn show superior performance to mixes with PP. This observation can be explained by the fact that a strong chemical bond forms between the PVA fibers and the concrete matrix, while PP and AR glass fibers merely form a mechanical bond with the concrete matrix.

When microfibers are introduced into the mixture, the efficiency of the PVA macrofibers decreases, and mixes with AR glass fibers show increasingly superior performance as the microfiber content increases. When PP microfibers are added to a matrix that already contains some amount of macrofiber, the grading of the fibers is enhanced, which can contribute to the mechanical properties of the FRC. However, as stated above, PVA macrofibers form a strong chemical bond with the matrix, and the addition of PP microfibers introduces some weak spots in the matrix due to their weak fiber-matrix bonds, which undermines the tensile behavior of the PVA FRC. For instance, at a macrofiber dosage of 0.125%, mixes with PVA lose 7% of their tensile strength when 0.125% microfiber is added, while mixes with PP and AR glass gain 13% and 6%, respectively. Similarly, at a macrofiber dosage of 0.25%, the addition of 0.125% microfiber does not change the tensile strength of mixes with PVA, while it increases the tensile strength of mixes with PP and AR glass by 7% and 20%, respectively.

Flexural Strength

The flexural strengths of the hybrid FRC mixtures are plotted in Figure 36.

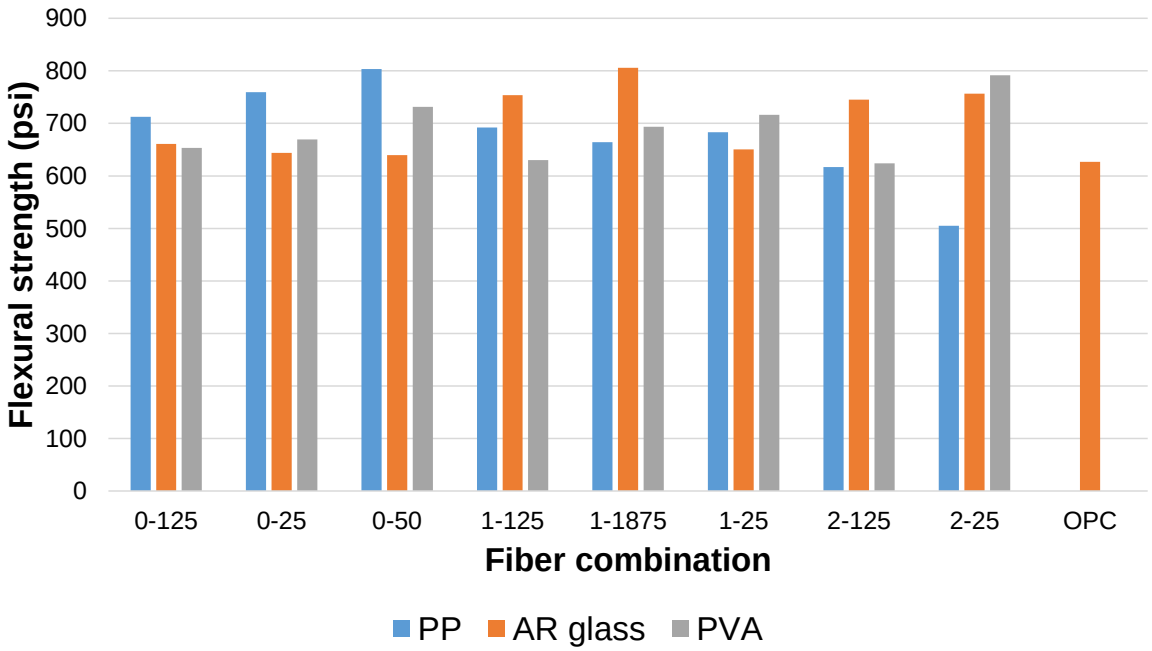

Figure 36. Flexural strengths of hybrid FRC with PP, AR glass, and PVA macrofibers

As shown in Figure 36, the FRC samples show similar or higher flexural strengths compared to the control sample, regardless of the type and quantity of the fibers. The only irregularity is the P2-25 mixture, in which cracking occurred outside of the middle section. When no microfibers are incorporated into the FRC, increasing the dosage of PP and PVA macrofibers increases the flexural strength of the FRC. At a dosage of 0.5%, this flexural strength enhancement is 28% and 17% for PP and PVA, respectively. However, the flexural strength of the AR glass FRC is not affected by the macrofiber volume. Consequently, mixes with PP macrofibers show superior flexural performance to mixes with PVA and AR glass fibers when no microfibers are present.

In hybrid FRC, mixtures made with AR glass macrofibers show higher flexural strengths at lower macrofiber dosages (i.e., 0.125% and 0.1875%), with G1-1875 exhibiting a 29% increase in flexural strength compared to the control sample. PVA exhibits superior performance at a macrofiber dosage of 0.25%, with V2-25 showing a 27% increase in flexural strength compared to the control sample. It is noteworthy that regardless of the microfiber dosage, increasing the PVA content results in an increase in the flexural strength of FRC, which can be attributed to the strong fiber-matrix bond that shifts the failure mode of the PVA macrofibers to rupture rather than pull-out.

Toughness

The toughness of each mixture can be measured by calculating the area under the load-deflection curve. The toughness values of the FRC specimens that showed some level of residual strength are presented in Table 14.

Table 14. Toughness of FRC specimens

Specimen	Toughness (in./lb)	Specimen	Toughness (in./lb)	Specimen	Toughness (in./lb)
OPC	-	-	-	-	-
P0-125	-	G0-125	49.67	V0-125	-
P0-25	-	G0-25	51.88	V0-25	123.07
P0-50	-	G0-50	131.48	V0-50	86.12
P1-125	-	G1-125	117.3	V1-125	-
P1-1875	-	G1-1875	106.82	V1-1875	124.43
P1-25	102.47	G1-25	84.05	V1-25	100.51
P2-125	-	G2-125	113.86	V2-125	-
P2-25	58.87	G2-25	100.07	V2-25	112.61

The results presented in this table suggest that AR glass FRC reaches a higher toughness when microfibers are incorporated into the matrix. Microfibers do not provide similar benefits to PVA FRC because the strong fiber-matrix bond of the PVA fibers means that the PP microfibers fail faster than the PVA macrofibers, which limits the microfibers' contribution to toughness. In general, PVA FRC shows higher toughness compared to AR glass FRC. This can be attributed to the higher deflection occurring at the failure point of PVA FRC compared to that occurring at the failure point of AR glass FRC. This deflection is controlled by the governing mode of failure, which is rupture of the fibers in PVA FRC and pull-out of the fibers in AR glass FRC. In the latter, pull-out is restricted by the twisted shape of the monofilaments. Furthermore, AR glass macrofibers have a significantly higher modulus of elasticity compared to PVA and PP macrofibers, which further limits crack widths.

CHAPTER 7. CONCLUSIONS AND RECOMMENDATIONS

In this study, a comprehensive investigation was conducted on the properties of FRC for use in bridge decks. Three stages of research were designed to achieve this goal. The first stage was dedicated to finding the best performing binder composition to withstand plastic shrinkage. In the second stage, FRC with microfibers was investigated for its crack resistance, mechanical properties, and chloride resistivity. The third stage focused on the mechanical properties of hybrid FRC and involved an investigation of various dosages of PP microfibers and three types of macrofibers, i.e., PP, AR glass, and PVA.

Key Findings

The results of the investigations carried out for this research are summarized in the findings presented below.

Stage 1

- In general, increasing the proportion of Type K expansive cement resulted in an increase in the rate of capillary pressure development for all types and percentages of SCMs investigated in this project. Silica fume was found to have a negative effect on the rate of capillary pressure development, while Class F fly ash decreased the rate of capillary pressure. Therefore, Class F fly ash was incorporated into the mix design of the FRC in subsequent stages of this research.

- For each type of concrete investigated, an increase in Type K expansive cement led to a reduction in plastic shrinkage crack widths at six hours after casting. For concrete containing Class F fly ash or silica fume, increasing the dosage of Type K cement resulted in a reduction in the rate of plastic shrinkage crack propagation, provided that adequate workability was achieved through the use of superplasticizer.

- The DIC results suggest that after the six-hour testing period, the specimens experienced reduced plastic shrinkage-induced tensile strain at the location of cracking with increasing proportions of Type K expansive cement up to 22.5%. Doses of Type K cement up to 22.5% showed a substantial relative reduction in plastic shrinkage-induced tensile strain.

Stage 2

- For PP microfiber percentages from 0.25% up to 1.0% by volume, an increase in fiber proportion did not significantly affect the rate of drying-induced strain development or the final magnitude of strain in a concrete ring.

- Tensile strength increased with both age and PP microfiber percentage among all ages and mixes of FRC for fiber doses up to 1.0% by volume. The largest relative increase in tensile

strength occurred at lower PP microfiber doses in the range of 0.25%. The ability of PP microfibers to improve the tensile strength of concrete decreased in efficiency at fiber volumes of 1.0% or higher.

- Cracking potential, defined as the ratio of the maximum shrinkage-induced stress experienced by an FRC mix to the tensile strength of the same FRC mix, decreased with an increase in PP microfiber percentage for fiber doses up to 1.0%. At volumes of 1.0% and higher, the relative reduction in cracking potential significantly decreased compared to the relative reduction in cracking potential at lower doses.

- In general, the data show that the 28-day compressive strength of FRC increases with PP microfiber proportion for fiber doses up to 1.0% by volume. At PP microfiber volumes of 1.0% and higher, the relative increase in compressive strength provided by the fibers significantly decreased compared to the relative increase in compressive strength at lower doses.

- An increase in PP microfiber proportion up to 1.0% by volume corresponded to a decrease in the rate and magnitude of chloride ion penetration into FRC after 24 hours. Increasing the fiber dosage to 1.0% appeared to result in less efficient mitigation of chloride penetration compared to the mitigation provided at lower fiber proportions.

Stage 3

- PVA macrofibers reduced the workability of FRC more significantly than AR glass and PP macrofibers due to the water absorption of the PVA fibers.

- PP and PVA macrofibers reduced the compressive strength of concrete, while AR glass macrofibers provided a compressive strength similar to that of the control sample. In the case of hybrid FRC, the addition of AR glass macrofibers resulted in superior compressive strength, which was augmented by increasing the macrofiber dosage.

- FRC with PP macrofibers showed weaker performance under tensile loads compared to FRC with AR glass or PVA macrofibers.

- The mechanical test results suggest that AR glass macrofibers show a promising synergy with PP microfibers, which makes AR glass macrofibers an appropriate choice for hybrid FRC.

- Regardless of the fiber combination and dosage, the FRC samples studied in Stage 3 exhibited a flexural strength similar to or higher than that of the control sample. FRC with PP macrofibers showed superior performance in terms of flexural strength when no microfibers were added to the mixture. However, when microfibers were introduced into the mixture, FRC with PP macrofibers lost its superiority. Furthermore, in hybrid FRC with low

macrofiber dosages (i.e., 0.125% and 0.1875%), AR glass FRC had the highest flexural strength. However, at a macrofiber dosage of 0.25%, PVA FRC outperformed the FRCs with other macrofibers.

- The addition of AR glass macrofibers to concrete, even at a dosage of 0.125%, provided FRC with some level of post-peak residual strength and toughness. However, PP and PVA macrofibers provided FRC with post-peak flexural strength and toughness at dosages of 0.25% and 0.1875%, respectively. Moreover, at a macrofiber dosage of 0.5%, AR glass FRC, in contrast to PP or PVA FRC, showed a well-formed residual flexural strength stretching beyond 1/150 of the span length.

Conclusions and Recommendations

Based on the research conducted and the literature reviewed for this study, it can be concluded that replacing a portion of portland cement with Class F fly ash has a positive effect on the resistance of concrete to plastic shrinkage as well as on the workability and long-term durability of concrete. Although the addition of Type K cement showed promise in restricting crack width, it increased the rate of capillary pressure development in concrete, which has a destructive effect on the resistance of concrete to plastic shrinkage. Therefore, it is not recommended that Type K cement be included in final mix designs, while it is recommended that Class C fly ash replace 20% of the portland cement to address dimensional stability, workability, and durability concerns.

The addition of PP microfibers, even in doses as low as 0.25% by volume, proved to significantly reduce the cracking potential of concrete due to drying shrinkage. Furthermore, PP microfibers were found to be helpful in enhancing the mechanical and chloride resistance of FRC, but increasing the volume of PP microfibers beyond a certain percentage decreased the fibers' efficiency. On the other hand, PP microfibers, similar to other microfibers, increase the water demand of concrete, which is a restrictive operational parameter. Therefore, practical considerations limit the dosage of PP microfibers; the maximum practical dosage is recommended to be 0.125%, which corresponds to 2 lb/yd^3.

Another drawback of microfibers is their inability to provide post-peak strength, which can be addressed with the addition of macrofibers. Based on the pre- and post-peak mechanical strength results, AR glass monofilaments are recommended to be used as macrofibers. These fibers showed superior performance over PP and PVA macrofibers. The recommended fiber combination is 0.125% PP microfiber along with 0.25% AR glass macrofiber, which can satisfy practical restrictions as well as provide suitable pre- and post-peak mechanical properties.

REFERENCES

Abeysinghe, T. M., G. Tanapornraweekit, S. Tangtermsirikul, W. Pansuk, and N. Nuttayasakul. 2017. Performance of Aramid Fiber Reinforced Concrete Panels Under Blast Loads. *Fourth Asian Conference on Defence Technology-Japan (ACDT)*, pp. 1–6.

Adhikari, S. 2013. Mechanical and Structural Characterization of Mini-Bar Reinforced Concrete Beams. PhD dissertation. University of Akron, Akron, OH.

Adhikary, S. K., Z. Rudzionis, A. Balakrishnan, and V. Jayakumar. 2019. Investigation on the Mechanical Properties and Post-Cracking Behavior of Polyolefin Fiber Reinforced Concrete. *Fibers,* Vol. 7, No. 1, pp. 5–15.

Ahmad, S. and A. Umar. 2018. Rheological and Mechanical Properties of Self-Compacting Concrete with Glass and Polyvinyl Alcohol Fibres. *Journal of Building Engineering,* Vol. 17, pp. 65–74.

Akihama, S., T. Suenaga, and T. Banno. 1984. The Behaviour of Carbon Fibre Reinforced Cement Composites in Direct Tension. *International Journal of Cement Composites and Lightweight Concrete,* Vol. 6, No. 3, pp. 159–168.

Alberti, M., A. Enfedaque, and J. Gálvez. 2014. On the Mechanical Properties and Fracture Behavior of Polyolefin Fiber-Reinforced Self-Compacting Concrete. *Construction and Building Materials,* Vol. 55, pp. 274–288.

Ali, M., A. Majumdar, and D. Rayment. 1972. Carbon Fibre Reinforcement of Cement. *Cement and Concrete Research,* Vol. 2, No. 2, pp. 201–212.

Alipour, A., B. Shafei, and M. Shinozuka. 2011. Performance Evaluation of Deteriorating Highway Bridges in High Seismic Areas. *ASCE Journal of Bridge Engineering,* Vol. 16, No. 5, pp. 597–611.

Alipour, A., B. Shafei, and M. Shinozuka. 2013. Capacity Loss Evaluation of Reinforced Concrete Bridges Located in Extreme Chloride-Laden Environments. *Journal of Structure and Infrastructure Engineering,* Vol. 9, No. 1, pp. 8–27.

Allahham, J., A. Bordelon, L. Li, and R. Siddartha. 2016. *Review and Specification for Shrinkage Cracks of Bridge Decks*. Utah Department of Transportation, Salt Lake City, UT.

Aly, T., J. G. Sanjayan, and F. Collins. 2008. Effect of Polypropylene Fibers on Shrinkage and Cracking of Concretes. *Materials and Structures,* Vol. 41, No. 10, article 1741.

Amat, T., M. Blanco, and A. Palomo. 1994. Acrylic Fibres as Reinforcement for Cement Pastes. *Cement and Concrete Composites,* Vol. 16, No. 1, pp. 31–37.

Arslan, M. E. 2016. Effects of Basalt and Glass Chopped Fibers Addition on Fracture Energy and Mechanical Properties of Ordinary Concrete: CMOD Measurement. *Construction and Building Materials,* Vol. 114, pp. 383–391.

Attiogbe, E. K., S. Schaef, C. O. Kerobo, D. Vojtko, and C. K. Nmai. 2014. A New Fiber for Enhanced Crack Control: Polypropylene Fiber with Chemical Bond to Concrete. *Concrete International,* Vol. 36, No. 12, pp. 35–39.

Auchey, F. L. and P. K. Dutta. 1996. The Use of Recycled High Density Polyethylene Fibers as Secondary Reinforcement in Concrete Subjected to Severe Environment. Sixth International Offshore and Polar Engineering Conference, May 26–31, Los Angeles, CA.

Ayub, T., N. Shafiq, and M. F. Nuruddin. 2014. Mechanical Properties of High-Performance Concrete Reinforced with Basalt Fibers. *Procedia Engineering,* Vol. 77, pp. 131–139.

Balaguru, P. 1994. *Thin Reinforced Concrete Products and Systems*. ACI Special Publication SP-146, American Concrete Institute. pp. 43–68.
Banthia, N. and R. Gupta. 2006. Influence of Polypropylene Fiber Geometry on Plastic Shrinkage Cracking in Concrete. *Cement and Concrete Research,* Vol**.** 36, No. 7, pp. 1263–1267.
Banthia, N. and C. Yan. 2000. Shrinkage Cracking in Polyolefin Fiber-Reinforced Concrete. *Materials Journal,* Vol. 97, No. 4, pp. 432–437.
Barluenga, G. and F. Hernández-Olivares. 2007. Cracking Control of Concretes Modified with Short AR-Glass Fibers at Early Age. Experimental Results on Standard Concrete and SCC. *Cement and Concrete Research,* Vol. 37, No. 12, pp. 1624–1638.
Battaglia, I. K. 2012. *Experimental Use of Type K Cement Concrete in Wisconsin Highway Bridge Decks*. Wisconsin Department of Transportation, Madison, WI.
Benmokrane, B., P. Wang, T. M. Ton-That, H. Rahman, and J.-F. Robert. 2002. Durability of Glass Fiber-Reinforced Polymer Reinforcing Bars in Concrete Environment. *Journal of Composites for Construction,* Vol. 6, No. 3, pp. 143–153.
Bentur A. and S. Mindess. 2006. *Fibre Reinforced Cementitious Composites*. CRC Press.
Bentz, D. P. and O. M. Jensen. 2004. Mitigation Strategies for Autogenous Shrinkage Cracking. *Cement and Concrete Composites,* Vol. 26, No. 6, pp. 677–685.
Bertelsen, I. M. G., L. M. Ottosen, and G. Fischer. 2019. Influence of Fibre Characteristics on Plastic Shrinkage Cracking in Cement-Based Materials: A Review. *Construction and Building Materials,* Vol. 230, pp. 1–17.
Betterman, L., C. Ouyang, and S. P. Shah. 1995. Fiber-Matrix Interaction in Microfiber-Reinforced Mortar. *Advanced Cement Based Materials,* Vol. 2, No. 2, pp. 53–61.
Borg, R. P., O. Baldacchino, and L. Ferrara. 2016. Early Age Performance and Mechanical Characteristics of Recycled PET Fibre Reinforced Concrete. *Construction and Building Materials,* Vol. 108, pp. 29–47.
Branston, J., S. Das, S. Y. Kenno, and C. Taylor. 2016. Mechanical Behaviour of Basalt Fibre Reinforced Concrete. *Construction and Building Materials,* Vol. 124, pp. 878–886.
Cengiz, O. and L. Turanli. 2004. Comparative Evaluation of Steel Mesh, Steel Fibre, and High-Performance Polypropylene Fibre Reinforced Shotcrete in Panel Test. *Cement and Concrete Research,* Vol. 34, No. 8, pp. 1357–1364.
Chan, L., G. Tanapornraweekit, and S. Tangtermsirikul. 2016. Investigation of Aramid Fibers Compared with Steel Fiber on Bending Behavior of Hybrid RC Beams. *Materials Science Forum*, Vol. 860, pp. 117–120.
Chand, S. 2000. Review Carbon Fibers for Composites. *Journal of Materials Science,* Vol. 35, No. 6, pp. 1303–1313.
Chen, P. W. and D. Chung. 1996. Low-Drying-Shrinkage Concrete Containing Carbon Fibers. *Composites Part B: Engineering,* Vol. 27, No. 3–4, pp. 269–274.
Chen, M., P. Gao, F. Geng, L. Zhang, and H. Liu. 2017. Mechanical and Smart Properties of Carbon Fiber and Graphite Conductive Concrete for Internal Damage Monitoring of Structure. *Construction and Building Materials,* Vol. 142, pp. 320–327.
Choi, Y., and R. L. Yuan. 2005. Experimental Relationship between Splitting Tensile Strength and Compressive Strength of GFRC and PFRC. *Cement and Concrete Research,* Vol. 35, No. 8, pp. 1587–1591.

Cifuentes, H., F. García, O. Maeso, and F. Medina. 2013. Influence of the Properties of Polypropylene Fibres on the Fracture Behaviour of Low-, Normal- and High-Strength FRC. *Construction and Building Materials,* Vol. 45, pp. 130–137.

Cohen, M. D. 1983. Theories of Expansion in Sulfoaluminate-Type Expansive Cements: Schools of Thought. *Cement and Concrete Research*, Vol. 13, No. 6, pp. 809–818.

Cohen, M. D., J. Olek, and W. L. Dolch. 1990. Mechanism of Plastic Shrinkage Cracking in Portland Cement and Portland Cement-Silica Fume Paste and Mortar. *Cement and Concrete Research,* Vol. 20, No. 1, pp. 103–119.

Combrinck, R., L. Steyl, and W. P. Boshoff. 2018. Interaction Between Settlement and Shrinkage Cracking in Plastic Concrete. *Construction and Building Materials,* Vol. 185, pp. 1–11.

Cordon, W. A. and J. D. Thorpe. 1965. Control of Rapid Drying of Fresh Concrete by Evaporation Control. *Materials Journal*, Vol. 62, No. 8, pp. 977–986.

Cui, Z, A. Alipour, and B. Shafei. 2019. Structural Performance of Deteriorating Reinforced Concrete Columns under Multiple Earthquake Events. *Journal of Engineering Structures*, Vol. 191, pp. 460–468.

Deák, T. and T. Czigány. 2009 Chemical Composition and Mechanical Properties of Basalt and Glass Fibers: A Comparison. *Textile Research Journal*, Vol. 79, No. 7, pp. 645–651.

Dehghan, A., K. Peterson, and A. Shvarzman. 2017. Recycled Glass Fiber Reinforced Polymer Additions to Portland Cement Concrete. *Construction and Building Materials*, Vol. 146, pp. 238–250.

Derombise, G., L. V. Van Schoors, and P. Davies. 2009. Degradation of Technora Aramid Fibres in Alkaline and Neutral Environments. *Polymer Degradation and Stability*, Vol. 94, No. 10, pp. 1615–1620.

Diab, S. H., A. M. Soliman, M. Nokken. 2020. Performance-Based Design for Fiber-Reinforced Concrete: Potential Balancing Corrosion Risk and Strength. *Journal of Materials in Civil Engineering*, Vol. 32, No. 2, 04019362.

Dopko, M. 2018. Fiber Reinforced Concrete: Tailoring Composite Properties with Discrete Fibers. MS thesis. Iowa State University, Ames, IA.

Dopko, M., M. Najimi, B. Shafei, X. Wang, P. Taylor, and B. M. Phares. 2018. Flexural Performance Evaluation of Fiber-Reinforced Concrete Incorporating Multiple Macro-Synthetic Fibers. *Transportation Research Record: Journal of the Transportation Research Board,* Vol. 2672, No. 27, pp. 1–12.

Dopko, M., M. Najimi, B. Shafei, X. Wang, P. Taylor, and B. Phares. 2020. Strength and Crack Resistance of Carbon Microfiber Reinforced Concrete. *Materials Journal,* Vol. 117, No. 2, pp. 11–23.

Eren, Ö. and K. Marar. 2010. Effect of Steel Fibers on Plastic Shrinkage Cracking of Normal and High Strength Concretes. *Materials Research*, Vol. 13, No. 2, pp. 135–141.

Eisenbeisz, H. G. 2001. South Dakota's First HPC Bridge. *Concrete Bridge Views*, Vol. 16, pp. 1–6.

Esping, O. and I. Löfgren. 2005. *Cracking Due to Plastic and Autogenous Shrinkage – Investigation of Early Age Deformation of Self-Compacting Concrete-Experimental Study*. Technical report. Chalmers University of Technology, Sweden.

Fan, S. J. 2015. Mechanical and Durability Performance of Polyacrylonitrile Fiber Reinforced Concrete. *Materials Research*, Vol. 18, No. 6, pp. 1298–1303.

Fiore, V., T. Scalici, G. Di Bella, and A. Valenza. 2015. A Review on Basalt Fibre and Its Composites. *Composites Part B: Engineering*, Vol. 74, pp. 74–94.

Fraternali, F., V. Ciancia, R. Chechile, G. Rizzano, L. Feo, and L. Incarnato. 2011. Experimental Study of the Thermo-Mechanical Properties of Recycled PET Fiber-Reinforced Concrete. *Composite Structures*, Vol. 93, No. 9, pp. 2368–2374.

Fraternali, F., S. Spadea, and V. P. Berardi. 2014. Effects of Recycled PET Fibres on the Mechanical Properties and Seawater Curing of Portland Cement-Based Concretes. *Construction and Building Materials*, Vol. 61, pp. 293–302.

Gao, S.-L., E. Mäder, A. Abdkader, and P. Offermann. 2003. Sizings on Alkali-Resistant Glass Fibers: Environmental Effects on Mechanical Properties. *Langmuir*, Vol. 19, No. 6, pp. 2496–2506.

Ghourchian, S., M. Wyrzykowski, M. L. Baquerizo, and P. Lura. 2018a. Performance of Passive Methods in Plastic Shrinkage Cracking Mitigation. *Cement and Concrete Composites*. 2018, Vol. 91, pp. 148–155.

Ghourchian, S., M. Wyrzykowski, M. L. Baquerizo, and P. Lura. 2018b. Susceptibility of Portland Cement and Blended Cement Concretes to Plastic Shrinkage Cracking. *Cement and Concrete Composites*, Vol. 85, pp. 44–55.

Ghourcian, S., M. Wyrzykowski, and P. A. Lura. 2018c. A Poromechanics Model for Plastic Shrinkage of Fresh Cementitious Materials. *Cement and Concrete Research*, Vol. 109, pp. 120–132.

Ghugal, T. M. and S. B. Deshmukh. 2006. Performance of Alkali-Resistant Glass Fiber Reinforced Concrete. *Journal of Reinforced Plastics and Composites*, Vol. 25, No. 6, pp. 617–630.

Giles Jr, H. F., E. M. Mount III, and J. R. Wagner Jr. 2004. *Extrusion: The Definitive Processing Guide and Handbook*. William Andrew, Norwich, NY.

Girgle, F., L. Bodnárová, A. Kučerová, P. Janák, and J. Prokeš. 2016. Experimental Verification of Behavior of Glass and Carbon Fibers in Alkali Environment. *Key Engineering Materials*, Vol. 677, pp. 43–48.

Grdic, Z. J., G. A. T. Curcic, N. S. Ristic, and I. M. Despotovic. 2012. Abrasion Resistance of Concrete Micro-Reinforced with Polypropylene Fibers. *Construction and Building Materials*, Vol. 27, No. 1, pp. 305–312.

Hahne, H., S. Karl, and J. Worner. 1987. Properties of Polyacrylonitrile Fiber Reinforced Concrete. *American Concrete Institute Symposium Paper*, Vol. 105, pp. 211–224.

Hajilar, S. and B. Shafei. 2014. Nano-Scale Characterization of Elastic Properties of AFt and AFm Phases of Hydrated Cement Paste. *Proceedings of the European Conference on Computational Modeling of Concrete Structures (EURO-C)*, pp. 299–306.

Hajilar, S. and B. Shafei. 2015. Nano-Scale Investigation of Elastic Properties of Hydrated Cement Paste Constituents using Molecular Dynamics Simulations. *Journal of Computational Materials Science*, Vol. 101, pp. 216–226.

Hajilar, S. and B. Shafei. 2016a. Mechanical Failure Mechanisms of Hydrated Products of Tricalcium Aluminate: A Molecular Dynamics Study. *Journal of Materials and Design*, Vol. 90, pp. 165–176.

Hajilar, S. and B. Shafei. 2016b. Assessment of Structural, Thermal, and Mechanical Properties of Portlandite through Molecular Dynamics Simulations. *Journal of Solid State Chemistry*, Vol. 244, pp. 164–174.

Hajilar, S. and B. Shafei. 2018a. Atomic-Scale Investigation of Physical Adsorption of Water Molecules and Aggressive Ions to Ettringite's Surfaces. *Journal of Colloid and Interface Science*, Vol. 513, pp. 104–116.

Hajilar, S. and B. Shafei. 2018b. Structure, Orientation, and Dynamics of Water-Soluble Ions Adsorbed to Basal Surfaces of Calcium Monosulfoaluminate Hydrates. *Journal of Physical Chemistry Chemical Physics*, Vol. 20, pp. 24681–24694.

Hajilar, S. and B. Shafei. 2019. Strength Anisotropy and Tension-Compression Asymmetry in Complex Sulfate-Bearing Crystals. *International Journal of Mechanical Sciences*, Vol. 150, pp. 304–313.

Hamoush, S., T. Abu-Lebdeh, and T. Cummins. 2010. Deflection Behavior of Concrete Beams Reinforced with PVA Micro-Fibers. *Construction and Building Materials,* Vol. 24, No. 11, pp. 2285–2293.

Han, T. Y., W. T. Lin, A. Cheng, R. Huang, and C. C. Huang. 2012. Influence of Polyolefin Fibers on the Engineering Properties of Cement-Based Composites Containing Silica Fume. *Materials and Design*, Vol. 37, pp. 569–576.

Han, J., D. Jia, and P. Yan. 2016. Understanding the Shrinkage Compensating Ability of Type K Expansive Agent in Concrete. *Construction and Building Materials*. Vol. 116, pp. 36–44.

Hao, Y., L. Cheng, H. Hao, and M. A. Shahin. 2018. Enhancing Fiber/Matrix Bonding in Polypropylene Fiber Reinforced Cementitious Composites by Microbially Induced Calcite Precipitation Pre-Treatment. *Cement and Concrete Composites,* Vol. 88, pp. 1–7.

Hargis, C. W., A. Telesca, and P. J. M. Monteiro. 2014. Calcium Sulfoaluminate (Ye'elimite) Hydration in the Presence of Gypsum, Calcite, and Vaterite. *Cement and Concrete Research*, Vol. 65, pp. 15–20.

Hasan, M., M. Afroz, and H. Mahmud. 2011. An Experimental Investigation on Mechanical Behavior of Macro Synthetic Fiber Reinforced Concrete. *International Journal of Civil and Environmental Engineering,* Vol. 11, No. 3, pp. 19–23.

He, S., J. Qiu, J. Li, and E. H. Yang. 2017. Strain Hardening Ultra-High Performance Concrete (SHUHPC) Incorporating CNF-Coated Polyethylene Fibers. *Cement and Concrete Research*, Vol. 98, pp. 50–60.

Hemalatha, T. and G. Ramesh. 2019. Mitigation of Plastic Shrinkage in Fly Ash Concrete Using Basalt Fibers. *Canadian Journal of Civil Engineering,* Vol. 46, pp. 759–769.

Henkensiefken, R., P. Briatka, D. P. Bentz, T. Nantung, and J. Weiss. 2010. Plastic Shrinkage Cracking in Internally Cured Mixtures: Prewetted Lightweight Aggregate can Reduce Cracking. *Concrete International*, Vol. 32, No. 2, pp. 49–54.

Heo, Y. S., J. G. Sanjayan, C. G. Han, and M. C. Han. 2011. Critical Parameters of Nylon and Other Fibres for Spalling Protection of High Strength Concrete in Fire. *Materials and Structures*, Vol. 44, No. 3, pp. 599–610.

Hoff, G. C., and K. A. Mather. 1978. *A Look at Type K Shrinkage-Compensating Cement Production and Specifications*. Paper C-78-2. U.S. Army Engineer Waterways Experiment Station Concrete Laboratory, Washington, DC.

Hossain, A. B., and J. Weiss. 2006. The Role of Specimen Geometry and Boundary Conditions on Stress Development and Cracking in the Restrained Ring Test. *Cement and Concrete Research*, Vol**.** 36, No 1, pp. 189–199.

Hossain, K., M. Lachemi, M. Sammour, and M. Sonebi. 2012. Influence of Polyvinyl Alcohol, Steel, and Hybrid Fibers on Fresh and Rheological Properties of Self-Consolidating Concrete. *Journal of Materials in Civil Engineering,* Vol. 24, No. 9, pp. 1211–1220.

Hossain, K., M. Lachemi, M. Sammour, and M. Sonebi, 2013. Strength and Fracture Energy Characteristics of Self-Consolidating Concrete Incorporating Polyvinyl Alcohol, Steel, and Hybrid Fibres. *Construction and Building Materials,* Vol. 45, pp. 20–29.

Hsie, M., C. Tu, and P. Song. 2008. Mechanical Properties of Polypropylene Hybrid Fiber-Reinforced Concrete. *Materials Science and Engineering: A,* Vol. 494, No. 1–2, pp. 153–157.

Huang, C. and G. Zhao. 1995. Properties of Steel Fibre Reinforced Concrete Containing Larger Coarse Aggregate. *Cement and Concrete Composites,* Vol. 17, No. 3, pp. 199–206.

Ibrahim, K. 2016. Mechanical Properties of Glass Fiber Reinforced Concrete (GFRC). *Journal of Mechanical and Civil Engineering,* Vol. 13, No. 4, pp. 47–50.

Islam, G. M. S. and S. D. Gupta. 2016. Evaluating Plastic Shrinkage and Permeability of Polypropylene Fiber Reinforced Concrete. *International Journal of Sustainable Built Environment,* Vol. 5, No. 2, pp. 345–354.

Jaber, T. M. 2007. Silica Fume for Concrete Bridge Decks. *Concrete Construction*. pp. 43–53.

Jalasutram, S., D. R. Sahoo, and V. Matsagar. 2017. Experimental Investigation of the Mechanical Properties of Basalt Fiber-Reinforced Concrete. *Structural Concrete,* Vol. 18, No. 2, pp. 292–302.

Jamshidi, M. and M. Karimi. 2010. Characterization of Polymeric Fibers as Reinforcements of Cement-Based Composites. *Journal of Applied Polymer Science,* Vol. 115, No. 5, pp. 2779–2785.

Jiang, C., K. Fan, F. Wu, and D. Chen. 2014. Experimental Study on the Mechanical Properties and Microstructure of Chopped Basalt Fibre Reinforced Concrete. *Materials and Design,* Vol. 58, pp. 187–193.

Johnston, C. D. 2014. *Fiber-Reinforced Cements and Concretes*. CRC Press.

Kabay, N. 2014. Abrasion Resistance and Fracture Energy of Concretes with Basalt Fiber. *Construction and Building Materials,* Vol. 50, pp. 95–101.

Karim, R., M. Najimi, and B. Shafei. 2019. Assessment of Transport Properties, Volume Stability, and Frost Resistance of Non-Proprietary Ultra-High Performance Concrete. *Journal of Construction and Building Materials*, Vol. 227, 117031.

Karim, R. and B. Shafei. 2021a. Performance of Fiber-Reinforced Concrete Link Slabs with Embedded Steel and GFRP Rebars. *Journal of Engineering Structures*, Vol. 229, 111590.

Karim, R. and B. Shafei. 2021b. Flexural Response Characteristics of Ultra-High Performance Concrete Made with Steel Microfibers and Macrofibers. *Journal of Structural Concrete*, Vol. 22, No. 6, pp. 3476–3490.

Karim, R. and B. Shafei. 2021c. Investigation of Five Synthetic Fibers as Potential Replacements of Steel Fibers in Ultra-High Performance Concrete. *ASCE Journal of Materials in Civil Engineering* [In Press].

Kang, S. H., S. G. Hong, and J. Moon. 2018. Shrinkage Characteristics of Heat-Treated Ultra-High Performance Concrete and Its Mitigation Using Superabsorbent Polymer Based Internal Curing Method. *Cement and Concrete Composites*, Vol. 89, pp. 130–138.

Khan, M. and M. Ali. 2016. Use of Glass and Nylon Fibers in Concrete for Controlling Early Age Micro Cracking in Bridge Decks. *Construction and Building Materials*, Vol. 125, pp. 800–808.

Khan, I., T. Xu, M. S. H. Khan, A. Castel, and R. I. Gilbert. 2020. Effects of Various Supplementary Cementitious Materials on Early-Age Concrete Cracking. *Journal of Materials in Civil Engineering*, Vol. 32, No. 4, pp. 1–9.

Khatami, D., B. Shafei, and O. Smadi. 2016. Management of Bridges under Aging Mechanisms and Extreme Events: A Risk-Based Approach. *Transportation Research Record: Journal of the Transportation Research Board*, Vol. 2550, No. 1, pp. 89–95.

Khatami, D., S. Hajilar, and B. Shafei. 2021. Investigation of Oxygen Diffusion and Corrosion Potential through a Cellular Automaton Framework. *Journal of Corrosion Science*, Vol. 187, 109496.

Khatami, D., and B. Shafei. 2021. Impact of Climate Conditions on Deteriorating Reinforced Concrete Bridges in the U.S. Midwest Region. *ASCE Journal of Performance of Constructed Facilities*, Vol. 35, No. 1, 04020129.

Kim, S. B., N. H. Yi, H. Y. Kim, J. H. J. Kim, and Y. C. Song. 2010. Material and Structural Performance Evaluation of Recycled PET Fiber Reinforced Concrete. *Cement and Concrete Composites*, Vol. 32, No. 3, pp. 232–240.

King, D. 2012. The Effect of Silica Fume on the Properties of Concrete as Defined in Concrete Society Report 74, Cementitious Materials. 37th Conference on Our World in Concrete and Structures, August 29–31, Singapore.

Kizilkanat, A. B., N. Kabay, V. Akyüncü, S. Chowdhury, and A. H. Akça. 2015. Mechanical Properties and Fracture Behavior of Basalt and Glass Fiber Reinforced Concrete: An Experimental Study. *Construction and Building Materials*, Vol. 100, pp. 218–224.

Kobayashi, K. and R. Cho. 1981. Flexural Behaviour of Polyethylene Fibre Reinforced Concrete. *International Journal of Cement Composites and Lightweight Concrete*, Vol. 3, No. 1, pp. 19–25.

Kulkarni, A., and B. Shafei. 2018. Impact of Extreme Events on Transportation Infrastructure in Iowa: A Bayesian Network Approach. *Transportation Research Record: Journal of the Transportation Research Board*, Vol. 2672, No. 48, pp. 45–57.

Kwan, A. K. H. and S. H. Chu. 2018. Direct Tension Behaviour of Steel Fibre Reinforced Concrete Measured by a New Test Method. *Engineering Structures*, Vol. 176, pp. 324–336.

Larson, B. K., L. T. Drzal, and P. Sorousian. 1990. Carbon Fibre-Cement Adhesion in Carbon Fibre Reinforced Cement Composites. *Composites*, Vol. 21, No. 3, pp. 205–215.

Lee, G., D. Han, M.-C. Han, C.-G. Han, and H. J. Son. 2012. Combining Polypropylene and Nylon Fibers to Optimize Fiber Addition for Spalling Protection of High-Strength Concrete. *Construction and Building Materials*, Vol. 34, pp. 313–320.

Leemann, A., P. Nygaard, and P. Lura. 2014. Impact of Admixtures on the Plastic Shrinkage Cracking of Self-Compacting Concrete. *Cement and Concrete Composites*, Vol. 46, pp. 1–7.

Lepoutre, P. 2013. *The Manufacture of Polyethylene*. New Zealand Institute of Chemistry.

Li, V. C., T. Horikoshi, A. Ogawa, S. Torigoe, and T. Saito. 2004. Micromechanics-Based Durability Study of Polyvinyl Alcohol-Engineered Cementitious Composite. *Materials Journal*, Vol. 101, No. 3, pp. 242–248.

Li, Y., W. Li, D. Deng, K. Wang, and W. H. Duan. 2018. Reinforcement Effects of Polyvinyl Alcohol and Polypropylene Fibers on Flexural Behaviors of Sulfoaluminate Cement Matrices. *Cement and Concrete Composites*, Vol. 88, pp. 139–149.

Lin, T., S. Wu, J. Lai, and S. Shyu. 2000. The Effect of Chemical Treatment on Reinforcement/Matrix Interaction in Kevlar-Fiber/Bismaleimide Composites. *Composites Science and Technology*, Vol. 60, No. 9, pp. 1873–1878.

Lipatov, Y., V. S. Gutnikov, M. Manylov, E. Zhukovskaya, and B. Lazoryak. 2015. High Alkali-Resistant Basalt Fiber for Reinforcing Concrete. *Materials and Design,* Vol. 73, pp. 60–66.

López-Buendía, A. M., M. D. Romero-Sánchez, V. Climent, and C. Guillem. 2013. Surface Treated Polypropylene (PP) Fibres for Reinforced Concrete. *Cement and Concrete Research,* Vol. 54, pp. 29–35.

Malathy, R., K. Subramanian, and M. Rameshkumar. 2007. Effect of Glass Fibers on Restrained Plastic Shrinkage Cracking of HPC with Silica Fume. *Journal of Scientific and Industrial Research,* Vol. 66, pp. 748–751.

Marissen, R. 2011. Design With Ultra Strong Polyethylene Fibers. *Materials Sciences and Applications,* Vol. 2, No. 5, pp. 319–331.

Micelli, F. and A. Nanni. 2004. Durability of FRP Rods for Concrete Structures. *Construction and Building Materials,* Vol. 18, No. 7, pp. 491–503.

Mingchao, W., Z. Zuoguang, L. Yubin, L. Min, and S. Zhijie. 2008. Chemical Durability and Mechanical Properties of Alkali-Proof Basalt Fiber and its Reinforced Epoxy Composites. *Journal of Reinforced Plastics and Composites,* Vol. 27, No. 4, pp. 393–407.

Mirza, F. A. and P. Soroushian. 2002. Effects of Alkali-Resistant Glass Fiber Reinforcement on Crack and Temperature Resistance of Lightweight Concrete. *Cement and Concrete Composites,* Vol. 24, No. 2, pp. 223–227.

Mo, K. H., U. J. Alengaram, M. Z. Jumaat, and M. Y. J. Liu. 2015. Contribution of Acrylic Fibre Addition and Ground Granulated Blast Furnace Slag on the Properties of Lightweight Concrete. *Construction and Building Materials*, Vol. 95, pp. 686–695.

Mohammadi Mohaghegh, A. 2016. *Use of Macro Basalt Fibre Concrete for Marine Applications*. KTH Royal Institute of Technology, Stockholm.

Mohod, M. V. 2015. Performance of Polypropylene Fibre Reinforced Concrete. *Journal of Mechanical and Civil Engineering,* Vol. 12, No. 1, pp. 28–36.

Mora-Ruacho, J., R. Gettu, and A. Aguado. 2009. Influence of Shrinkage-Reducing Admixtures on the Reduction of Plastic Shrinkage Cracking in Concrete. *Cement and Concrete Research*, Vol. 39, No. 3, pp. 141–146.

Mufti, A. A., N. Banthia, B. Benmokrane, M. Boulfiza, and J. P. Newhook. 2007. Durability of GFRP Composite Rods. *Concrete International,* Vol. 29, No. 2, pp. 37–42.

Nagataki, S. and H. Gomi. 1998. Expansive Admixtures (Mainly Ettringite). *Cement and Concrete Composites*, Vol. 20, No. 2–3, pp. 163–170.

Nam, J., G. Kim, J. Yoo, G. Choe, H. Kim, H. Choi, Y. Kim. 2016. Effectiveness of Fiber Reinforcement on the Mechanical Properties and Shrinkage Cracking of Recycled Fine Aggregate Concrete. *Materials*, Vol. 9, No. 3, pp. 1-15.

Nanni, A. 1992. Properties of Aramid-Fiber Reinforced Concrete and SIFCON. *Journal of Materials in Civil Engineering,* Vol. 4, No. 1, pp. 1–15.

Nishioka, K., S. Yamakawa, and K. Shirakawa. 1986. Properties and Applications of Carbon Fiber Reinforced Cement Composites. Development in Fiber Reinforced Cement and Concrete, RILEM, Symposium, Sheffield, South Yorkshire, England.

Niu, Y., H. Huang, J. Zhang, W. Jin, J. Wei, and Q. Yu. 2019. Development of the Strain Field Along the Crack in Ultra-High-Performance Fiber-Reinforced Concrete (UHPFRC) Under Bending by Digital Image Correlation Technique. *Cement and Concrete Research*, Vol. 125, pp. 1–11.

Nkurunziza, G., A. Debaiky, P. Cousin, and B. Benmokrane. 2005. Durability of GFRP Bars: A Critical Review of the Literature. *Progress in Structural Engineering and Materials,* Vol. 7, No. 4, pp. 194–209.

Nochaiya, T., W. Wongkeo, and A. Chaipanich. 2010. Utilization of Fly Ash with Silica Fume and Properties of Portland Cement–Fly Ash–Silica Fume Concrete. *Cement and Concrete Research*, Vol. 89, No. 3, pp. 768–774.

Noushini, A., B. Samali, and K. Vessalas. 2013. Effect of Polyvinyl Alcohol (PVA) Fibre on Dynamic and Material Properties of Fibre Reinforced Concrete. *Construction and Building Materials,* Vol. 49, pp. 374–383.

Ochi, T., S. Okubo, and K. Fukui. 2007. Development of Recycled PET Fiber and Its Application as Concrete-Reinforcing Fiber. *Cement and Concrete Composites,* Vol. 29, No. 6, pp. 448–455.

Ogawa, A. and H. Hoshiro. 2011. Durability of Fibres. *Durability of Strain-Hardening Fibre-Reinforced Cement-Based Composites (SHCC).* Springer, Netherlands. pp. 81–88.

Oh, B. H., J. C. Kim, and Y. C. Choi. 2007. Fracture Behavior of Concrete Members Reinforced with Structural Synthetic Fibers. *Engineering Fracture Mechanics,* Vol. 74, No. 1–2, pp. 243–257.

Okeil, A., K. Matsumoto, and K. Nagai. 2020. Investigation on Local Bond Behavior in Concrete and Cement Paste around a Deformed Bar by Using DIC Technique. *Cement and Concrete Composites,* Vol. 109.

Ozsar, D. S., F. Ozalp, H. D. Yilmaz, and B. Akcay. 2017. Effects of Nylon Fibre and Concrete Strength on the Shrinkage and Fracture Behaviour of Fibre Reinforced Concrete. International Conference on Strain-Hardening Cement-Based Composites, September 18–20, Dresden, Germany, pp. 188–194.

Ozger, O. B., F. Girardi, G. M. Giannuzzi, V. A. Salomoni, C. E. Majorana, L. Fambri, N. Baldassino, and R. Di Maggio. 2013. Effect of Nylon Fibres on Mechanical and Thermal Properties of Hardened Concrete for Energy Storage Systems. *Materials and Design*, Vol. 51, pp. 989–997.

Passuello, A., G. Moriconi, and S. P. Shah. 2009. Cracking Behavior of Concrete with Shrinkage Reducing Admixtures and PVA Fibers. *Cement and Concrete Composites,* Vol. 31, No. 10, pp. 699–704.

Patnaik, A., L. Miller, S. Adhikari, and P. C. Standal. 2013. Basalt FRP Minibar Reinforced Concrete. Fibre Concrete 2013, September 12–13, Prague, Czech Republic, pp. 51–52.

Patnaik, A., L. Miller, and P. C. Standal. 2014. Fiber Reinforced Concrete Made from Basalt FRP Minibar. 1st Concrete Innovation Conference (CIC), June 11–13, Oslo, Norway.

Patnaik, A., P. Baah, P. Ricciardi, and W. Khalifa. 2017. Reduction of Crack Widths in Steel Reinforced Concrete Bridge Decks with Fiber *American Concrete Institute Symposium Paper,* Vol. 319, pp. 1.1–1.20.

Pelisser, F., A. B. d. S. S. Neto, H. L. La Rovere, and R. C. de Andrade Pinto. 2010. Effect of the Addition of Synthetic Fibers to Concrete Thin Slabs on Plastic Shrinkage Cracking. *Construction and Building Materials,* Vol. 24, No. 11, pp. 2171–2176.

Pešić, N., S. Živanović, R. Garcia, and P. Papastergiou. 2016. Mechanical Properties of Concrete Reinforced with Recycled HDPE Plastic Fibres. *Construction and Building Materials,* Vol. 115, pp. 362–370.

Pezeshkian, M., A. Delnavaz, and M. Delnavaz. 2020. Effect of Natural Zeolite on Mechanical Properties and Autogenous Shrinkage of Ultrahigh-Performance Concrete. *Journal of Materials in Civil Engineering*, Vol. 32, No. 5, article 04020093.

PCA. 2002. *Types and Causes of Concrete Deterioration*. PCA R&D Serial No. 2617. Portland Cement Association, Skokie, IL.

Qi, C. 2003. Quantitative Assessment of Plastic Shrinkage Cracking and Its Impact on the Corrosion of Steel Reinforcement. PhD dissertation. Purdue University, West Lafayette, IN.

Ramakrishnan, V. 1999. Structural Application of Polyolefin Fiber Reinforced Concrete. *American Concrete Institute Symposium Paper,* Vol. 182, pp. 235–253.

Ramachandran, V. S., P. J. Sereda, and R. F. Feldman. 1964. Mechanism of Hydration of Calcium Oxide. *Nature*, Vol. 201, pp. 288–289.

Ramezanianpour, A., M. Esmaeili, S. Ghahari, and M. Najafi. 2013. Laboratory Study on the Effect of Polypropylene Fiber on Durability, and Physical and Mechanical Characteristic of Concrete for Application in Sleepers. *Construction and Building Materials,* Vol. 44, pp. 411–418.

Ramsayer, C. 2017. Type K Engineered Expansive Cements: Boyd's Hollow Bridge. Presentation from the Illinois Transportation and Highway Engineering Conference, February 28–March 1, Urbana, IL.

Rice, E. K. 2012. Shrinkage-Compensating Concrete – Past, Present, and Future, Part 1. Presentation from the ACI Fall 2012 Convention, October 21–24, Toronto, Canada.

Roque, R., N. Kim, B. Kim, and G. Lopp. 2009. *Durability of Fiber-Reinforced Concrete in Florida Environments*. Florida Department of Transportation, Tallahassee, FL.

Rostami, R., M. Zarrebini, M. Mandegari, K. Sanginabadi, D. Mostofinejad, and S. M. Abtahi. 2019. The Effect of Concrete Alkalinity on Behavior of Reinforcing Polyester and Polypropylene Fibers with Similar Properties. *Cement and Concrete Composites,* Vol. 97, pp. 118–124.

Rouquerol, J., D. Avnir, C. W. Fairbridge, D. H. Everett, J. H. Haynes, N. Pernicone, J. D. F. Ramsay, K. S. W. Sing., and K. K. Unger. 1994. Recommendations for the Characterization of Porous Solids. *Pure Applied Chemistry*, Vol. 66, No. 8, pp. 1739–1758.

Rybin, V., A. Utkin, and N. Baklanova. 2013. Alkali Resistance, Microstructural and Mechanical Performance of Zirconia-Coated Basalt Fibers. *Cement and Concrete Research,* Vol. 53, pp. 1–8.

Saradar, A., B. Tahmouresi, E. Mohseni, and A. Shadmani. 2018. Restrained Shrinkage Cracking of Fiber-Reinforced High-Strength Concrete. *Fibers,* Vol. 6, No. 1, p. 12.

Sayahi, F. 2019. Plastic Shrinkage Cracking in Concrete: Mitigation and Modelling. PhD dissertation. Luleå University of Technology, Luleå, Sweden.

Sayyar, M., P. Soroushian, M. M. Sadiq, A. Balachandra, and J. Lu. 2013. Low-Cost Glass Fiber Composites with Enhanced Alkali Resistance Tailored Towards Concrete Reinforcement. *Construction and Building Materials,* Vol. 44, pp. 458–463.

Scarpas, A., N. Kringos, I. Al-Qadi, and A. Loizos. 2012. *7th RILEM International Conference on Cracking in Pavements: Mechanisms, Modeling, Testing, Detection, and Prevention Case Histories*. Springer, New York, NY.

Scheffler, C., T. Förster, E. Mäder, G. Heinrich, S. Hempel, and V. Mechtcherine. 2009. Aging of Alkali-Resistant Glass and Basalt Fibers in Alkaline Solutions: Evaluation of the Failure Stress by Weibull Distribution Function. *Journal of Non-Crystalline Solids,* Vol. 355, No. 52–54, pp. 2588–2595.

Scheffler, C., S. Zhandarov, and E. Mäder. 2017. Alkali Resistant Glass Fiber Reinforced Concrete: Pull-Out Investigation of Interphase Behavior Under Quasi-Static and High Rate Loading. *Cement and Concrete Composites,* Vol. 84, pp. 19–27.

Schmidt, M. and V. Slowik. 2009. Capillary Shrinkage Cracking and Its Prevention by Controlled Concrete Curing. *Concrete Durability and Service Life Planning – ConcreteLife '09*. RILEM Publications, Paris, France.

Shaeles, C. A. and K. C. Hover. 1988. Influence of Mix Proportions and Constructions Operation,s on Plastic Shrinkage Cracking in Thin Slabs. *Materials Journal*, Vol. 85, No. 6, pp. 495–504.

Shafei, B. 2011. Stochastic Finite-Element Analysis of Reinforced Concrete Structures Subjected to Multiple Environmental Stressors. Ph.D. Dissertation. University of California, Irvine.

Shafei, B., A. Alipour, and M. Shinozuka. 2012. Prediction of Corrosion Initiation in Reinforced Concrete Members Subjected to Environmental Stressors: A Finite-Element Framework. *Journal of Cement and Concrete Research*, Vol. 42, No. 2, pp. 365–376.

Shafei, B., A. Alipour, and M. Shinozuka. 2013. A Stochastic Computational Framework to Investigate the Initial Stage of Corrosion in Reinforced Concrete Superstructures. *Journal of Computer-Aided Civil and Infrastructure Engineering*, Vol. 28, No. 7, pp. 482–494.

Shafei, B., and A. Alipour. 2015a. Application of Large-Scale Non-Gaussian Stochastic Fields for the Study of Corrosion-Induced Structural Deterioration. *Journal of Engineering Structures*, Vol. 88, pp. 262–276.

Shafei, B., and A. Alipour. 2015b. Estimation of Corrosion Initiation Time in Reinforced Concrete Bridge Columns: How to Incorporate Spatial and Temporal Uncertainties. *ASCE Journal of Engineering Mechanics*, Vol. 141, No. 10, 04015037.

Shafei, B., M. Kazemian, M. Dopko, and M. Najimi. 2021. State-of-the-Art Review of Capabilities and Limitations of Polymer and Glass Fibers Used in Fiber-Reinforced Concrete. *Journal of Materials*, Vol. 14, No. 2, 409.

Shafiq, N., T. Ayub, and S. U. Khan. 2016. Investigating the Performance of PVA and Basalt Fibre Reinforced Beams Subjected to Flexural Action. *Composite Structures,* Vol. 153, pp. 30–41.

Shi, W., B. Shafei, Z. Liu, and B. Phares. 2019. Early-Age Performance of Longitudinal Bridge Joints Made with Shrinkage-Compensating Cement Concrete. *Journal of Engineering Structures,* Vol. 197, 109391.

Shi, W., B. Shafei, Z. Liu, and B. Phares. 2020a. Longitudinal Box-Beam Bridge Joints under Monotonic and Cyclic Loads. *Journal of Engineering Structures,* Vol. 220, 110976.

Shi, W., M. Najimi, and B. Shafei. 2020b. Reinforcement Corrosion and Transport of Water and Chloride Ions in Shrinkage-Compensating Cement Concretes. *Journal of Cement and Concrete Research*, Vol. 135, 106121.

Shi, W., M. Najimi, and B. Shafei. 2020c. Chloride Penetration in Shrinkage-Compensating Cement Concretes. *Journal of Cement and Concrete Composites*, Vol. 113, No. 103656.

Shi, W., and B. Shafei. 2021. Bond Characteristics Between Conventional Concrete and Six High-Performance Patching Materials. *Journal of Construction and Building Materials*, Vol. 308, 124898.

Shizong, L, W. Yanrong, and L. Chen. 1995 Investigation on the Formation of Ettringite in the Presence of BaO. *Cement and Concrete Research*, Vol. 25, No. 7, pp. 1417–1422.
Silica Fume Association. 2014. What is Silica Fume? Silica Fume Association, Lovettsville, VA. https://www.silicafume.org/general-silicafume.html.
Silva, D., A. Betioli, P. Gleize, H. Roman, L. Gomez, and J. Ribeiro. 2005. Degradation of Recycled PET Fibers in Portland Cement-Based Materials. *Cement and Concrete Research*, Vol. 35, No. 9, pp. 1741–1746.
Sivakumar, A. and M. Santhanam. 2007. Mechanical Properties of High Strength Concrete Reinforced with Metallic and Non-Metallic Fibres. *Cement and Concrete Composites*, Vol. 29, No. 8, pp. 603–608.
Slowik, V., M. Schmidt, and R. Fritzsch. 2008. Capillary Pressure in Fresh Cement-Based Materials and Identification of the Air Entry Value. *Cement and Concrete Research*, Vol. 30, No. 7, pp. 557–565.
Smirnova, O. M., A. A. Shubin, and I. V. Potseshkovskaya. 2017. Strength and Deformability Properties of Polyolefin Macrofibers Reinforced Concrete. *International Journal of Applied Engineering Research*, Vol. 12, No. 20, pp. 9397–9404.
Song, P., S. Hwang, and B. Sheu. 2005. Strength Properties of Nylon- and Polypropylene-Fiber-Reinforced Concretes. *Cement and Concrete Research*, Vol. 35, No. 8, pp. 1546–1550.
Song, M., P. Purnell, and I. Richardson. 2015. Microstructure of Interface Between Fibre and Matrix in 10-Year Aged GRC Modified by Calcium Sulfoaluminate Cement. *Cement and Concrete Research*, Vol. 76, pp. 20–26.
Soranakom, C., M. Bakhshi, and B. Mobasher. 2008. Role of Alkali Resistant Glass Fibers in Suppression of Restrained Shrinkage Cracking of Concrete Materials. 15th Congress of the International Glass Fibre Reinforced Concrete Association (GRCA), April 20–23. Prague, Czech Republic.
Sorelli, L., A. Meda, and G. Plizzari. 2005. Bending and Uniaxial Tensile Tests on Concrete Reinforced with Hybrid Steel Fibers. *Journal of Materials in Civil Engineering*, Vol. 17, No. 5, pp. 519–527.
Soroushian, P., A. Khan, and J. W. Hsu. 1992. Mechanical Properties of Concrete Materials Reinforced with Polypropylene or Polyethylene Fibers. *Materials Journal*, Vol. 89, No. 6, pp. 535–540.
Soroushian, P., J. Plasencia, and S. Ravanbakhsh. 2003. Assessment of Reinforcing Effects of Recycled Plastic and Paper in Concrete. *Materials Journal*, Vol. 100, No. 3, pp. 203–207.
Söylev, T. and T. Özturan. 2014. Durability, Physical, and Mechanical Properties of Fiber-Reinforced Concretes at Low-Volume Fraction. *Construction and Building Materials*, Vol. 73, pp. 67–75.
Sutter, L., R. D. Hooton, and S. Schlorholtz. 2013. *NCHRP Report 749: Methods for Evaluating Fly Ash for Use in Highway Concrete*. National Cooperative Highway Research Program, Washington, DC.
Sutter, L. L. 2016. *Best Practices for Concrete Pavements: Supplementary Cementitious Materials*. FHWA-HIF-16-001. Technical Brief. Federal Highway Administration. Washington, DC.
Swamy, R. N. and B. Barr. 1989. *Fibre Reinforced Cement and Concretes: Recent Developments*. CRC Press.

Tagnit-Hamou, A., Y. Vanhove, and N. Petrov. 2005. Microstructural Analysis of the Bond Mechanism between Polyolefin Fibers and Cement Pastes. *Cement and Concrete Research*, Vol. 35, No. 2, pp. 364–370.

Takemoto, K. and H. Uchikawa. 1980. Hydration of Pozzolanic Cements. 7th International Congress on the Chemistry of Cement, Paris, France.

Tan, Y., X. Lu, R. He, H. Chen, and Z. Wang. 2020. Influence of Superabsorbent Polymers (SAPs) Type and Particle Size on the Performance of Surrounding Cement-Based Materials. *Construction and Building Materials*, Vol. 270, article 121442.

Thomas, M. 2007. *Optimizing the Use of Fly Ash in Concrete*. Portland Cement Association. Skokie, IL.

Toutanji, H., S. McNeil, and Z. Bayasi. 1998. Chloride Permeability and Impact Resistance of Polypropylene-Fiber-Reinforced Silica Fume Concrete. *Cement and Concrete Research*, Vol. 28, No. 7, pp. 961–968.

Uomoto, T. and T. Nishimura. 1999. Deterioration of Aramid, Glass, and Carbon Fibers due to Alkali, Acid, and Water in Different Temperatures. *American Concrete Institute Symposium Paper*, Vol. 188, pp. 515–522.

Uomoto, T., H. Mutsuyoshi, F. Katsuki, and S. Misra. 2002. Use of Fiber Reinforced Polymer Composites as Reinforcing Material for Concrete. *Journal of Materials in Civil Engineering*, Vol. 14, No. 3, pp. 191–209.

Van Tuan, N., G. Ye, K. Van Breugel, and O. Copuroglu. 2011. Hydration and Microstructure of Ultra High Performance Concrete Incorporating Rice Husk Ash. *Cement and Concrete Research*, Vol. 41, No. 11, pp. 1104–1111.

Veigas, M. G., M. Najimi, and B. Shafei. 2022. Investigation of Cementitious Composites Made with Uncoated and Coated Sisal Fibers. *Journal of Case Studies in Construction Materials*, Vol. 16, E00788.

Vosoughi, P. 2019. Improving Engineering Properties of Cement-Based Materials by Internal Curing. PhD dissertation. Iowa State University, Ames, IA.

Wang, Y., V. C. Li, and S. Backer. 1987. Analysis of Synthetic Fiber Pull-Out from a Cement Matrix. *MRS Online Proceedings Library*: *Symposium R – Bonding in Cementitious Composites*, Vol. 114, pg. 159.

Wang, X., K. Wang, F. Bektas, and P. Taylor. 2012. Drying shrinkage of ternary blend concrete in Transportation Structures. *Journal of Sustainable Cement-Based Materials*. Vol. 1, No. 1, pp. 56–66.

Wei, B., H. Cao, and S. Song. 2010. Tensile Behavior Contrast of Basalt and Glass Fibers after Chemical Treatment. *Materials and Design,* Vol. 31, No. 9, pp. 4244–4250.

Wongtanakitcharoen, T. and A. E. Naaman. 2007. Unrestrained Early Age Shrinkage of Concrete with Polypropylene, PVA, and Carbon Fibers. *Materials and Structures,* Vol. 40, No. 3, pp. 289–300.

Wu, H. C. and V. C. Li. 1999. Fiber/Cement Interface Tailoring with Plasma Treatment. *Cement and Concrete Composites,* Vol. 21, No. 3, pp. 205–212.

Wu, G., X. Wang, Z. Wu, Z. Dong, and G. Zhang. 2015. Durability of Basalt Fibers and Composites in Corrosive Environments. *Journal of Composite Materials,* Vol. 49, No. 7, pp. 873–887.

Yamaguchi, M., K. Murakami, K. Takeda, and Y. Mitsui. 2011. Blast Resistance of Polyethylene Fiber Reinforced Concrete to Contact Detonation. *Journal of Advanced Concrete Technology,* Vol. 9, No. 1, pp. 63–71.

Yan, L., R. Pendleton, and C. Jenkins. 1998. Interface Morphologies in Polyolefin Fiber Reinforced Concrete Composites. *Composites Part A: Applied Science and Manufacturing,* Vol. 29, No. 5–6, pp. 643–650.
Yang, Y. X. and J. Lian. 2011. Basalt Fiber Reinforced Concrete. *Advanced Materials Research,* Vol. 194, pp. 1103–1108.
Yao, W., J. Li, and K. Wu. 2003. Mechanical Properties of Hybrid Fiber-Reinforced Concrete at Low Fiber Volume Fraction. *Cement and Concrete Research,* Vol. 33, No. 1, pp. 27–30.
Yap, S. P., U. J. Alengaram, and M. Z. Jumaat. 2013. Enhancement of Mechanical Properties in Polypropylene- and Nylon-Fibre Reinforced Oil Palm Shell Concrete. *Materials and Design,* Vol. 49, pp. 1034–1041.
Yeganeh, A. E., F. Kouroshnezhad, S. Dadsetan, K. M. Hossain, and M. Lachemi. 2019. Experimental Investigation on Mechanical Properties of Fiber Reinforced Lightweight Self-Consolidating Concrete. *Rheology and Processing of Construction Materials,* pp. 536–543.
Yin, S., R. Tuladhar, T. Collister, M. Combe, N. Sivakugan, and Z. Deng. 2015. Post-Cracking Performance of Recycled Polypropylene Fibre in Concrete. *Construction and Building Materials,* Vol. 101, Part 1, pp. 1069–1077.
Yin, S., R. Tuladhar, J. Riella, D. Chung, T. Collister, M. Combe, and N. Sivakugan. 2016. Comparative Evaluation of Virgin and Recycled Polypropylene Fibre Reinforced Concrete. *Construction and Building Materials*, Vol. 114, pp. 134–141.
Zaroudi, M., R. Madandoust, and K. Aghaee. 2020. Fresh and Hardened Properties of an Eco-Friendly Fiber Reinforced Self-Consolidated Concrete Composed of Polyolefin Fiber and Natural Zeolite. *Construction and Building Materials,* Vol. 241.
Zhang, S., G. Z. Li, and H. Y. Yuan. 2011. Effect of the Chemical Treated Kevlar Fiber on the Behaviors of Cement Mortars. *Advanced Materials Research,* Vol. 306, pp. 758–761.
Zhang, P. and Q. F. Li. 2013. Combined Effect of Polypropylene Fiber and Silica Fume on Workability and Carbonation Resistance of Concrete Composite Containing Fly Ash. *Proceedings of the Institution of Mechanical Engineers, Part L: Journal of Materials: Design and Applications,* Vol. 227, No. 3, pp. 250–258.
Zhang, J., J. Cheng, Y. Dou, and Q. Xin. 2017. Mechanical Properties and Durability of Fiber-Reinforced Concrete. *Journal of Engineering Science and Technology Review,* Vol. 10, No. 5, pp. 68–75.
Zhao, X. and X. J. He. 2014. High-Toughness and Durability Performance Characterization of Concrete Reinforced with Poly (Vinyl Alcohol) Fibers. *Materials Express,* Vol. 4, No. 3, pp. 247–252.
Zhao, Y., R. Guo, and Y. Zhou. 2018. Research on Drying Shrinkage and Early-Age Crack Resistance of Aramid Fiber Reinforced Concrete. 97th Annual Meeting of the Transportation Research Board, January 7–11, Washington, DC.
Zheng, Z. and D. Feldman. 1995. Synthetic Fibre-Reinforced Concrete. *Progress in Polymer Science,* Vol. 20, No. 2, pp. 185–210.
Zia, A. and M. Ali. 2017. Behavior of Fiber Reinforced Concrete for Controlling the Rate of Cracking in Canal-Lining. *Construction and Building Materials,* Vol. 155, pp. 726–739.

THE INSTITUTE FOR TRANSPORTATION IS THE FOCAL POINT FOR TRANSPORTATION AT IOWA STATE UNIVERSITY.

InTrans centers and programs perform transportation research and provide technology transfer services for government agencies and private companies;

InTrans contributes to Iowa State University and the College of Engineering's educational programs for transportation students and provides K–12 outreach; and

InTrans conducts local, regional, and national transportation services and continuing education programs.

IOWA STATE UNIVERSITY

Visit **InTrans.iastate.edu** for color pdfs of this and other research reports.